University of Naples "Federico II" Polytechnic and Basic Sciences School

Ph.D. School in Chemical Sciences – Cycle XXXVIII

"Structural And Functional Characterization of Immunomodulatory Glycoconjugates Provided by The Gut Microbiota"

Roberta Cirella

Tutors

Prof. Flaviana Di Lorenzo

Prof. Antonio Molinaro

Examiner

Prof. Angela Arciello

This PhD was funded through the **ERC-funded project DEBUGGING-LPS** (Grant Agreement No. 101040202) under the European Union's Horizon 2020 research and innovation programme, led by **Prof. Flaviana Di Lorenzo** at the University of Naples Federico II.

As part of the doctoral training, a research stay was conducted at the *Forschungszentrum Borstel, Leibniz Lungenzentrum* in Borstel, Germany, under the supervision of **Dr. Katarzyna Anna Duda**, providing additional expertise and collaborative input to the project.

Index

Abbreviations

AA	Acetylated Alditols
AMG	Acetylated Methyl Glycosides
COSY	Correlation Spectroscopy
CPS	Capsular Polysaccharide
DC	Dendritic Cells
DMSO	Dimethyl Sulphoxide
DNase	Deoxyribonuclease I From Bovine Pancreas
DOSY	Diffusion Ordered Spectroscopy
EPS	Exopolysaccharide
F/B Ratio	Firmicutes/Bacteroidetes Ratio
GC-MS	Gas Chromatography Mass Spectrometry
GF	Germ Free (Mice)
GM	Gut Microbiota
HEK	Human Embryonic Kidney (Cells)
HMBC	Heteronuclear Multiple Bond Correlation Spectroscopy
HSQC	Heteronuclear Single-Quantum Correlation Spectroscopy
IBD	Inflammatory Bowel Disease
IL	Interleukin
LBP	LPS Binding Protein
LipA	Lipid A
LPS	Lipopolysaccharides
LTA	Lipoteichoic Acid
MALDI -TOF	Matrix-Assisted Laser Desorption/Ionisation Mass Spectrometry
MAMP	Microbe Associated Molecular Pattern
MAPK	Mitogen-Activate Protein Kinase
MD-2	Myeloid Differentiation Factor 2
MS	Mass Spectrometry
MWCO	Molecular Weight Cut Off
$NABD_4$	Sodium borodeuteride
NMR	Nuclear Magnetic Resonance

NOE	Nuclear Overhauser Effect
NOESY	Nuclear Overhauser Spectroscopy
OM	Outer Membrane
OS	Oligosaccharide
PAGE	Polyacrylamide Gel Electrophoresis
PCP	Petroleum/Chloroform/Phenol
PDB	Protein Data Bank
PGN	Peptidoglycan
PMAA	Partially Methylated Acetylated Alditols
PS	Polysaccharides
RNase	Ribonuclease A
ROESY	Rotating Frame Nuclear Overhauser Effect
SDS	Sodium Dodecyl Sulphate
SEC	Size-Exclusion Chromatography
TFA	Trifluoroacetic Acid
TLR	Toll-Like Receptor
TNF-α	Tumour Necrosis Factor α
TOCSY	Total Correlation Spectroscopy
WT	Wild Type
WTA	Wall Teichoic Acid

Sugar abbreviations

Fuc	Fucose
Gal	Galactose
GalA	Galacturonic acid
GalN	Galactosamine
GalNAc	*N*-Acetylgalactosamine
Glc	Glucose
GlcA	Glucuronic acid

GlcN	Glucosamine
GlcNAc	*N*-Acetylglucosamine
Hep	Heptose
Kdo	3-deoxy-D-*manno*-octulosonic acid
Ko	D-glycero-D-talo-oct-2-ulosonic acid
Man	Mannose
MurNAc	*N*-acetylmuramic acid
Rha	Rhamnose

Chapter I

1.1 Introduction

The human digestive system is not only anatomically complex but also hosts one of the most densely populated microbial ecosystems known in biology. The human gut is home to an estimated 150 to 400 different bacterial species species [1], which, together with the intestinal system itself constitute a complex and dynamic structure, now recognized as a true functional organ: **the gut microbiota**. This ecosystem is composed of trillions of microorganisms that coexist in a delicate state of interdependence and competition. Although bacteria are the most studied components, and are the primary focus of my PhD project, the gut microbiota also includes viruses, phages, and fungi. The network of signals present in this system is characterized not only by specific interactions but also by a symbiotic relationship with the host. The balance of this ecosystem is intrinsically fragile and influenced by factors such as diet, lifestyle, and immune response, and is crucial for maintaining homeostasis and overall health [2]. One of the central concepts that emerged from my doctoral project is **that the gut microbiota is a primary source of regulatory signals**, capable of influencing not only the local intestinal environment but also distant physiological systems, including the immune, metabolic, and neuroendocrine systems. Within this complex signalling cascade, particular attention has been paid to Gram-negative bacteria and their outer membrane glycoconjugates, which play a central role in the interaction with the host. **These components are immunologically active and capable of triggering both inflammatory responses and immune tolerance mechanisms.**

1.2 Methodological Approaches in Gut Microbiota Studies

In recent years, advances in microbial isolation techniques and the low-cost sequencing technologies have significantly expanded our understanding of this "microbial organ". These discoveries have paved the way for the development of new diagnostic tools, preventive strategies, and targeted therapies. Among these, 16S ribosomal RNA gene sequencing has become one of the most widely used methods for identifying and classifying bacterial taxa within the gut microbiota [3]. Even more pivotal has been the development of metagenomics, which goes beyond species composition to investigate the genetic and metabolic functions of entire microbial communities [4]. This approach enables the simultaneous analysis of all microorganisms in a complex environment, making it possible to study both microbial diversity and the dynamic interactions among community members and their surroundings. These methodological advancements have laid the groundwork for major international initiatives, such as the **Human Microbiome Project** in the United States and the European consortium MetaHIT (*Metagenomics of the Human Intestinal Tract*), both of which are central to advancing our understanding of the human microbiota [5]. The goal of these projects is the systemic characterization of the human microbiome for diagnostic purposes and to distinguish between healthy and pathological states. In this context, understanding the gut microbiota and its genetic makeup, along with its role in maintaining organismal homeostasis, represents one of the most promising frontiers in biomedicine, opening new avenues in diagnosis, therapy, and prevention.

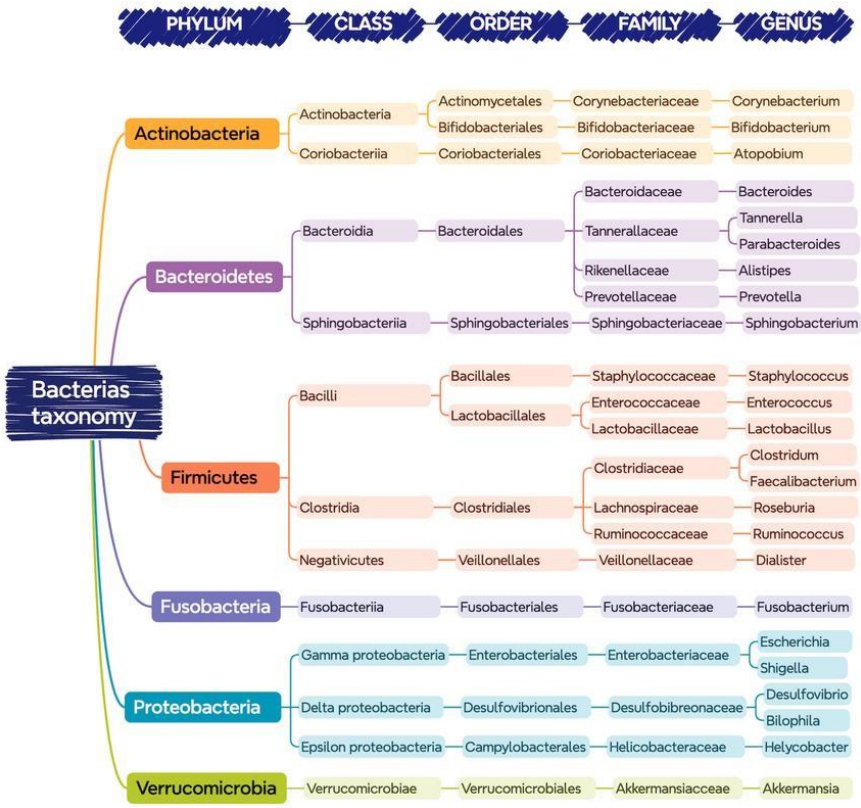

Figure 1.1 Bacteria in the gastrointestinal tract are classified based on their taxonomy, including phylum, class, order, family, and genus. Figure taken from Martínez-Martínez et al. (2024) [6]

1.3 From Eubiosis to Dysbiosis: Microbial Dynamics, Immune Modulation, and Disease Onset

The term *eubiosis*, derived from the Ancient Greek *eu* (good) and *bios* (life), refers to a state of equilibrium and optimal functionality within the gut microbiota. In this

condition, the diverse microbial communities are balanced in a way that supports host homeostasis and contributes positively to physiological processes including immune modulation, metabolic regulation, and gut-brain communication. Conversely, a disruption of this balance, termed *dysbiosis*, may impair the gut environment and trigger inappropriate immune responses, potentially leading to pathological conditions. Dysbiosis encompasses a broad spectrum of alterations in microbial structure and function [7]. In severe cases, dysbiosis is associated with significant changes in the microbial genome, transcriptome, and metabolome, which may provoke chronic inflammatory responses in the host. Numerous diseases have been linked to dysbiosis states, including type 1 diabetes, inflammatory bowel diseases (IBD), asthma, and certain types of cancer [8]. However, studying the gut microbiota is particularly challenging due to its remarkable complexity and adaptability. Not only its composition varies greatly between individuals, but it also changes dynamically within the same person over the course of life. Current research is therefore focused on identifying **robust biomarkers** capable of distinguishing between *eubiotic* and *dysbiotic* states, a crucial step toward advancing personalized medicine. Developing a standardized model that reliably defines a microbial profile as "healthy" or "pathological" would represent a breakthrough in the field, enabling targeted therapeutic interventions aimed at modulating the microbiota to restore or maintain host health. Among the most investigated non-invasive therapeutic approaches are dietary and lifestyle modifications, the use of antibiotics, prebiotics, probiotics, and symbiotic [9] (*Table 1*). In severe cases, more invasive strategies may be required, such as fecal microbiota transplantation (FMT), a medical procedure in which processed stool from a healthy donor is transferred into the recipient's gastrointestinal tract with the aim to restoring the composition and function of the gut microbiota.

Critical steps in the host-microbiota communication involve surface glycans expressed by gut-resident bacterial strains. These include peptidoglycans, exo- and capsular polysaccharides (EPS and CPS), and lipopolysaccharides (LPS) . By modulating immune recognition, influencing epithelial barrier function, and

mediating microbial competition, **these complex glycans act as key molecular interfaces between gut bacteria and the host**, with profound implications for health and disease.

Antibiotic	A pharmacological agent that exerts bactericidal or bacteriostatic effects by targeting essential cellular processes in pathogenic bacteria—such as cell-wall synthesis, protein synthesis, nucleic-acid replication, or metabolic pathways—while exhibiting selective toxicity toward microbial rather than host cells.
Prebiotic	A substrate that is selectively utilized by host microorganisms conferring a health benefit. Prebiotics typically consist of nondigestible carbohydrates (e.g., inulin, fructo-oligosaccharides, galacto-oligosaccharides) that reach the colon intact and promote the proliferation or metabolic activity of specific beneficial microbial taxa.
Probiotic	Live microorganisms which, when administered in adequate amounts, confer a health benefit on the host. These strains—commonly *Lactobacillus*, *Bifidobacterium*, or certain yeasts—must be well-characterized, viable during administration, and capable of exerting functional effects such as modulation of the gut microbiota, immune regulation, or improvement of barrier function.
Postbiotic	Preparations of inanimate microorganisms and/or their components, or metabolites produced by these microorganisms, that confer health benefits on the host. Postbiotics include short-chain fatty acids, microbial cell-wall fragments, peptides, enzymes, and other bioactive molecules capable of influencing host physiology without requiring viable cells.
Synbiotic	A synergistic formulation comprising both probiotics and prebiotics, designed such that the prebiotic substrate is selectively utilized by the included probiotic strain(s). The combination aims to optimize microbial viability, colonization, and functional activity, thereby enhancing host–microbiota interactions and delivering measurable health benefits.

Table 1: Key terms related to gut microbiota modulation

1.4 Microbiota, Immunity, and Life: A Lifelong Interdependence

The gastrointestinal tract hosts a large compartment of immune cells, making it a key site for maintaining host homeostasis. The intestinal epithelium forms the first barrier against pathogens, while underlying immune cells in the *lamina propria* provide rapid innate defences through pattern recognition receptors (PRRs), such as Toll-like receptors (TLRs) [10], [11]. This interaction is **bidirectional**: the immune system must discriminate between harmful and beneficial microbes, while a balanced microbiota is essential for the proper development and function of immune responses. Numerous studies have confirmed the essential role of the gut microbiota in immune

development, particularly those using germ-free (GF) mice, which lack intestinal microbes and exhibit underdeveloped immune systems compared to conventional mice [11]. Similar effects are seen in animals repeatedly treated with antibiotics,which drastically reduce microbial populations and lead to lower lymphocyte counts and impaired inflammatory cytokine production [12]. The influence of the microbiota begins before birth, as maternal microbial composition, shaped by diet and lifestyle, affects the infant microbiota and early immune development. At birth, delivery mode determines initial colonization: vaginally delivered infants acquire *Lactobacillus*, *Bacteroides*, and *Prevotella*, whereas caesarean-born infants are more often colonized by skin-associated species such as *Staphylococcus* and *Streptococcus* [13]. Breastfeeding further supports immune maturation by transferring immunoglobulins and immune cells [14]. By 2-3 years of age, the microbiota generally stabilizes into an adult-like composition, which remains relatively constant unless disrupted by conditions such as chronic inflammation, obesity, inflammatory bowel disease (IBD), or psoriasis. Of note, early-life dysbiosis has been linked to asthma, with low abundance of *Lachnospira*, *Veillonella*, and *Rothia* increasing disease risk [15]. With aging, microbial diversity declines (known as “micro-aging”), characterized by a loss of beneficial commensals (*Clostridiales*, *Bifidobacterium*) and an expansion of opportunistic pathobionts (*Enterobacteriaceae*) [15]. Given these age-associated changes, numerous studies are now exploring strategies to restore microbial balance, with the aim of enhancing immune function and promoting healthy longevity.

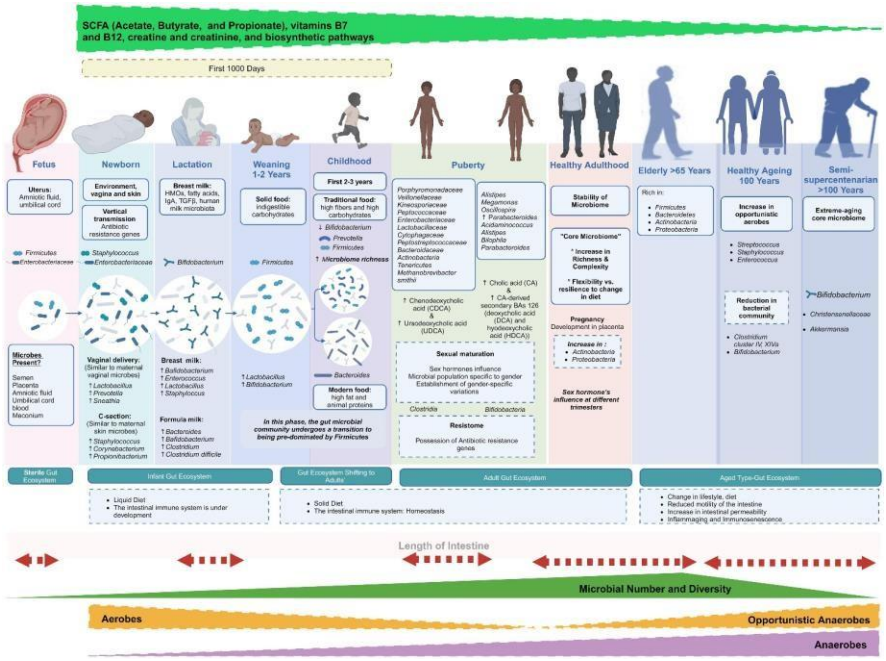

Figure 1.2 Graphic representation of changes in the composition and diversity of the gut microbiota through the different stages of life, from childhood to old age. Figure taken from Ira et al. (2004) [16]

1.5 Microbial Homeostasis in the Gut: Focus on Firmicutes and Bacteroidetes

Within the human gut microbiota, Bacteroidetes and Firmicutes represent the dominant phyla, followed by lower proportions of *Actinobacteria*, *Verrucomicrobia*, and *Proteobacteria* [21]. Alterations in the *Firmicutes*/*Bacteroidetes* (F/B) ratio, normally maintained within defined ranges under healthy, non-pathological conditions, have been frequently associated with gut-related diseases, including diabetes and IBDs [17]. The Firmicutes phylum is predominantly composed of Gram-

positive bacteria, except for two classes, *Negativicutes* and *Halanaerobiales*, that, although classified as Gram-positive, exhibit characteristics typical of Gram-negative bacteria, such as the presence of an **outer membrane (OM).** Within this phylum, the *Lactobacillales* and *Clostridiales* orders are of particular significance and are the most extensively studied in relation to dysbiosis [18]. Certain species within the *Clostridiales* order are known to contribute to important protective mechanisms, including resistance to colonization by enteric pathogens and prevention of allergic sensitization [19]. Conversely, members of the *Lactobacillales* order play a crucial role in modulating the host's immune system, enhancing mucus production in the gastrointestinal epithelium, and inhibiting the growth of pathogenic bacteria through lactic acid production.[20] In contrast, the phylum *Bacteroidetes* (now often referred to as *Bacteroidota*) consists entirely of Gram-negative bacteria. Within the human gut, this phylum is mainly represented by four families, Bacteroidaceae, Prevotellaceae, Rikenellaceae, and Porphyromonadaceae, which include prominent genera such as *Bacteroides*, *Prevotella*, *Rikenella*, and *Porphyromonas*. [21]. Scientific literature on this phylum presents a complex and sometimes contradictory picture. On one hand, several studies have shown that certain *Bacteroides* species are positively associated with disease development, for example, *Bacteroides fragilis* has been implicated in the pathogenesis of colorectal cancer, especially for ETBF (Enterotoxigenic *Bacteroides fragilis*) strains, secreting the BFT (Bacteroides fragilis toxin) metalloprotease, directly implicated in the alteration of the integrity of the intestinal epithelium. [22]. On the other hand, other species, such as *Bacteroides thetaiotaomicron*, have demonstrated beneficial properties; this species, as example, has been used in FMT protocols to alleviate colitis, suggesting a potential therapeutic role for specific *Bacteroides* species in the treatment of IBDs.

References:

[1] W.-L. Hao and Y.-K. Lee, “Microflora of the Gastrointestinal Tract: A Review,” in *Public Health Microbiology*, New Jersey: Humana Press, pp. 491–502. doi: 10.1385/1-59259-766-1:491.

[2] V. B. Young and T. M. Schmidt, “Overview of the Gastrointestinal Microbiota,” in *GI Microbiota and Regulation of the Immune System*, New York, NY: Springer New York, pp. 29–40. doi: 10.1007/978-0-387-09550-9_3.

[3] M.-A. Osman, H. Neoh, N.-S. Ab Mutalib, S.-F. Chin, and R. Jamal, “16S rRNA Gene Sequencing for Deciphering the Colorectal Cancer Gut Microbiome: Current Protocols and Workflows,” *Front Microbiol*, vol. 9, Apr. 2018, doi: 10.3389/fmicb.2018.00767.

[4] D. Peterson, K. S. Bonham, S. Rowland, C. W. Pattanayak, and V. Klepac-Ceraj, “Comparative Analysis of 16S rRNA Gene and Metagenome Sequencing in Pediatric Gut Microbiomes,” *Front Microbiol*, vol. 12, Jul. 2021, doi: 10.3389/fmicb.2021.670336.

[5] K. Aagaard *et al.*, “The Human Microbiome Project strategy for comprehensive sampling of the human microbiome and why it matters,” *The FASEB Journal*, vol. 27, no. 3, pp. 1012–1022, Mar. 2013, doi: 10.1096/fj.12-220806.

[6] A. Martínez-Martínez, B. Lamban-Per, M. Lezaun, A. Rezusta, and J. Arbones-Mainar, “Exploring Functional Products and Early-Life Dynamics of Gut Microbiota,” *Nutrients*, vol. 16, no. 12, p. 1823, Jun. 2024, doi: 10.3390/nu16121823.

[7] V. Iebba *et al.*, “Eubiosis and dysbiosis: the two sides of the microbiota.,” *New Microbiol*, vol. 39, no. 1, pp. 1–12, Jan. 2016.

[8] A. B. Shreiner, J. Y. Kao, and V. B. Young, “The gut microbiome in health and in disease,” *Curr Opin Gastroenterol*, vol. 31, no. 1, pp. 69–75, Jan. 2015, doi: 10.1097/MOG.0000000000000139.

[9] P. Y. Wong, C. Yip, D. A. Lemberg, A. S. Day, and S. T. Leach, “Evolution of a Pathogenic Microbiome,” *J Clin Med*, vol. 12, no. 22, p. 7184, Nov. 2023, doi: 10.3390/jcm12227184.

[10] N. Dera *et al.*, “Impact of Early-Life Microbiota on Immune System Development and Allergic Disorders,” *Biomedicines*, vol. 13, no. 1, p. 121, Jan. 2025, doi: 10.3390/biomedicines13010121.

[11] M.-C. Arrieta and B. B. Finlay, “The commensal microbiota drives immune homeostasis.,” *Front Immunol*, vol. 3, p. 33, 2012, doi: 10.3389/fimmu.2012.00033.

[12] G. Bamias *et al.*, “Down-Regulation of Intestinal Lymphocyte Activation and Th1 Cytokine Production by Antibiotic Therapy in a Murine Model of Crohn’s Disease,” *The Journal of Immunology*, vol. 169, no. 9, pp. 5308–5314, Nov. 2002, doi: 10.4049/jimmunol.169.9.5308.

[13] J. Molès *et al.*, “Breastmilk cell trafficking induces microchimerism-mediated immune system maturation in the infant,” *Pediatric Allergy and Immunology*, vol. 29, no. 2, pp. 133–143, Mar. 2018, doi: 10.1111/pai.12841.

[14] A. Ver Heul, J. Planer, and A. L. Kau, “The Human Microbiota and Asthma.,” *Clin Rev Allergy Immunol*, vol. 57, no. 3, pp. 350–363, Dec. 2019, doi: 10.1007/s12016-018-8719-7.

[15] E. Biagi, M. Candela, S. Fairweather-Tait, C. Franceschi, and P. Brigidi, “Aging of the human metaorganism: the microbial counterpart.,” *Age (Dordr)*, vol. 34, no. 1, pp. 247–67, Feb. 2012, doi: 10.1007/s11357-011-9217-5.

[16] R. Ira *et al.*, “Understanding Aging through the Lense of Gut Microbiome,” *Explor Res Hypothesis Med*, vol. 000, no. 000, pp. 000–000, Aug. 2024, doi: 10.14218/ERHM.2024.00008.

[17] Y.-C. Tsai *et al.*, “Alternations of the gut microbiota and the Firmicutes/Bacteroidetes ratio after biologic treatment in inflammatory bowel disease,” *Journal of*

Microbiology, Immunology and Infection, vol. 58, no. 1, pp. 62–69, Feb. 2025, doi: 10.1016/j.jmii.2024.09.006.

[18] C. Zhu *et al.*, "Determine independent gut microbiota-diseases association by eliminating the effects of human lifestyle factors," *BMC Microbiol*, vol. 22, no. 1, p. 4, Jan. 2022, doi: 10.1186/s12866-021-02414-9.

[19] A. M. Seekatz, N. Safdar, and S. Khanna, "The role of the gut microbiome in colonization resistance and recurrent Clostridioides difficile infection.," *Therap Adv Gastroenterol*, vol. 15, p. 17562848221134396, 2022, doi: 10.1177/17562848221134396.

[20] Y.-T. Tsai, P.-C. Cheng, and T.-M. Pan, "The immunomodulatory effects of lactic acid bacteria for improving immune functions and benefits," *Appl Microbiol Biotechnol*, vol. 96, no. 4, pp. 853–862, Nov. 2012, doi: 10.1007/s00253-012-4407-3.

[21] Z. J. Zhang *et al.*, "Comprehensive analyses of a large human gut Bacteroidales culture collection reveal species and strain level diversity and evolution.," *bioRxiv*, Mar. 2024, doi: 10.1101/2024.03.08.584156.

[22] C. Lucas, N. Barnich, and H. T. T. Nguyen, "Microbiota, Inflammation and Colorectal Cancer.," *Int J Mol Sci*, vol. 18, no. 6, Jun. 2017, doi: 10.3390/ijms18061310.

Chapter II

2.1 Introduction to Gram-Negative Bacteria

One of the most widely used classifications of bacteria divides them into Gram-positive and Gram-negative groups. This classification originates from an experiment conducted by Hans Christian Gram in 1884. In this staining procedure, bacterial cells are first treated with a crystal violet-iodine complex, which stains all bacteria purple, regardless of their structural composition. However, during the subsequent decolorization step using safranin, only Gram-positive bacteria retain the violet stain, while Gram-negative bacteria do not, while taking on the pink colour of the safranin. This differential staining behaviour is due to the inability of safranin to penetrate the thick cell wall of Gram-positive bacteria, which prevents the decolorization of the crystal violet-iodine complex [23]. Therefore, this behaviour originates from the fundamental **structural differences between Gram-positive and Gram-negative bacterial cell envelopes**. Both groups possess an inner membrane (IM), composed of a phospholipid bilayer enclosing the cytoplasm, and a periplasmic space containing a peptidoglycan layer, a rigid macromolecular network providing mechanical strength and osmotic protection. Peptidoglycan is made of alternating *N*-acetylglucosamine (GlcNAc) and *N*-acetylmuramic acid (MurNAc) residues, cross-linked by short peptides containing both L- and D-amino acids. Notably, the peptide cross-links differ between the two groups: lysine is common in Gram-positive bacteria, while *meso*-diaminopimelic acid (m-DAP) is typical of Gram-negative bacteria. In Gram-positive bacteria, the peptidoglycan layer is much thicker and lies directly outside the inner membrane. It contains teichoic acids and other anionic polymers that contribute to cell wall stability [24]. By contrast, in **Gram-negative bacteria**, the peptidoglycan layer is much thinner and located between the inner and an additional **OM.** The OM is an asymmetric bilayer: its inner leaflet is composed of phospholipids, while its outer

leaflet contains membrane proteins and **lipopolisaccarides (LPS).** As stated above, both Gram-positive and Gram-negative bacteria may also possess extracellular structures, such as capsular polysaccharide (CPS) and exopolysaccharide (EPS), which play roles in interactions with host organisms, communication with other bacteria, and provide protection against environmental stress. [25]

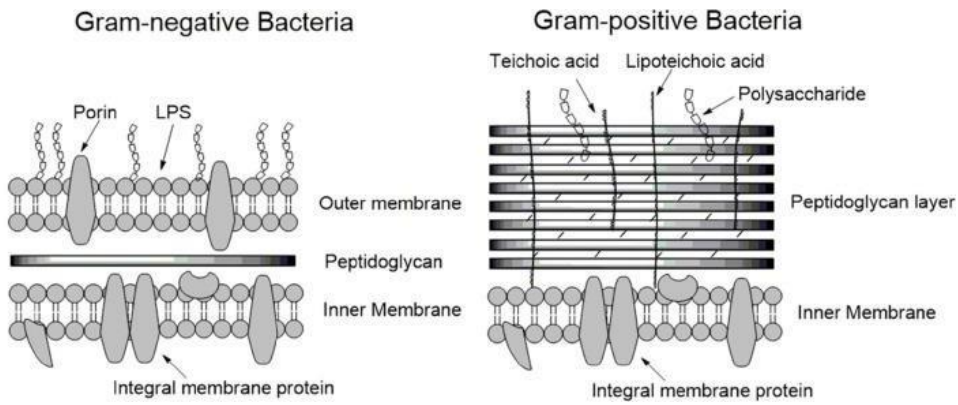

Figure 1.3 Simplified graphic representation of the membrane in Gram-positive and Gram-negative bacteria. The image compares the main structural differences between the two types of bacteria: Gram-positives have a thick cell wall composed of several layers of peptidoglycan and no outer membrane, while Gram-negatives have a thinner wall but enclosed between two membranes, with an outer membrane rich in LPSs. Figure taken from Li et al. (2017) [26]

2.2 LPS: Key Molecules in Membrane Integrity and Environmental Interaction

LPS are the predominant components of the OM of Gram-negative bacteria and are essential amphipathic molecules necessary for the survival and growth of these microorganisms [27]. They play a crucial role in organizing and stabilizing the OM, providing structural protection against potentially harmful environmental factors. Their chemical composition, usually characterized by negative charges, enables

interactions with environmental divalent cations such as calcium (Ca^{2+}) and magnesium (Mg^{2+}), generating electrostatic forces that strengthen the cohesion of the OM. These interactions grant bacteria significant resistance to external substances, including various antibiotics. Moreover, due to their peripheral location on the bacterial surface, LPSs participate in complex biological processes such as immune response activation and modulation, virulence, surface adhesion, and colonization. Structurally, each LPS molecule is composed of three distinct regions: the **lipid A**, the hydrophobic anchor embedded in the OM; the **core oligosaccharide** (core OS), a variable-length sugar chain that connects lipid A to the outermost and third component of an LPS that is the **O-antigen**, a polysaccharide chain made up of repetitive carbohydrate units, highly variable across strains and species [27]. However, not all LPS possess the O-antigen: when present, they are referred to as smooth LPS (S-LPS), whereas its absence defines rough LPS (R-LPS) or lipooligosaccharides (LOS). This structural variation is often reflected in colony morphology: bacteria producing S-LPS typically form smooth-appearing colonies, while those lacking the O-antigen display a rough phenotype [28]. Beyond this distinction, it is important to highlight the **remarkable structural heterogeneity of LPS molecules**. Such variability occurs not only between different species, but also among strains of the same species, and can involve any region of the molecule, both saccharide and lipid domains, varying in composition, number of constituents, and specific structural arrangements. Importantly, LPS is widely recognized for its ability to trigger a potent immune inflammatory response; however, due to its extreme structural complexity and variability, this long-standing notion warrants reconsideration. As example, **certain LPS molecules from pathogenic bacteria possess distinct structural features that render them more immunostimulatory than others, enabling their specific recognition by immune system receptors. It has been observed that pro-inflammatory LPS share common structural motifs that are absent in LPS produced by commensal bacteria**. Therefore, it is essential to precisely characterize the fine structure of these complex and heterogeneous glycoconjugates to gain a clear

understanding of their impact on the human immune system and overall health and well-being.

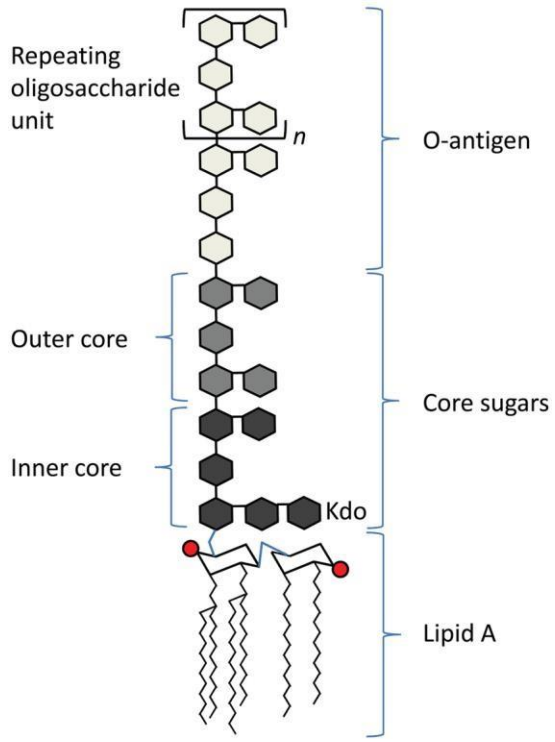

Figure 1.4 Structural representation of a generic bacterial LPS. The picture shows the typical composition of an LPS. It is divided into three regions: the membrane-anchored lipid A; the core OS; and the O-specific chain (or O-antigen). Figure taken from Maeshima, N., & Fernandez, R. C. (2013). [29]

2.3 Lipid A: The Glycolipid Anchor that activates the TLR4-mediated signalling

The component that anchors the entire LPS to the OM is the **Lipid A**. Historically, Lipid A has been recognized as the structural portion of LPS primarily responsible for triggering the innate immune response against pathogenic Gram-negative bacteria. The receptors that detect this domain belong mainly to the innate immune system, particularly Toll-like Receptor 4 (TLR4) in complex with the co-receptor myeloid differentiation protein-2 (MD2) [30] (see chapter III, paragraph 3.3 more details). Lipid A was first described by Westphal and Lüderitz in 1954. Structurally, it (typically) consists of a disaccharide of glucosamines (GlcN) linked via a β (1→6) bond. This disaccharide is typically phosphorylated, usually at position 1 of the α-glucosamine and position 4' of the β-GlcN. Each GlcN unit can be acylated at positions 2, 2', 3, and 3' by hydroxylated fatty acids, linked through amide and ester bonds [27]. Secondary (typically not-hydroxylated) acyl chains are then found linked at these primary fatty acids. To explain the mechanism of TLR4-mediated immune activation, the structure of *E. coli* lipid A is often used as a reference, as it represents one of the best characterized forms. *E. coli* lipid A is hexa-acylated and *bis*-phosphorylated, containing four primary fatty acid chains 14:0 (3-OH) and two secondary acyl chains (C12:0 and C14:0), linked to the primary ones decorating the non-reducing GlcN. This asymmetric distribution of fatty acids, commonly known as the "4+2" arrangement, **allows optimal interaction with the hydrophobic pocket of the MD2 receptor**, the key co-receptor of TLR4 activation (see chapter III, paragraph 3.3 more details). Specifically, five of the six acyl chains of lipid A fit into the MD2 cavity, while the sixth remains exposed, allowing direct interaction with TLR4. This promotes dimerization with a second TLR4/MD2 complex, which in turn activates downstream intracellular immune signalling. **Both the number and length of acyl chains are critical for receptor activation**: chains slightly shorter or longer than those of *E. coli* lipid A significantly reduce TLR4 activation [31]. Similarly, hypo-acylated variants or Lipid A structures with a symmetrical acyl chain distribution display weak immunostimulatory activity [32]. Phosphorylation is also essential: both hypo- and hyper-phosphorylated species are associated with decreased immune-

stimulating potential [29]. Moreover, chemical modifications of the phosphate groups, such as the addition of glucuronic acid (GlcA) or 2-aminoethyl groups (PEtN), negatively impact the immunostimulatory properties of Lipid A [29]. Interestingly, certain Lipid A molecules can act as antagonists of TLR4 activation. These antagonists have specific chemical features that allow them to bind the TLR4/MD2 complex without initiating downstream signaling, thereby blocking the binding of proinflammatory molecules and suppressing the immune response [33], [34]. A well-known example is Lipid IVA, a biosynthetic precursor of *E. coli* Lipid A, which functions as a potent antagonist in human cells [35]. Additionally, several Lipid A molecules isolated from environmental bacteria also exhibit antagonistic properties [36].

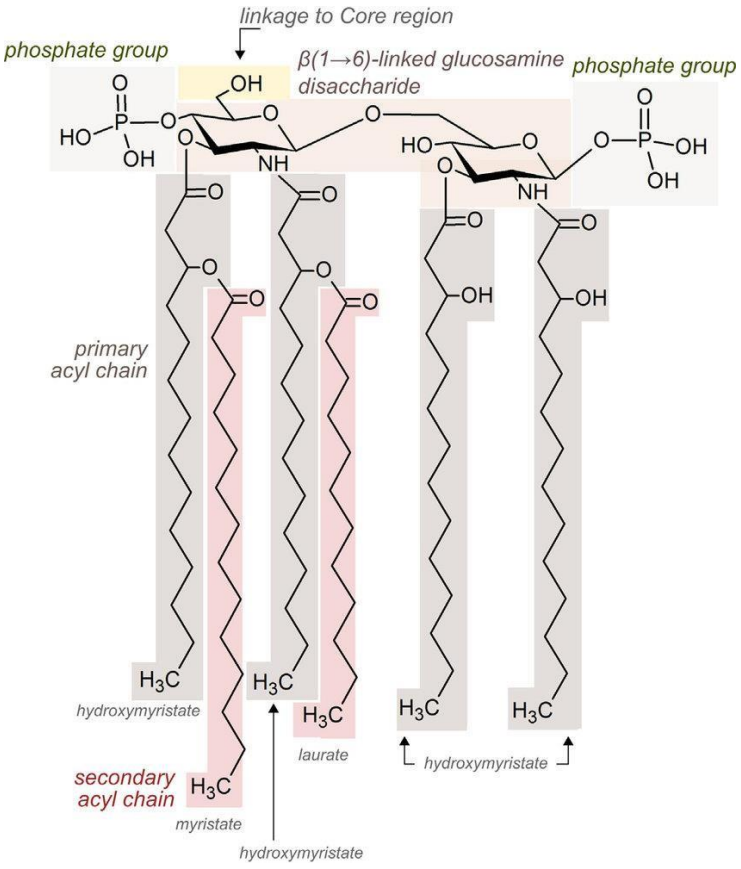

Figure 1.5: Detailed structure of Lipid A from *E. coli*. It consists of a glucosamine disaccharide backbone linked through a β (1→6) bond, typically carrying two phosphate groups. The hydroxyl group of the non-reducing glucosamine residue provides the attachment site for the core OS region of the LPS. The primary acyl chains (in light grey) are directly bound to the sugar residues, while the secondary acyl chains (in light red) are esterified on the hydroxyl groups of the primary chains. Figure taken from Steimle et al. (2016) [37]

2.4 Inner and Outer Core Oligosaccharide: Their Role in Membrane Integrity and Host Immune Response

The core OS is the region of the LPS molecule directly connected to the lipid A. It consists of a variable number of monosaccharides, typically up to fifteen units, arranged in either linear or branched structures [27]. Together with Lipid A, the core OS plays a critical role in maintaining the structural integrity and stability of the OM. Structurally, the core OS is divided into two distinct portions: the inner core and the outer core. The inner core is highly conserved and begins with one or more residues of 3-deoxy-D-*manno*-oct-2-ulosonic acid (Kdo), which are linked to the glucosamine backbone of Lipid A via an α (2→6) bond. Kdo is the most conserved sugar within the entire LPS molecule and is often used as a diagnostic marker for its presence. Despite this high degree of conservation, exceptions do exist. For example, in certain strains of *Acinetobacter*, Kdo may be replaced by D-*glycero*-D-*talo*-oct-2-ulosonic acid (Ko) [38], while in *Shewanella* species, Kdo8N, a modified form of Kdo, may be found instead [39]. Surrounding the Kdo residues are typically negatively charged groups such as phosphates and uronic acids, which contribute to the overall negative charge of an LPS. These groups are essential for stabilizing the OM and facilitating interactions with host immune defences. In many bacterial species, the Kdo residues

are followed by heptoses, usually L,D-heptose or D,D-heptose, which also belong to the conserved architecture of the inner core [40]. In contrast, the outer core is more variable, and its composition depends largely on the bacterial species or strain. It is generally composed of hexoses such as glucose, mannose, and galactosamine. In S-LPS, the outer core functions as a linker between the inner core and the O-antigen, while in R- LPS, which lack the O-antigen, it represents the terminal portion of the molecule. Although Lipid A is widely recognized as the principal trigger of the immune response through activation of TLR4, the structure of the inner core significantly influences this interaction [41]. Changes in the inner core whether through alterations in charge distribution, conformational flexibility, or the addition of functional groups, such as phosphates or amino sugars, **can profoundly impact receptor binding and subsequent immune signalling**. Moreover, experimental studies, including those on mutant strains of *E. coli*, have highlighted the importance of inner core phosphorylation in maintaining the permeability barrier and stability of the OM [42].

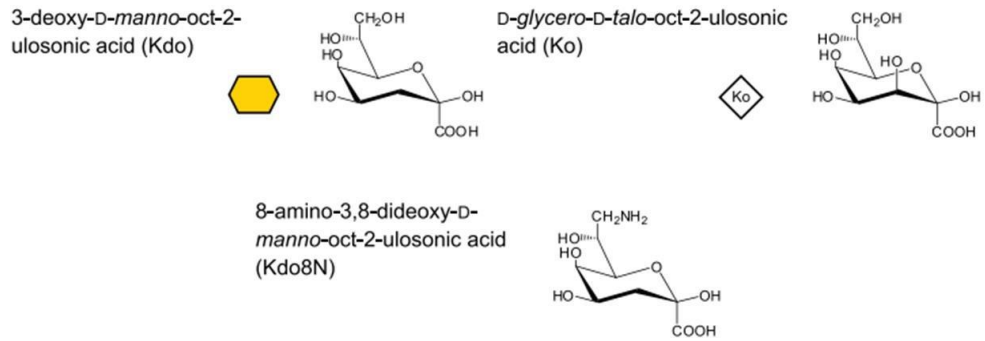

Figure 1.6 Comparative chemical representation of three keto-deoxy acids belonging to the ulosonic acid family: Kdo (3-deoxy-D-*manno*-oct-2-ulosonic acid), Ko (D-*glycero*-D-*talo*-oct-2-ulosonic acid) and Kdo8N (an aminated variant of Kdo). Figure taken from Di Lorenzo et al. (2022) [27]

2.5 Structural variability and Immunological Role of the O-antigen

The O-antigen is described as a repetitive polysaccharide chain located in the outermost portion of the LPS . It is highly variable and plays a key role in immune recognition and serotype determination [46]. Its structural diversity arises from differences in the number and composition of constituent monosaccharides, the presence of branching motifs, and the occasional addition of non-carbohydrate substituents covalently, but not stoichiometrically, attached to the backbone [45]. This high degree of variability has made the O-antigen an ideal target for bacterial serotyping. *E. coli*, for example, has over 170 distinct types [43], while *Salmonella* presents 46 [44]. Immunologically, as the outermost component of LPS, it plays a central role in modulating the adaptive immune response. Moreover, in many pathogenic bacteria, the O-antigen has evolved the ability to mimic human-like glycoconjugates, thereby evading host immune surveillance. Such mimicry mechanisms are observed in *Helicobacter pylori* [45], *Neisseria gonorrhoeae*, and *Neisseria meningitidis* [46]. The structure and length of the polysaccharide directly influence bacterial survival. In *Salmonella enteritidis*, for instance, a very long O-antigen chain enhances resistance to complement-mediated cytolysis compared to strains expressing shorter chains [47]. Similarly, in *Salmonella typhimurium*, mutations in length regulators, such as the *wzz* locus, affect membrane permeability, sensitivity to polymyxin B and sodium deoxycholate, as well as colonization ability and complement resistance [48]. Moreover, the protective role of the O-antigen extends beyond immune evasion to include resistance to environmental stressors, such as oxidative agents, bile salts, and cationic antimicrobial peptides (CAMPs), thereby granting bacteria a survival advantage in the intestinal niche [49].

References:

[23] E. J. Chung *et al.*, "MEK1/2 inhibition enhances the radiosensitivity of cancer cells by downregulating survival and growth signals mediated by EGFR ligands.," *Int J Oncol*, vol. 42, no. 6, pp. 2028–36, Jun. 2013, doi: 10.3892/ijo.2013.1890.

[24] M. Rajagopal and S. Walker, "Envelope Structures of Gram-Positive Bacteria.," *Curr Top Microbiol Immunol*, vol. 404, pp. 1–44, 2017, doi: 10.1007/82_2015_5021.

[25] T. Pang, "Germs, genomics and global public health: How can advances in genomic sciences be integrated into public health in the developing world to deal with infectious diseases?," *Hugo J*, vol. 3, no. 1–4, pp. 5–9, Dec. 2009, doi: 10.1007/s11568-009-9131-4.

[26] J. Li, J.-J. Koh, S. Liu, R. Lakshminarayanan, C. S. Verma, and R. W. Beuerman, "Membrane Active Antimicrobial Peptides: Translating Mechanistic Insights to Design," *Front Neurosci*, vol. 11, Feb. 2017, doi: 10.3389/fnins.2017.00073.

[27] F. Di Lorenzo, K. A. Duda, R. Lanzetta, A. Silipo, C. De Castro, and A. Molinaro, "A Journey from Structure to Function of Bacterial Lipopolysaccharides," *Chem Rev*, vol. 122, no. 20, pp. 15767–15821, Oct. 2022, doi: 10.1021/acs.chemrev.0c01321.

[28] I. Zanoni *et al.*, "Similarities and differences of innate immune responses elicited by smooth and rough LPS," *Immunol Lett*, vol. 142, no. 1–2, pp. 41–47, Feb. 2012, doi: 10.1016/j.imlet.2011.12.002.

[29] N. Maeshima and R. C. Fernandez, "Recognition of lipid A variants by the TLR4-MD-2 receptor complex," *Front Cell Infect Microbiol*, vol. 3, 2013, doi: 10.3389/fcimb.2013.00003.

[30] A. Molinaro *et al.*, "Chemistry of Lipid A: At the Heart of Innate Immunity," *Chemistry – A European Journal*, vol. 21, no. 2, pp. 500–519, Jan. 2015, doi: 10.1002/chem.201403923.

[31] N. Maeshima and R. C. Fernandez, “Recognition of lipid A variants by the TLR4-MD-2 receptor complex,” *Front Cell Infect Microbiol*, vol. 3, 2013, doi: 10.3389/fcimb.2013.00003.

[32] A. Zamyatina and H. Heine, “Lipopolysaccharide Recognition in the Crossroads of TLR4 and Caspase-4/11 Mediated Inflammatory Pathways.,” *Front Immunol*, vol. 11, p. 585146, 2020, doi: 10.3389/fimmu.2020.585146.

[33] C. Cravotto, O. Claux, M. Bartier, A.-S. Fabiano-Tixier, and S. Tabasso, “Leading Edge Technologies and Perspectives in Industrial Oilseed Extraction,” *Molecules*, vol. 28, no. 16, p. 5973, Aug. 2023, doi: 10.3390/molecules28165973.

[34] Q. ul Ain, M. Batool, and S. Choi, “TLR4-Targeting Therapeutics: Structural Basis and Computer-Aided Drug Discovery Approaches,” *Molecules*, vol. 25, no. 3, p. 627, Jan. 2020, doi: 10.3390/molecules25030627.

[35] S. -i. Saitoh, “Lipid A antagonist, lipid IVa, is distinct from lipid A in interaction with Toll-like receptor 4 (TLR4)-MD-2 and ligand-induced TLR4 oligomerization,” *Int Immunol*, vol. 16, no. 7, pp. 961–969, May 2004, doi: 10.1093/intimm/dxh097.

[36] S. H. Joo, “Lipid A as a Drug Target and Therapeutic Molecule,” *Biomol Ther (Seoul)*, vol. 23, no. 6, pp. 510–516, Nov. 2015, doi: 10.4062/biomolther.2015.117.

[37] A. Steimle, I. B. Autenrieth, and J.-S. Frick, “Structure and function: Lipid A modifications in commensals and pathogens,” *International Journal of Medical Microbiology*, vol. 306, no. 5, pp. 290–301, Aug. 2016, doi: 10.1016/j.ijmm.2016.03.001.

[38] H. S. Chung and C. R. H. Raetz, “Dioxygenases in *Burkholderia ambifaria* and *Yersinia pestis* that hydroxylate the outer Kdo unit of lipopolysaccharide,” *Proceedings of the National Academy of Sciences*, vol. 108, no. 2, pp. 510–515, Jan. 2011, doi: 10.1073/pnas.1016462108.

[39] A. Casillo *et al.*, “Structural Elucidation of a Novel Lipooligosaccharide from the Cold-Adapted Bacterium OMVs Producer Shewanella sp. HM13,” *Mar Drugs*, vol. 17, no. 1, p. 34, Jan. 2019, doi: 10.3390/md17010034.

[40] S. Gronow, G. Xia, and H. Brade, “Glycosyltransferases involved in the biosynthesis of the inner core region of different lipopolysaccharides,” *Eur J Cell Biol*, vol. 89, no. 1, pp. 3–10, Jan. 2010, doi: 10.1016/j.ejcb.2009.10.002.

[41] J. Meng, E. Lien, and D. T. Golenbock, “MD-2-mediated Ionic Interactions between Lipid A and TLR4 Are Essential for Receptor Activation,” *Journal of Biological Chemistry*, vol. 285, no. 12, pp. 8695–8702, Mar. 2010, doi: 10.1074/jbc.M109.075127.

[42] J. A. Yethon, D. E. Heinrichs, M. A. Monteiro, M. B. Perry, and C. Whitfield, “Involvement of waaY, waaQ, and waaP in the Modification of Escherichia coliLipopolysaccharide and Their Role in the Formation of a Stable Outer Membrane,” *Journal of Biological Chemistry*, vol. 273, no. 41, pp. 26310–26316, Oct. 1998, doi: 10.1074/jbc.273.41.26310.

[43] A. Iguchi *et al.*, “A complete view of the genetic diversity of the Escherichia coli O-antigen biosynthesis gene cluster,” *DNA Research*, vol. 22, no. 1, pp. 101–107, Feb. 2015, doi: 10.1093/dnares/dsu043.

[44] B. Liu *et al.*, “Structural diversity in *Salmonella* O antigens and its genetic basis,” *FEMS Microbiol Rev*, vol. 38, no. 1, pp. 56–89, Jan. 2014, doi: 10.1111/1574-6976.12034.

[45] A. P. Moran and M. M. Prendergast, “Molecular Mimicry in Campylobacter jejuni and Helicobacter pylori Lipopolysaccharides: Contribution of Gastrointestinal Infections to Autoimmunity,” *J Autoimmun*, vol. 16, no. 3, pp. 241–256, May 2001, doi: 10.1006/jaut.2000.0490.

[46] S. Ram, J. Shaughnessy, R. B. DeOliveira, L. A. Lewis, S. Gulati, and P. A. Rice, “Utilizing complement evasion strategies to design complement-based antibacterial immunotherapeutics: Lessons from the pathogenic Neisseriae,” *Immunobiology*, vol. 221, no. 10, pp. 1110–1123, Oct. 2016, doi: 10.1016/j.imbio.2016.05.016.

[47] E. Krzyżewska-Dudek *et al.*, “Lipopolysaccharide with long O-antigen is crucial for Salmonella Enteritidis to evade complement activity and to facilitate bacterial survival in vivo in the Galleria mellonella infection model,” *Med Microbiol Immunol*, vol. 213, no. 1, p. 8, Dec. 2024, doi: 10.1007/s00430-024-00790-3.

[48] R. Tamayo, S. S. Ryan, A. J. McCoy, and J. S. Gunn, “Identification and Genetic Characterization of PmrA-Regulated Genes and Genes Involved in Polymyxin B Resistance in *Salmonella enterica* Serovar Typhimurium,” *Infect Immun*, vol. 70, no. 12, pp. 6770–6778, Dec. 2002, doi: 10.1128/IAI.70.12.6770-6778.2002.

[49] R. W. Crawford *et al.*, “Very Long O-antigen Chains Enhance Fitness during Salmonella-induced Colitis by Increasing Bile Resistance,” *PLoS Pathog*, vol. 8, no. 9, p. e1002918, Sep. 2012, doi: 10.1371/journal.ppat.1002918.

Chapter III

LPS in immune mechanisms

3.1 Fundamentals of Innate and Adaptive Immunity

The immune system is a complex network of organs, tissues, cells, and molecules that work together to protect the body from potentially harmful external agents. It is commonly divided into two branches: innate immunity and adaptive immunity. Innate immunity represents the body's first line of defence. It is present from birth, responds rapidly but non-specifically, and does not require prior exposure to a pathogen to be activated. This type of immunity includes physical barriers (such as the skin and mucous membranes) and chemical barriers (such as gastric acidity and enzymes), as well as specific cells such as macrophages, neutrophils, natural killer cells, and various proteins, including those of the complement system, defensins, ficolins, cytokines, and chemokines. Many innate immune responses are activated through the recognition by **pattern recognition receptors** (**PRRs**) of molecular structures commonly found in microorganisms. These structures, known as MAMPs (**Microbe-Associated Molecular Patterns**) trigger a signalling cascade upon recognition. This process leads to the activation of transcription factors, which promote the transcription of genes involved in the innate immune response. The innate response is essential for the subsequent activation of adaptive immunity, which by constrast takes longer to develop but is highly specific [50]. It requires a first encounter with the pathogen to generate what is known as **immunological memory**, which allows a more rapid and effective response to subsequent exposures to the same antigen. It involves mature lymphocytes, namely B cells, T cells, NK cells and NK-T cells, in addition to immunoglobulins.

3.2 Immunomodulatory Mechanisms of LPS in the Innate Immunity

The recognition of microorganisms by the innate immune system, as previously mentioned, is primarily mediated by the detection of MAMPs. Among these, **LPS represent the most potent and best-characterized MAMPs**. However, **not all LPS are immunologically identical**: there is considerable structural variability, which is reflected in their varying ability to activate or modulate the immune response. It is important to clarify a substantial difference between LPS from defined pathogenic bacteria and those from commensals. A properly functioning immune system must be able to discriminate between these two categories of microorganisms. It is now known that immune balance is based on a sophisticated signalling system, in which bacterial glycoconjugates play a fundamental role, acting in some cases as activators of the inflammatory response and in others as modulators of immune tolerance. Understanding how immune receptors recognize LPS and distinguish molecules that induce an inflammatory response from those that do not is crucial to elucidating the mechanisms of the immune response.

3.3 Mechanism of TLR4 Activation

TLRs are transmembrane proteins characterized by a bipartite structure: an extracellular domain composed of leucine-rich repeats (LRR), responsible for ligand recognition, and a conserved intracellular signalling domain known as the TIR (Toll/IL-1 receptor) domain. These receptors are widely expressed in various tissues and organs, where they play essential roles in modulating immune responses [51]. Among the members of the TLR family, **TLR4 is the one most associated with LPS recognition**, it requires an accessory protein, MD-2, for ligand binding and signal transduction. The functional receptor is composed of a heterotetramer composed of

two TLR4 molecules and two MD-2 molecules, forming the active TLR4/MD-2 dimer [52]. LPS recognition occurs almost exclusively through the Lipid A domain. For this reason, the MD-2 molecule plays a crucial role by presenting a hydrophobic pocket, formed by antiparallel β-sheets, which accommodates the acyl chains of Lipid A. This structural feature is essential to stabilize the interaction between LPS and the receptor complex, thus modulating the intensity and nature of the immune response [53]. For the immune system to detect LPS, Lipid A must be released and presented to the TLR4 complex, a process that generally occurs following bacterial lysis or through the action of the host-derived LPS-binding protein (LBP). LBP binds to LPS through its N-terminal domain and transfers it to CD14, a glycoprotein present in both soluble and membrane-anchored forms. Acting as a molecular chaperone, CD14 subsequently delivers LPS to MD-2, allowing the assembly of the active TLR4/MD-2 complex. The efficiency of this process strongly depends on the structural characteristics of the lipid ligand. Dimerization of TLR4 complexes brings the intracellular TIR domains closer together, initiating two distinct downstream signalling pathways (*Figure 1.7*): the rapid, pro-inflammatory MyD88-dependent pathway and the TRIF-dependent pathway, mediated via the adaptors TRAM (TRIF-related adaptor molecule) and TRIF (TIR-domain-containing adapter-inducing interferon-β) [54]. These pathways converge on the activation of MAP kinases (MAPKs) and transcription factors such as NF-κB and IRF (Interferon Regulatory Factors), which promote the transcription of pro-inflammatory cytokines and chemokines, including TNF-α, IL-1β, IL-6, IL-8, and IL-12. (*Figure 1.7*).

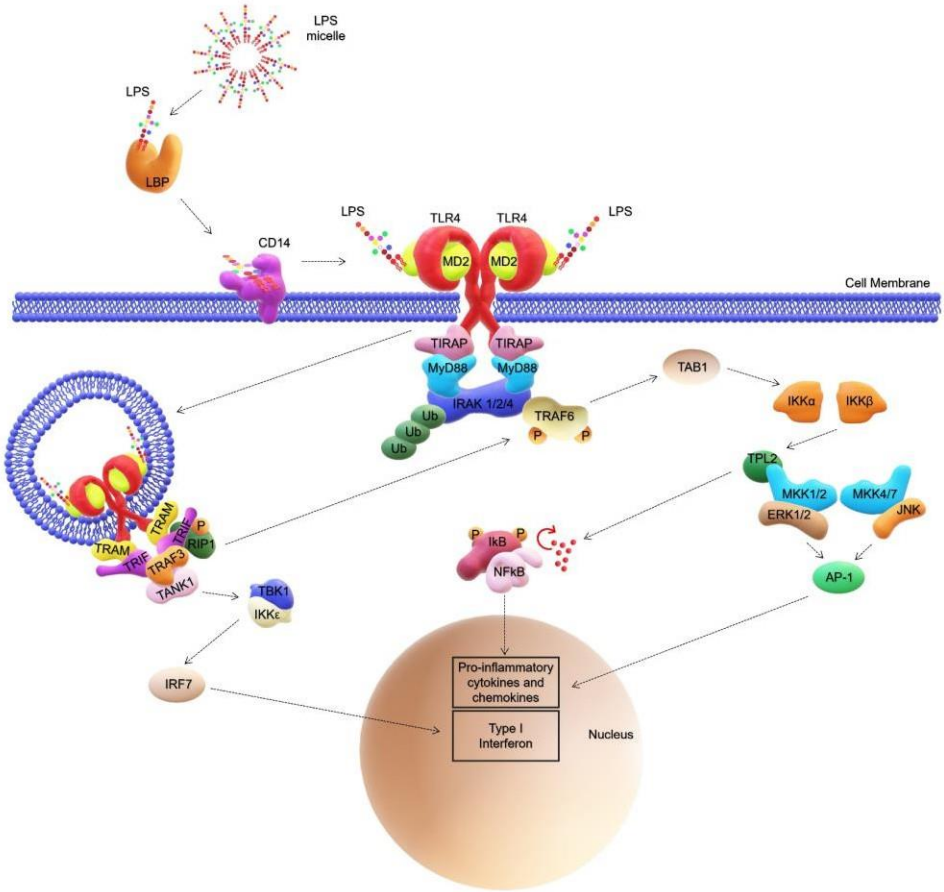

Figure 1.7: Simplified unscaled representation of MD-2/TLR4 complex signaling induced by extracellular LPS. Figure taken from De Chiara et all (2025) [55]

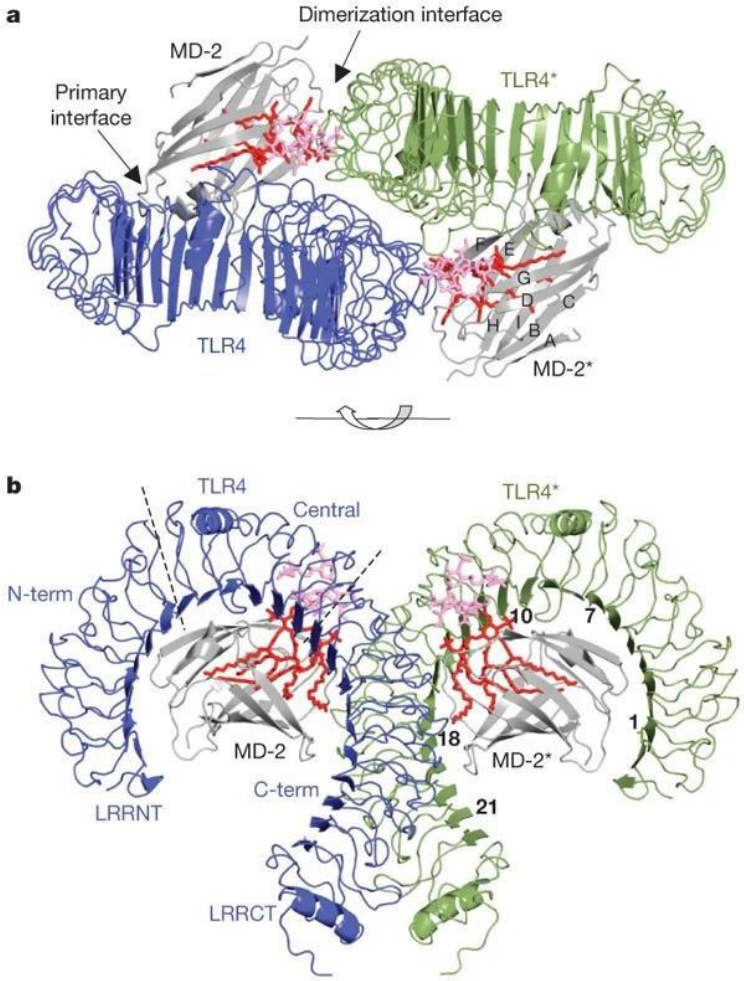

Figure 1.8: Overall structure of the TLR4-MD-2-LPS complex. The image shows the symmetrical complex between the TLR4 receptor, the co-receptor protein MD-2 and the LPS **a)** Top view of the TLR4-MD-2-LPS dimer: the primary interface between TLR4 and MD-2 is formed prior to LPS binding, while the dimerization interface is induced by LPS binding. **b)** Side view of the complex: the lipid A of the LPS is highlighted in red and the inner core carbohydrates in pink. Figure taken from Park et al. (2009) [52]

3.4 Beyond TLR4

As previously mentioned, the most well-characterized signalling pathway involving LPS is certainly the one involving TLR4. However, it is important to note that in recent years, numerous studies have highlighted **alternative pathways** to the canonical one. These pathways represent an additional level of complexity in LPS recognition and the resulting fine-tuning of the immune response. As also highlighted in the review by *De Chiara et al., 2025*[55], LPS can activate TLR4-independent pathways, such as those mediated by human caspase-4/5 and murine caspase-11 [55]. These proteins directly recognize Lipid A and trigger the formation of the non-canonical inflammasome, leading to pyroptosis and the subsequent release of IL-1β and IL-18 [55]. Inflammatory mechanisms involving guanylate-binding proteins (GBPs) have also been extensively studied, as they mediate intracellular responses to LPS. There are also pathways involving the co-receptor CD14, independent of the TLR4/MD-2 complex, that involve the activation of the transcription factor NFAT present in dendritic cells, or that promote the direct entry of LPS into the cytosol, thus activating the non-canonical inflammasome [55]. A further level of regulation involves lectin receptors, including C-type lectins such as DC-SIGN, which bind sugar residues, particularly fucose and mannose, commonly present in LPS [55]. Overall, LPS act as complex, multifactorial signal that, depending on its chemical structure, can activate distinct pathways and play a crucial role in maintaining immune homeostasis.

References:

[50] H. Kumar, T. Kawai, and S. Akira, "Pathogen Recognition by the Innate Immune System," *Int Rev Immunol*, vol. 30, no. 1, pp. 16–34, Jan. 2011, doi: 10.3109/08830185.2010.529976.

[51] N. D. Udeshi *et al.*, "Cell-surface Milieu Remodeling in Human Dendritic Cell Activation," *The Journal of Immunology*, vol. 213, no. 7, pp. 1023–1032, Oct. 2024, doi: 10.4049/jimmunol.2400089.

[52] B. S. Park, D. H. Song, H. M. Kim, B.-S. Choi, H. Lee, and J.-O. Lee, "The structural basis of lipopolysaccharide recognition by the TLR4–MD-2 complex," *Nature*, vol. 458, no. 7242, pp. 1191–1195, Apr. 2009, doi: 10.1038/nature07830.

[53] U. Ohto, K. Fukase, K. Miyake, and Y. Satow, "Crystal Structures of Human MD-2 and Its Complex with Antiendotoxic Lipid IVa," *Science (1979)*, vol. 316, no. 5831, pp. 1632–1634, Jun. 2007, doi: 10.1126/science.1139111.

[54] N. N. Kuzmich, K. V Sivak, V. N. Chubarev, Y. B. Porozov, T. N. Savateeva-Lyubimova, and F. Peri, "TLR4 Signaling Pathway Modulators as Potential Therapeutics in Inflammation and Sepsis.," *Vaccines (Basel)*, vol. 5, no. 4, Oct. 2017, doi: 10.3390/vaccines5040034.

[55] S. De Chiara *et al.*, "Beyond the Toll-Like Receptor 4. Structure-Dependent Lipopolysaccharide Recognition Systems: How far are we?," *ChemMedChem*, vol. 20, no. 6, Mar. 2025, doi: 10.1002/cmdc.202400780.

Chapter IV

During my PhD, my research focused primarily on characterizing the LPS molecules derived from key members of the human gut microbiota. This chapter details the methodologies used for their extraction and purification, along with the chemical, structural, and immunological analyses performed on both the carbohydrate and lipid components of the LPSs studied.

4.1 Cell preparation

The first crucial step in the characterization of LPS is their isolation from bacterial cells. In my work, the starting material consisted primarily of lyophilized bacterial cultures. While numerous protocols have been described in the literature for the extraction of LPS from environmental or pathogenic bacteria, fewer guidelines are available for bacteria belonging to the gut microbiota. For this reason, **established methods were modified and optimized to address the specific requirements and peculiar features of gut-derived strains**. One of the major challenges in working with gut microbiota is the low yield of LPS extraction. Most gut bacteria are in fact strict anaerobes, making their cultivation inherently difficult. In addition, they frequently express a variety of surface carbohydrate molecules, such CPS [56]. Because these molecules share similar chemical features, they are often co-extracted with LPS, complicating the structural resolution of the target molecule. It is therefore essential to have a clear understanding of the bacterial system under investigation to anticipate whether only LPS/LOS, or also other carbohydrate components such as CPS, are expected [57]. Despite this problem of "internal contamination," several strategies can be applied to improve LPS isolation, including specific cell washing steps, enzymatic digestions, and ultracentrifugation. During my PhD, all these

purification approaches were implemented and adapted to the specific requirements of the bacterial species analyzed.

4.2 LPS extraction

The extraction of LPS can be performed by means of two different methods, which differ mainly in the chemical composition of the solutions used. The choice of one technique over another depends on the structural composition of the LPS itself, i.e. whether it is a rough (R-LPS) or smooth (S-LPS) LPS. In fact, the presence of the O-antigen in S-LPS gives to the molecule a greater hydrophilicity compared to an R-LPS, which is preferably isolated using organic solvents. The first technique to be analyzed is called the Phenol/Chloroform/Petroleum Ether (PCP) extraction, which is mainly used to isolate R-LPS [58]. In this protocol, following the extraction, which is carried out using a solution in defined proportions of the three elements, the evaporation of the chloroform and petroleum ether allows the extracted product to remain in the phenol phase. If then a few drops of water are added to the phenol phase, the extracted product will be deposited in the water phase, which after centrifugation will be present in the form of a gelatinous precipitate. This procedure results in an extract that is generally free of cellular contaminants, which greatly facilitates the subsequent structural determination steps. The second approach, generally used for S-LPS, consists of preparing a phenol/water solution (1:1 v/v ratio) at 68°C into which the dried cells are mixed for a long time. In this extraction procedure, the LPSs are isolated in the aqueous phase, although depending on the chemical composition of the molecules they could also be isolated in the phenol phase [59]. For this reason, both phases after extraction are generally collected and subjected to subsequent purification steps. The purification steps immediately following extraction include hydrolysis with DNase, RNase, and Proteinase to eliminate contaminating nucleic acids and proteins. It is important to note that, although PCP extraction is preferred for R-type LPS, the water/phenol extraction method is effective for both types of LPS.

4.3 SDS PAGE

Sodium dodecyl sulfate polyacrylamide gel electrophoresis (SDS-PAGE) is typically used to verify the nature and degree of purification of the extracted material. By separating molecules based on their molecular weight, SDS-PAGE allows assessment of the purity and composition of the sample after extraction and purification steps. SDS acts by disaggregating LPS micelles, thereby facilitating their migration through the gel matrix. Following electrophoresis, gels are typically visualized using silver staining [60] or the PAS method [61]. S-LPS produces the characteristic “ladder-like” pattern, which reflects the lipid A-core region linked to an oligosaccharide backbone with a variable number of O-antigen repeating units. Each step of the ladder corresponds to molecules with an identical lipid A core but differing in the number of attached O-antigens. In contrast, R-LPSmigrates faster and accumulates in the lower part of the gel due to its lower molecular weight. To detect possible co-extracted contaminants, alternative stains can be used, such as Coomassie Blue brilliant, which is very useful for detecting any lipoproteins present in the sample. Alcian Blue is also used to detecting possible presence of the CPS as it could bind specifically to acid groups, which are commonly (but not always) present in these carbohydrate structures.

Figure 2.1: SDS-PAGE (12.5% acrylamide) with silver staining showing the migration patterns of two different type of glycoconjugate : *Lane 1*, LPS from *E. coli*, displays the characteristic ladder-like pattern due to the presence of O-antigen repeats; *Lane 2*, LOS from *Polaribacter* sp. 1127, appears as a lower molecular weight smear or discrete bands, consistent with the absence of O-antigen polysaccharide

4.4 Purification of LPS

Following LPS extraction, purification steps are performed to eliminate contaminants and obtain samples of high purity. These steps include enzymatic treatments with DNase, RNase, and Proteinase, ultracentrifugation, and size exclusion chromatography (SEC). SEC is particularly reliable when an appropriate resin cutoff is selected to effectively separate the target LPS from unwanted components. This technique separates molecules based on their hydrodynamic size: the sample, diluted in a mobile phase, passes through a stationary phase consisting of porous resin. Molecules larger than the resin pores are excluded and elute first, while smaller molecules enter the pores and elute later. Elution is monitored by a refractive index detector, which measures the refractive difference between the mobile phase and the eluted sample, generating a chromatogram. Individual peaks are subsequently analyzed by various methods to distinguish contaminants from the LPS fraction.[62].

4.5 Structural characterizationof saccharide portions

The structural characterization of LPSs presents many difficulties due to the enormous heterogeneity caused by their inherent variability [63]. Their composition usually includes monosaccharides that are widespread in nature such as pentoses, hexoses, hexosamines, 6-deoxy-hexoses, uronic acids, but also unusual monosaccharides that are usually found in certain bacterial strains. In addition, stereochemical variability (D or L), variability in monosaccharide ring closure (pyranose or furanose) and variability in anomeric configuration (α or β) can also be detected. Moreover, non-carbohydrate substitutions within the saccharide portion of LPSs, such as phosphates, amino acids etc are commonly found [64]. For these reasons, the characterization of the saccharide portion of LPS can be very complex and requires the combination of different techniques such as Nuclear Magnetic Resonance (NMR) and various Mass

Spectrometry (MS) always supported by compositional analyses via Gas Chromatography coupled with Mass Spectrometry (GC-MS) [65].

4.6 Structural characterization of saccharide portions via GC-MS

GC-MS combines the high separation efficiency of gas chromatography with the sensitivity and specificity of mass spectrometry, making it particularly suitable for analyzing glycoconjugates such as LPS. Through hydrolysis and derivatization, it enables detailed profiling of monosaccharide composition and acyl residues. One widely used approach is methanolysis in methanolic HCl at 85 °C, which cleaves glycosidic bonds to produce O-methyl glycosides (from sugars) and methyl esters (from lipids) [68]. These products are then acetylated with acetic anhydride in pyridine, yielding acetylated methyl glycosides (AMGs). Identification is based on retention times in gas chromatography and fragmentation patterns obtained via mass spectrometry. Another powerful derivatization method involves the preparation of partially methylated acetylated alditols (PMAAs), which provide insights into glycosidic linkages and ring configurations (pyranose vs furanose) [70]. This protocol includes four sequential steps: complete methylation of the saccharide portion, acid hydrolysis, reduction with $NaBD_4$, and acetylation. The resulting derivatives are then analyzed by GC-MS, where fragmentation typically occurs between adjacent methoxyl groups, aiding structural interpretation. GC-MS is also valuable for determining the absolute configuration of sugar monomers within LPS. This is achieved by converting enantiomers (D and L forms), which are indistinguishable under achiral conditions, into diastereoisomers using enantiomerically pure alcohols such as 2-(+)-octanol or 2-(+)-butanol. Diastereoisomers possess distinct physical properties and can be separated by GC-MS. After acetylation, enantiomeric discrimination is performed by comparing the retention times of the sample with those of a standard mixture of O-2-(±)-octyl glycosides in D or L configuration (*Figure 2.4*). Given the structural complexity of LPS, optimal characterization is typically achieved

by integrating multiple derivatization protocols and analytical techniques, allowing for a more accurate determination of monosaccharide composition and linkage patterns.

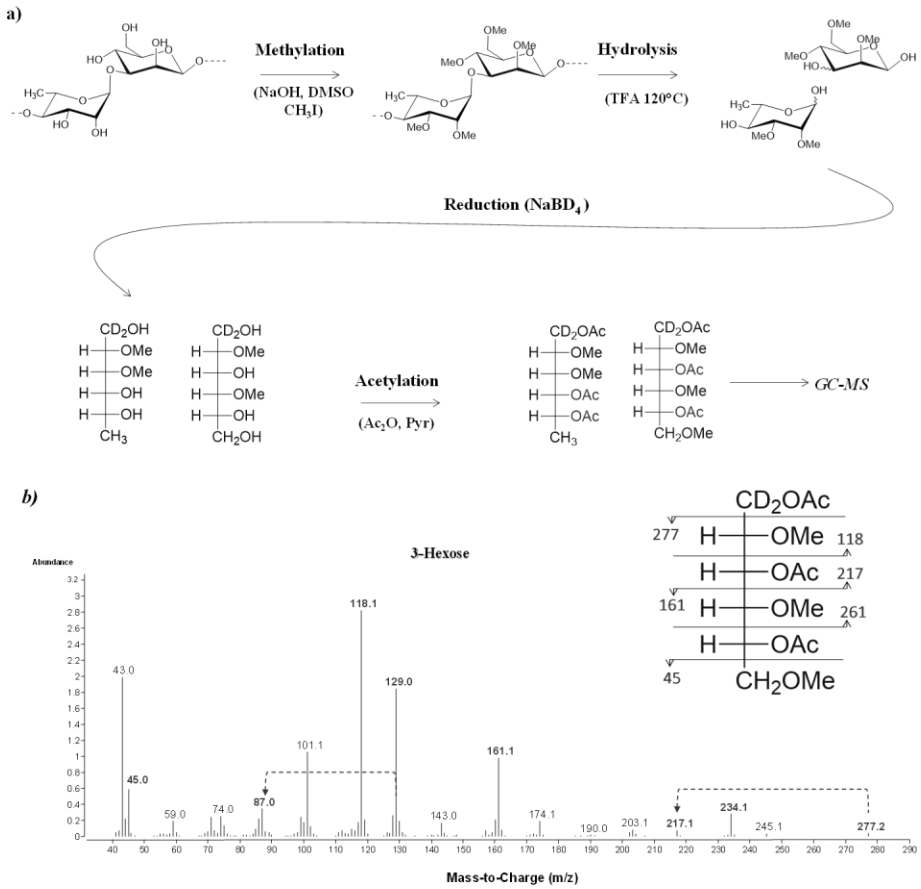

Figure 2.3: a) Schematic representation of the derivatization steps converting the disaccharide [→4) α-L-Rhap (1→3) α-D-Manp (1→] into the corresponding Partially Methylated Acetylated Alditol (PMAA). **b)** Mass spectrum of a PMAA derived from a 3-linked hexose, annotated with key alditol backbone fragmentations used to determine linkage positions. (*Figure adapted from https://glycopedia.eu/)*

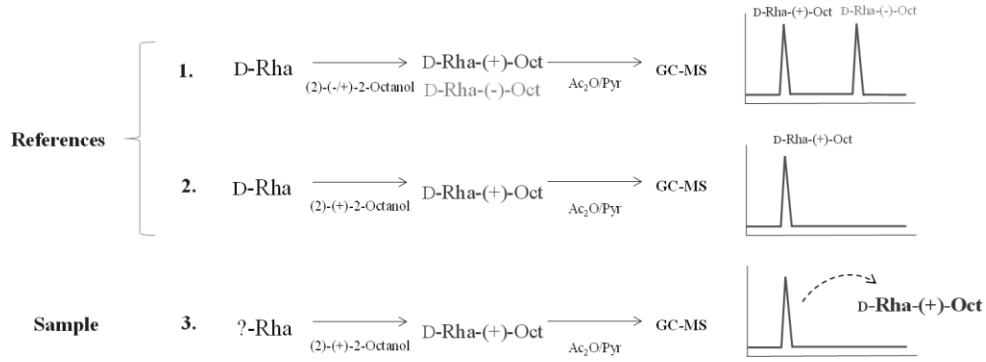

Figure 2.4: Illustration of the strategy used to study the configuration of monosaccharides. It starts with the construction of a standard, in this case D-ramose (D-Rha), which is reacted with a racemic mixture of 2- (±)-octanol. This gives rise to a mixture of diastereomers: D-Rha- (+)-oct and D-Rha- (-)-oct. The sample is then acetylated in the presence of pyridine, and the components are then analyzed by GC-MS. GC-MS analysis reveals two different retention times, representing the two different enantiomers. To distinguish the two forms, the same reaction is repeated using enantiomerically pure 2-octanol, thus obtaining only one of the two derivatives, D-Rha- (+)-oct and L-Rha- (+)-oct. In this way it is possible to distinguish by comparing the retention times the absolute configuration of the rhamnose present in the analyzed sample. (*Figure adapted from https://glycopedia.eu/)*

4.7 Chemical degradation techniques

The main challenge in studying LPS in its entirety lies not only in its structural complexity but also in the distinct chemical nature of its components, which hinders solubility in both aqueous and nonpolar solvents. To overcome this, the saccharide portions, specifically the O-antigen and core OS in LPS, and the core OS in LOS, are

typically analyzed separately from the Lipid A moiety. Separation of these components can be achieved either through complete deacylation or mild acid hydrolysis. Complete deacylation involves two sequential steps: O-deacylation, which removes the ester-linked acyl chains from Lipid A using methyl-hydrazine, and N-deacylation, which eliminates the amide-linked acyl chains via strong alkaline hydrolysis [66]. By contrast, through mild acid hydrolysis, the acid-labile bond between the GlcN of Lipid A and Kdo, the first sugar of the core oligosaccharide, is broken, thus enabling the separation of the water-soluble carbohydrate portion from the highly hydrophobic Lipid A. This separation is typically obtained by means of centrifugation that allows the precipitation of the Lipid A fraction which can be then further purified following the "Blight and Dyer protocol" [67]. In parallel, the water-soluble saccharide portion is also subjected to further purification protocols, which involve the use of size-exclusion chromatography. This acid-based procedure, however, has intrinsic limitations, as it can affect specific bonds and cause the loss of crucial structural information. Similarly, the complete deacylation method also presents drawbacks. For example, 4-substituted uronic acids are susceptible to β-elimination, Kdo di- and trisaccharides may undergo cleavage, and N-deacylation can lead to bond breakage, generating di- or monosaccharide fragments. Moreover, several labile groups under alkaline conditions, such as phosphoesters, pyrophosphates, diphosphodiesters, acetyls, and carbamyls, can also be cleaved during this treatment [68]. To minimize structural loss and obtain a more reliable analysis, an integrated approach, i.e. the merging of data from the two techniques, is recommended.

4.8 Structural characterization of saccharide portions by NMR spectroscopy

NMR spectroscopy represents a powerful and widely applied technique for the structural elucidation of the saccharide components of glycoconjugates. Its major

advantage lies in the ability to provide detailed structural information without altering or damaging the sample, supported by a broad range of established protocols. Nevertheless, NMR analysis requires highly pure preparations, free from contaminants, and sufficient sample quantities to ensure adequate spectral resolution. In addition, the interpretation of spectra containing multiple carbohydrate units, such as in the case of LPS, can be challenging, demanding specific expertise. The first step in resolving a polysaccharide spectrum is based on the acquisition of one-dimensional ^{1}H-NMR spectra that provide a preliminary overview of the sample composition and allow the identification of major signal regions. In the 1D proton spectrum, four characteristic regions can generally be distinguished:

• **2.7-1.0 ppm** (aliphatic region): This region is essential for the detection of deoxygenated sugars. It contains the signals of methyl groups and 6-deoxygenated residues such as rhamnose and fucose (approximately 1.1-1.3 ppm). It also contains the signals of diasterotopic protons, such as those from the methylene group at the C-3 position of Kdo

• **4.4-3.0 ppm** (carbinolic region): This region includes the signals of the ring protons of monosaccharide residues.

• **5.6-4.4 ppm** (anomeric region): It contains the signals of the anomeric protons of all the spin systems present.

• **8-7 ppm** (aromatic region): This region contains the signals related to aromatic protons, useful for identifying glycosides containing aromatic aglycones.

For a complete characterization of an unknown structure, two-dimensional NMR experiments, both homonuclear and heteronuclear, are essential. Homonuclear experiments include Correlation Spectroscopy (COSY) and Total Correlation Spectroscopy (TOCSY), as well as Nuclear Overhauser Effect Spectroscopy (NOESY) and Rotating Frame Overhauser Enhancement Spectroscopy (ROESY). Heteronuclear spectra, on the other hand, include experiments such as Heteronuclear Single Quantum Coherence (^{1}H, ^{13}C-HSQC), Heteronuclear Single Quantum

Coherence – TOtal Correlation SpectroscopY (HSQC-TOCSY), and Heteronuclear Multiple Bond Correlation (HMBC). COSY and TOCSY allow the identification and assignment of the chemical shifts of all protons belonging to the sugar ring. While NOESY and ROESY provide information on the correlations between protons close in space, useful for determining the anomeric configuration of individual monosaccharides. Typically, NOE correlations between H-1/H-3/H-5 are characteristic of sugars with a β configuration, while correlations between H-1 and H-2 indicate an α configuration. Inter-residue NOE correlations can also be observed, which are particularly useful for identifying glycosidic bonds by correlating protons belonging to different spin systems. HSQC spectrum allows the assignment of the carbon atoms in correlation with the protons directly bound to them. To determine the primary sequence, long-range heteronuclear correlation experiments such as HMBC are essential. These spectra detect scalar couplings across multiple bonds, allowing the identification of the hydrogen-carbon pairs involved in glycosidic bonds. HMBC data also provide information on ring shape: in pyranose residues, correlations between H-1/C-5 and C-5/H-1 are typically observed, while in furanose residues the corresponding correlations involve H-1/C-4 and C-1/H-4. Therefore, the combination of the spatial correlations obtained by NOESY/ROESY and the long-range heteronuclear correlations provided by HMBC allows for a comprehensive structural characterization of polysaccharides and oligosaccharides. [69]

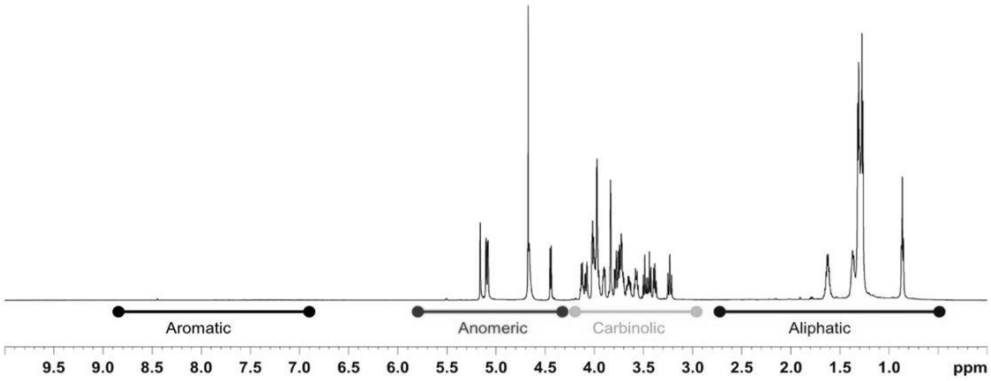

Figure 2.4: Example of a ^{1}H NMR spectrum highlighting the different spectral regions. Figure adapted from Speciale et al. (2022). [69]

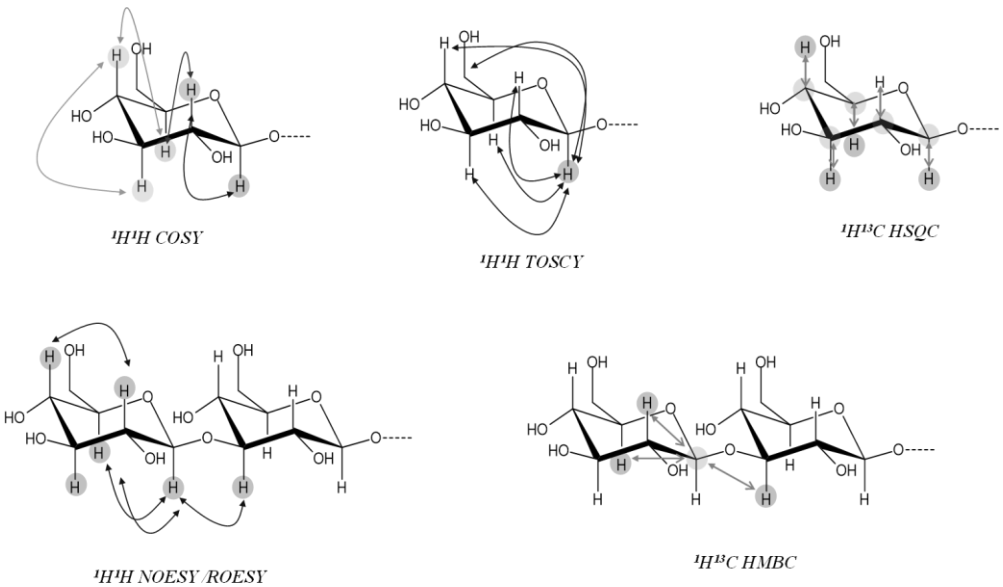

Figure 2.5: Schematic representation of the nuclei targeted in the main NMR techniques used for carbohydrate analysis. (*Figure adapted from https://glycopedia.eu/)*

4.9 Structural characterization of sugar and Lipid A fractions by mass spectrometry

Among the commonly employed techniques for elucidating the chemical structures of extracted LPS and Lipid A fractions, mass spectrometry (MS) stands out as particularly effective. Specifically, Electrospray Ionization (ESI) and Matrix-Assisted Laser Desorption/Ionization (MALDI) are essential tools for the analysis of oligo- and polysaccharides as well as intact LPS (R-LPS) [70]. With ESI, the liquid sample is passed through a narrow capillary, nebulized, and ionized by applying a defined voltage in a "soft" manner. The ability to generate multicharged ions makes ESI especially useful for studying high molecular weight species, such as LPS, and enables coupling with liquid chromatography (LC-ESI-MS) to pre-separate and purify the sample before analysis [71]. For the Lipid A portion, MALDI-TOF is widely preferred. This technique allows the analysis of diverse classes of molecules by a gentle ionization mechanism and measures the mass-to-charge (*m/z*) ratio of ions accelerated in a time-of-flight analyser [72]. The choice of MALDI-TOF is particularly advantageous for Lipid A due to its poor solubility in aqueous media [73]. Another major benefit is the minimal sample preparation required, often no extensive purification is needed prior to measurement. However, one critical aspect lies in the selection of the matrix, which absorbs the laser energy, shields the analyte, and promotes monoisotopic ion formation. The MALDI-TOF/TOF configuration further enables MS/MS experiments, which are indispensable for resolving challenging structural features such as glycosidic linkages and substituent positions within Lipid A. Thanks to these instrumental advancements, it is now feasible to characterize membrane glyco-conjugates with high sensitivity and resolution, even in extremely heterogeneous and high-mass molecules.

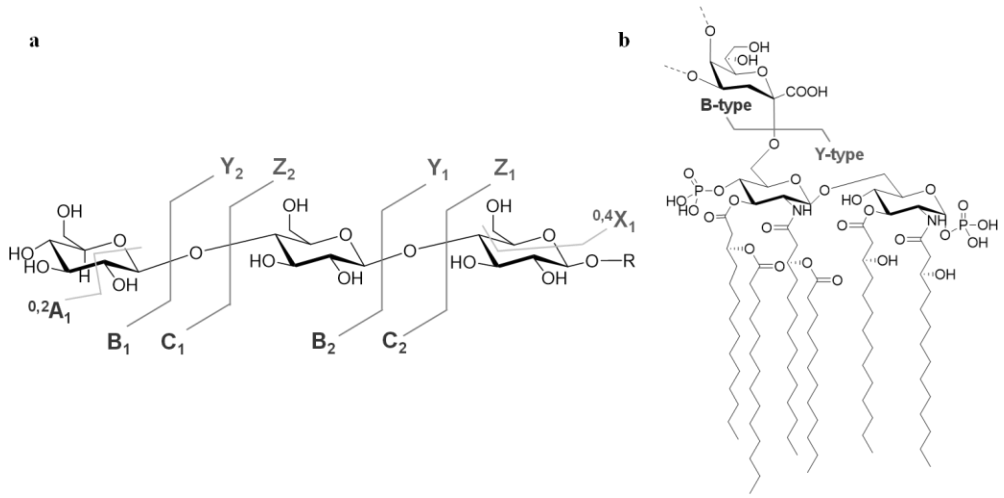

Figure 2.6: a) Scheme illustrating the systematic nomenclature of carbohydrate product ions generated by tandem MS, showing glycosidic cleavages (B-, C-, Y-, Z-types) and cross-ring cleavages (A-, X-types). Subscripts denote positions relative to termini; superscripts indicate ring cleavage sites. **b)** Schematic of cleavage patterns observed in MALDI-TOF MS analysis of an R-LPS, highlighting B-type ions (core oligosaccharide) and Y-type ions (lipid A). Figure adapted from Garcia-Vello et al. (2021). [74]

References

[56] F. Di Lorenzo, C. De Castro, R. Lanzetta, M. Parrilli, A. Silipo, and A. Molinaro, "Lipopolysaccharides as Microbe-associated Molecular Patterns: A Structural Perspective," in *Carbohydrates in Drug Design and Discovery*, The Royal Society of Chemistry, 2015, pp. 38–63. doi: 10.1039/9781849739993-00038.

[57] M. D. Pither, A. Silipo, A. Molinaro, and F. Di Lorenzo, "Extraction, Purification, and Chemical Degradation of LPS from Gut Microbiota Strains," 2023, pp. 153–179. doi: 10.1007/978-1-0716-2910-9_13.

[58] E. Sarmikasoglou and A. P. Faciola, "Ruminal Lipopolysaccharides Analysis: Uncharted Waters with Promising Signs," *Animals*, vol. 11, no. 1, p. 195, Jan. 2021, doi: 10.3390/ani11010195.

[59] G. Komazin *et al.*, "Substrate structure-activity relationship reveals a limited lipopolysaccharide chemotype range for intestinal alkaline phosphatase.," *J Biol Chem*, vol. 294, no. 50, pp. 19405–19423, Dec. 2019, doi: 10.1074/jbc.RA119.010836.

[60] S. Rezania *et al.*, "Extraction, Purification and Characterization of Lipopolysaccharide from Escherichia coli and Salmonella typhi.," *Avicenna J Med Biotechnol*, vol. 3, no. 1, pp. 3–9, Jan. 2011.

[61] L. Tan and P. S. Grewal, "Comparison of two silver staining techniques for detecting lipopolysaccharides in polyacrylamide gels.," *J Clin Microbiol*, vol. 40, no. 11, pp. 4372–4, Nov. 2002, doi: 10.1128/JCM.40.11.4372-4374.2002.

[62] S. Roy, V. B. Mahesh, and R. B. Greenblatt, "EFFECTS OF CLOMIPHENE ON THE PHYSIOLOGY OF REPRODUCTION IN THE RAT," *Acta Endocrinol (Copenh)*, vol. 47, no. 4, pp. 645–656, Dec. 1964, doi: 10.1530/acta.0.0470645.

[63] H. L. P. Tytgat and S. Lebeer, "The sweet tooth of bacteria: common themes in bacterial glycoconjugates.," *Microbiol Mol Biol Rev*, vol. 78, no. 3, pp. 372–417, Sep.

2014, doi: 10.1128/MMBR.00007-14.

[64] M. Matsuura, “Structural Modifications of Bacterial Lipopolysaccharide that Facilitate Gram-Negative Bacteria Evasion of Host Innate Immunity,” *Front Immunol*, vol. 4, 2013, doi: 10.3389/fimmu.2013.00109.

[65] A. Fox, “Carbohydrate profiling of bacteria by gas chromatography–mass spectrometry and their trace detection in complex matrices by gas chromatography–tandem mass spectrometry,” *J Chromatogr A*, vol. 843, no. 1–2, pp. 287–300, May 1999, doi: 10.1016/S0021-9673(98)00884-X.

[66] H. H. Yildirim, D. W. Hood, E. R. Moxon, and E. K. H. Schweda, “Structural analysis of lipopolysaccharides from *Haemophilus influenzae* serotype f,” *Eur J Biochem*, vol. 270, no. 15, pp. 3153–3167, Aug. 2003, doi: 10.1046/j.1432-1033.2003.03693.x.

[67] J. C. Henderson, J. P. O’Brien, J. S. Brodbelt, and M. S. Trent, “Isolation and Chemical Characterization of Lipid A from Gram-negative Bacteria,” *Journal of Visualized Experiments*, no. 79, Sep. 2013, doi: 10.3791/50623.

[68] E. Manzo, A. Molinaro, E. Bedini, C. De Castro, and M. Parrilli, “A very efficient method to cleave Lipid A and saccharide components in bacterial lipopolysaccharides,” *Carbohydr Res*, vol. 333, no. 4, pp. 339–342, Jul. 2001, doi: 10.1016/S0008-6215(01)00157-4.

[69] I. Speciale *et al.*, “Liquid-state NMR spectroscopy for complex carbohydrate structural analysis: A hitchhiker’s guide,” *Carbohydr Polym*, vol. 277, p. 118885, Feb. 2022, doi: 10.1016/j.carbpol.2021.118885.

[70] L. Sturiale *et al.*, “Reflectron MALDI TOF and MALDI TOF/TOF mass spectrometry reveal novel structural details of native lipooligosaccharides,” *Journal of Mass Spectrometry*, vol. 46, no. 11, pp. 1135–1142, Nov. 2011, doi: 10.1002/jms.2000.

[71] P. Liigand, J. Liigand, K. Kaupmees, and A. Kruve, “30 Years of research on ESI/MS response: Trends, contradictions and applications,” *Anal Chim Acta*, vol. 1152, p. 238117, Apr. 2021, doi: 10.1016/j.aca.2020.11.049.

[72] P. Zhou, E. Altman, M. B. Perry, and J. Li, “Study of Matrix Additives for Sensitive Analysis of Lipid A by Matrix-Assisted Laser Desorption Ionization Mass Spectrometry,” *Appl Environ Microbiol*, vol. 76, no. 11, pp. 3437–3443, Jun. 2010, doi: 10.1128/AEM.03082-09.

[73] J. Schiller, “MALDI-TOF MS in lipidomics,” *Frontiers in Bioscience*, vol. 12, no. 1, p. 2568, 2007, doi: 10.2741/2255.

[74] P. Garcia-Vello, I. Speciale, F. Di Lorenzo, A. Molinaro, and C. De Castro, “Dissecting Lipopolysaccharide Composition and Structure by GC-MS and MALDI Spectrometry,” 2022, pp. 181–209. doi: 10.1007/978-1-0716-2581-1_12.

Chapter V
Segatella copri

Decoding a Gut Commensal Signal: Structural and Immunological Profiling of Segatella copri Lipopolysaccharide

This study has beenpublished in

Angew Chem Int Ed Engl 2025 Sep30:e202512947. doi: 10.1002/anie.202512947.

5.1 Introduction

Segatella copri DSM 18205 (also known as *Prevotella copri*) is a bacterium found in the human oral cavity and gastrointestinal tract [75]. It has been the subject of numerous studies and has always been associated with both beneficial effects and pathological conditions. For this reason, the resolution of its structure together with immunological analyses represents an important step towards understanding the mechanisms that regulate its biological response and the way in which this bacterium modulates the immune response through its LPS. The study of *S. corpi DSM 18205* was carried out using the techniques described in Chapter XI, which include NMR and MALDI-TOF analysis, allowing the resolution of its unique chemical structure, which had never been described before. We have also analyzed its immunological properties by using different human cell models to analyze cytokine release but also mass cytometry (CyTOF).

5.2 Results and discussion: Structural characterization of S. copri DSM 18205 R-LPS

S. copri LPS was obtained by extraction from lyophilized cells as described in Chapter XI, paragraph 11.2. The profile of the extract was assessed by SDS-PAGE followed by silver nitrate gel staining, which revealed the rough nature of the LPS (R-LPS), i.e. the absence of the polysaccharide portion of the O-Antigen (*Figure 5.1, b*). The purity of the preparation was verified by complementary assays specifically designed to exclude typical immunostimulatory contaminants, such as phospholipids and lipoproteins/lipopeptides, as confirmed by negative results in SDS-PAGE with Coomassie Blue staining and in the micro-BCA assay (*Figure 5.1, a*). Monosaccharide composition analysis revealed the presence of terminal, 2-substituted, and 2,6-disubstituted D-mannopyranose (D-Man*p*), terminal, 2- and 6-substituted D-glucopyranose (D-Glc*p*), 6-substituted 2-amino-D-glucopyranose (Glc*p*N), and 4,5-disubstituted 3-deoxy-D-*manno*-oct-2-ulosonic acid (Kdo). The heterogenous fatty acid content of the lipid A portion was also defined. By combining matrix-assisted laser desorption/ionization time-of-flight MS (MALDI-TOF MS), electrospray (ESI) MS, tandem MS (MS/MS), and NMR spectroscopy data, we conducted a comprehensive structural elucidation of the R-LPS. To dissect the lipid A domain, an aliquot of sample was subjected to mild acid hydrolysis, a treatment that selectively cleaves the linkage between the non-reducing glucosamine of the lipid A portion and the Kdo, which anchors the core oligosaccharide to the lipid A. The released lipid A was mainly characterized by MALDI-TOF MS and MS/MS supported by compositional analyses. As for the carbohydrate moiety, structural determination was achieved via NMR investigation of R-LPS upon full deacylation followed by size-exclusion chromatography purification. Finally, an in-depth analysis of intact R-LPS was also performed by using both ESI-MS and MALDI-TOF MS.

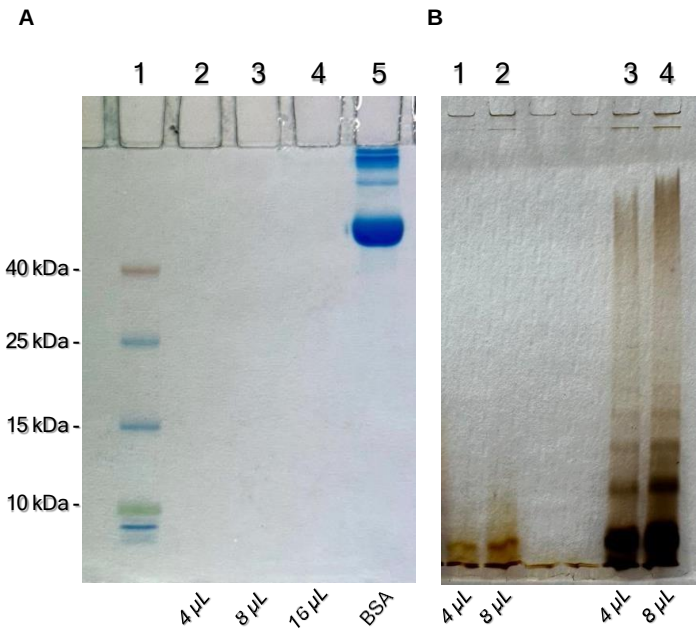

Figure 5.1 SDS-PAGE gels of R-LPS from *S. copri*, with silver staining (b) and Coomassie Brilliant Blue (a), respectively. In the Coomassie-stained gel, the BLUeye protein marker (2 µL, lane 1) and bovine serum albumin (BSA, 8 µL, lane 5) were used as references. In lanes 2, 3, and 4, 4, 8, and 16 µL of a 1 mg/mL concentration solution of *S. copri* R-LPS were loaded, respectively. In the silver-stained gel, *Salmonella typhimurium SH 2201* S-LPS was used as a control, loaded in quantities of 4 and 8 µL in lanes 3 and 4, while 4 and 8 µL of *S. copri* R-LPS, again at a concentration of 1 mg/mL, were loaded in lanes 1 and 2

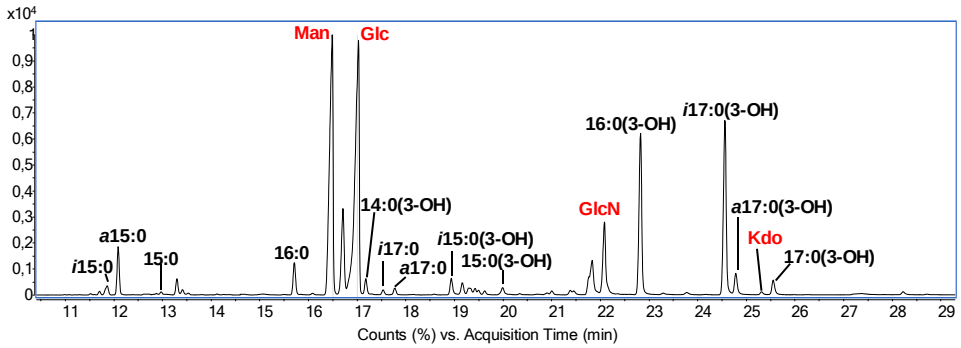

Figure 5.2 Results of GC-MS chromatogram profile of the acetylated methyl glycoside (AMG) and methyl ester derivatives of monosaccharides and fatty acids of *S. copri* R-LPS. Man: Mannose; Glc: Glucose; GlcN: 2-amino-D-glucopyranose; Kdo: 3-deoxy-D-manno-oct-2-ulosonic acid

5.3 Analysis via NMR of S. copri DSM 18205 R-LPS

The ^{1}H and ^{1}H, ^{13}C HSQC NMR spectra of the fully deacylated R-LPS (*Figure 5.3*) showed the presence of eleven anomeric signals, indicative of eleven spin systems (**A**–**H**), while H-3 methylene resonances of a Kdo residue (**K**/**K'**) were also detected in the spectra at δ_H 2.14/1.93-1.91 ppm and δ_C 34.4ppm. The identification of all spin systems was carried out by following the spin connectivity observed in the DQF-COSY and TOCSY spectra. Simultaneously, carbon atoms were assigned through interpretation of the HSQC spectrum (*Figure 5.3*)[69]. The anomeric configurations of the monosaccharide units were determined by examining intra-residue NOE correlations in the ROESY spectrum, along with the $^{3}J_{H1,H2}$ coupling constant values derived from the DQF-COSY. Additionally, vicinal $^{3}J_{H,H}$ coupling constants values were used to infer the relative configuration of each sugar residue, in turn supported by chemical analyses. Briefly, the fully deacylated R-LPS showed a core OS made up of a heptasaccharide composed of one α-Kdo (**K**/**K'**), three α-D-Man (**B**/**B'**,**C** and **E**), two β-D-Glc (**G**/**G'** and **H**), and one α-D-Glc (**D**), while the two glucosamine residues (α-D-GlcN and β-D-GlcN) composing the lipid A backbone were identified in spin systems **A** and **F**/**F'**, respectively Moreover, the Kdo was found to bear a 2-aminoethyl phosphate (PEtN) unit at its O-4 position, as proven by the correlation of H-4 **K**/**K'** with a signal at -0.75 ppm in the $^{31}P,^{1}H$ HSQC spectrum, in turn correlating with methylene proton resonances at δ_H 3.95 and 3.26 ppm. Moreover, two further monophosphate ester groups with chemical shifts at 3.61 ppm and 4.10 ppm, were found and correlated with anomeric proton signal of the lipid A non-reducing α-D-

GlcN **A** (5.52 ppm) and H-4 of α-D-Man **B** (3.77 ppm), respectively. The non-stoichiometric phosphorylation of α-D-Man **B** splits the NMR signals of sugar residues **B**, **G**, **K** and **F** resulting in additional spin systems **B'**, **G'**, **K'**, and **F'**. The core OS sequence was elucidated based on inter-residue NOE correlations detected in the ROESY, complemented by long-range correlations observed in the HMBC spectrum (*Figure 5.4*). Briefly, starting from Kdo unit (**K**), this was substituted at the O-5 position by α-D-Man **B**/**B'**, as indicated by the long-range correlation between the H-1 signal of **B**/**B'** and the C-5 signal of **K** (*Figure 5.4*). α-D-Man **B**/**B'** was in turn substituted at O-2 by β-D-Glc **G**/**G'** and at O-6 by β-D-Glc **H**, as indicated by the NOE correlation between H-1 of **G**/**G'** and H-2 of **B**/**B'** and between H-1 of H and H-6 of **B**/**B'**, as well as by the related HMBC correlations (*Figure 5.4*). The latter residue **H** showed to bear α-D-Glc **D** at its O-6 position, which in turn carried the α- D-Man-(1→2)-α-D-Man disaccharide (**E** and **C**, respectively) at its O-6 position. Hence, integration of the results obtained from the NMR analysis enabled the full structural characterization of the carbohydrate moiety from *S. copri* DSM 18205 R- LPS, as sketched in *Figure 5.5*

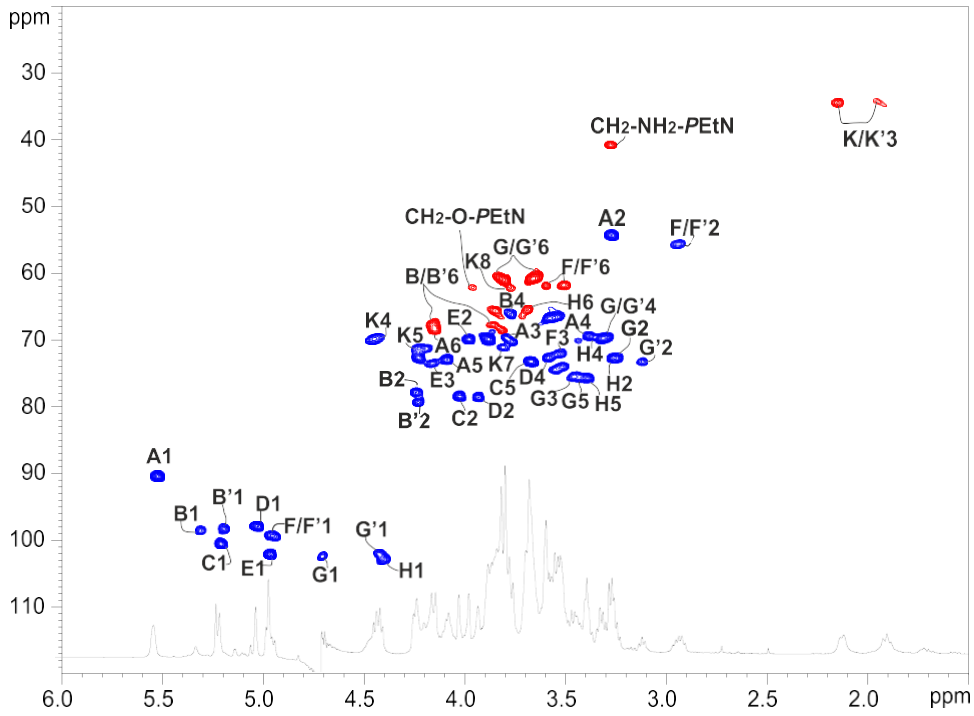

Figure 5.3: Structural analysis by NMR of *S. copri* R-LPS (600 MHz, 298 K, in D_2O; see Table S2). The picture shows the overlapping ^1H and ^1H, ^{13}C HSQC spectra (in red and blue) of the oligosaccharide core obtained after complete dealkylation of the R-LPS. The main one-bond heteronuclear correlations are indicated in the figure.

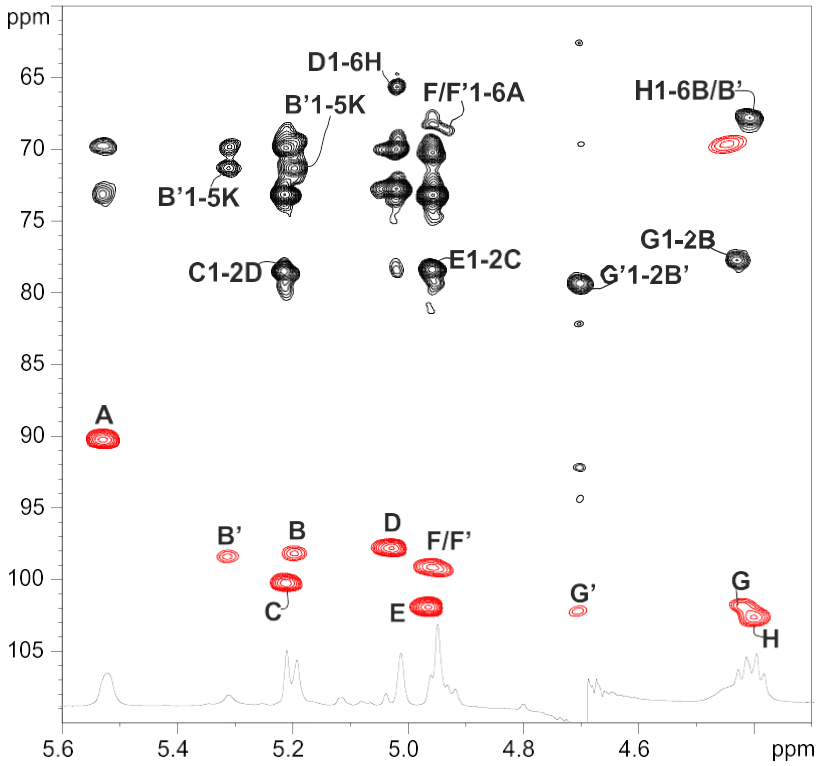

Figure 5.4: Zoom of the overlapped ^{1}H, ^{1}H, ^{13}C HSQC (red) and ^{1}H,^{13}C HMBC (black) spectra of the core OS from *S. copri* R-LPS. Key *inter*-residue long-range correlations involving sugar units are highlighted.

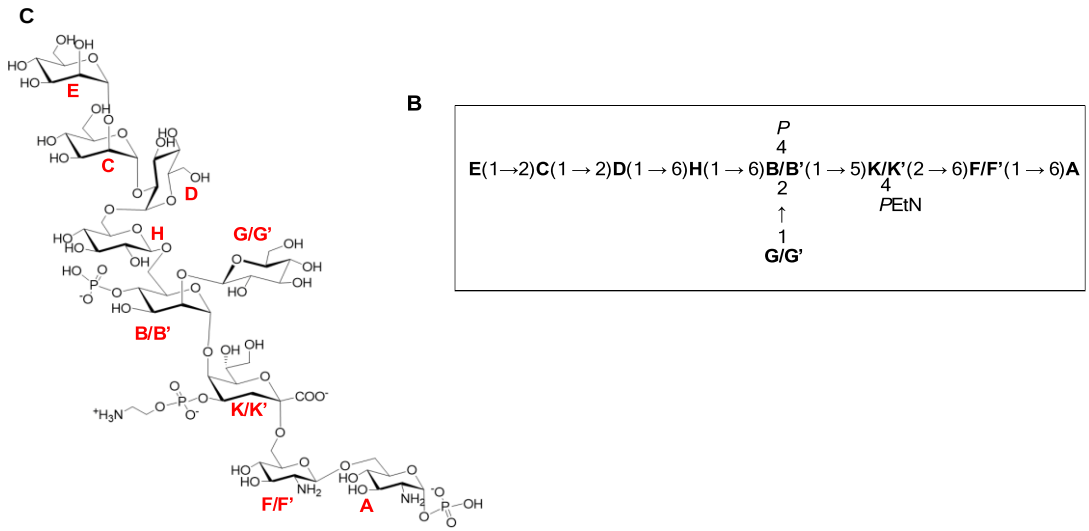

Figure 5.3: (b), (c) Structure of the core OS deduced by NMR spectroscopy.

5.4 Analysis via MS of S. copri DSM 18205 R-LPS

A comprehensive structural overview of the R-LPS was accomplished by ESI-MS, MALDI-TOF MS, and tandem MS analyses that were performed on the intact molecule. Direct infusion ESI-MS analysis of R-LPS in negative-ion mode revealed a complex distribution of ions corresponding to both intact R-LPS species and their characteristic fragment ions related to lipid A and the core OS. The intact R-LPS molecules were predominantly observed in the triply charged state ($[M\text{-}3H]^{3-}$), with a major signal detected at *m/z* 1022.767 (3070.582 Da) (*Figure 5.4, a*), consistent with the full R-LPS structure comprising a mono-phosphorylated penta-acylated lipid A moiety (m/z 1674.035) linked to a core OS consisting of six Hex, one Kdo, one phosphate group, and one 2-aminoethyl phosphate (PEtN), thus in agreement with NMR analysis. A minor population of $[M–3H]^{3-}$ ions was also detected at

approximately m/z 1076.775 (3232.665 Da) (*Figure 5.4, a*) and was assigned to R-LPS species carrying an additional Hex residue not identified by NMR, thereby suggesting minor heterogeneity within the core OS structure. A magnified view of the spectrum (*Figure 5.4, b*) in the m/z 1360–1710 range provided detailed insights into the heterogeneity of lipid A and R-LPS species. Multiple series of doubly charged ($[M-2H]^{2-}$) ions corresponding to R-LPS variants were observed, differing in acylation pattern, phosphorylation state, and presence of sodium adducts. Additionally, singly charged ions between m/z 1660.024 and 1702.057 were identified as mono-phosphorylated penta-acylated lipid A species (*Figure 5.4, a, b*). Further structural confirmation was obtained through MS/MS analysis of the $[M-2H]^{2-}$ ion at m/z 1534.609 and the $[M-3H]^{3-}$ ion at m/z 1022.767 (3070.582 Da) (*Figure5.4, c*). In particular, the MS/MS spectrum of the precursor ion at m/z 1534.609 revealed a complex fragmentation profile, with signals originating from both the lipid A and the core OS moieties (*Figure 5.4, c*). Prominent peaks at m/z 1674.019 and m/z 1394.175 were assigned to lipid A and core OS respectively. However, glycosidic and cross-ring fragments characteristic of the core region (e.g., Y could be observed in the m/z 50-1150 6, C4α, Y5αC6,...) [76] could be observed in the m/z 50-1200 range, which provided detailed structural information on the glycosidic sequence and branching points of the oligosaccharide thus corroborating NMR analysis.

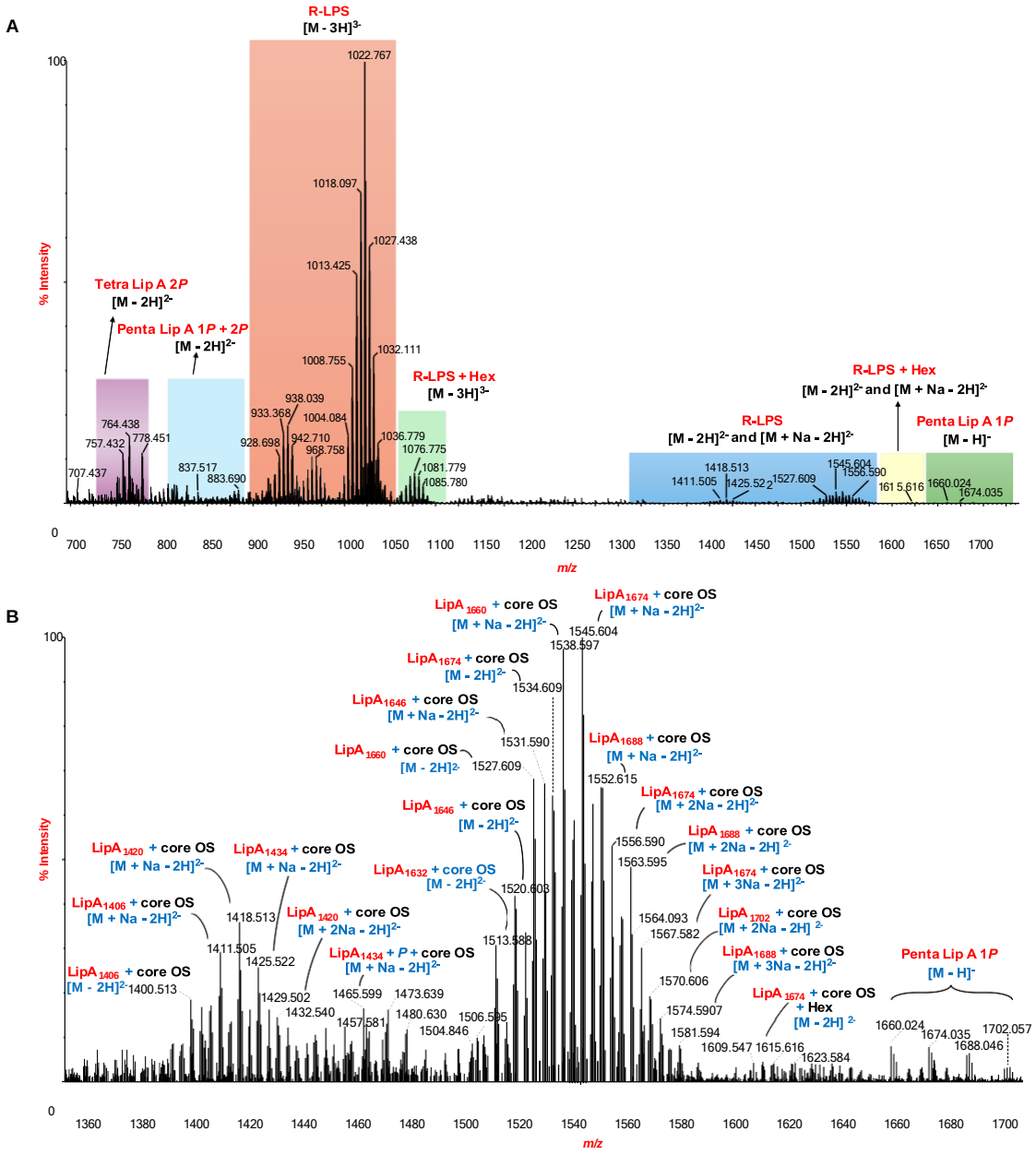

Figure 5.4: Mass spectrometry structural analysis of *S. copri* R-LPS. (A) Zoom of the negative-ion ESI mass spectrum of *S. copri* R-LPS. Coloured boxes indicate regions where $[M\text{-}3H]^{3-}$, $[M\text{-}2H]^{2-}$, and $[M+Na\text{-}2H]^{2-}$ ions corresponding to R-LPS are found. Coloured boxes have also been used to indicate the $[M\text{-}2H]^{2-}$ and [M-H] ions related to lipid A. (B) Magnified view of the region where $[M\text{-}2H]^{2-}$ and

$[M+Nan-2H]^{2-}$ ions corresponding to R-LPS and [M-H] ions related to lipid A are detected

Likewise, lipid A-related fragments (*Figure 5.5, a, b)* were clearly observed and confirmed that the species at *m/z* 1674.019 consists of two glucosamines, one phosphate, two *N*-linked primary 17:0(3-OH), one 15:0(3-OH) and one 16:0(3-OH) as *O*-linked primary acyl chains of the non-reducing and reducing glucosamine respectively, while 15:0 was the secondary acyl substituent in the acyloxyacylamide moiety of the non-reducing glucosamine (*Figure 5.5, b*). The spectrum also includes hybrid fragments containing both lipid and sugar elements (e.g., Y_3C_7, Z_3…), confirming extensive fragmentation across the glycosidic linkage between the core and lipid A. Of note, *Figure 5.4, a* also showed significant signals between *m/z* 757.432 and *m/z* 778.451 that were assigned to $[M-2H]^{2-}$ ions of tetra-acylated lipid A species bearing two phosphate groups. To further explore this lipid A structural variability and to determine the precise location of the second phosphate group on the glucosamine disaccharide backbone, negative-ion MS/MS analyses were performed on several precursor ions. This analysis enabled the assignment of the second phosphate group to the non-reducing glucosamine, as demonstrated by the observation in the MS/MS spectrum of the $[M - 2H]^{2-}$ precursor ion at *m/z* 764.4 (1529.016 Da) of both the Y_1- and C_2 ions at *m/z* 766.478 and *m/z* 778.899 that indicated the presence of two 16:0(3-OH) and one phosphate on the reducing glucosamine and of one 17:0(3-OH), one 17:0 and one phosphate on the non-reducing unit, respectively. Finally, full R-LPS also underwent a negative-ion MALDI-TOF MS analysis that provided complementary insights into its structural composition and confirmed the microheterogeneity of the R-LPS preparation almost fully occurring in the lipid A moiety. In particular, the MALDI-TOF spectrum clearly displayed distinct ion clusters corresponding to lipid A species that were both *mono*- and *bis*-phosphorylated tetra- and penta-acylated, which were likewise identified as components of the related R-LPS molecules.

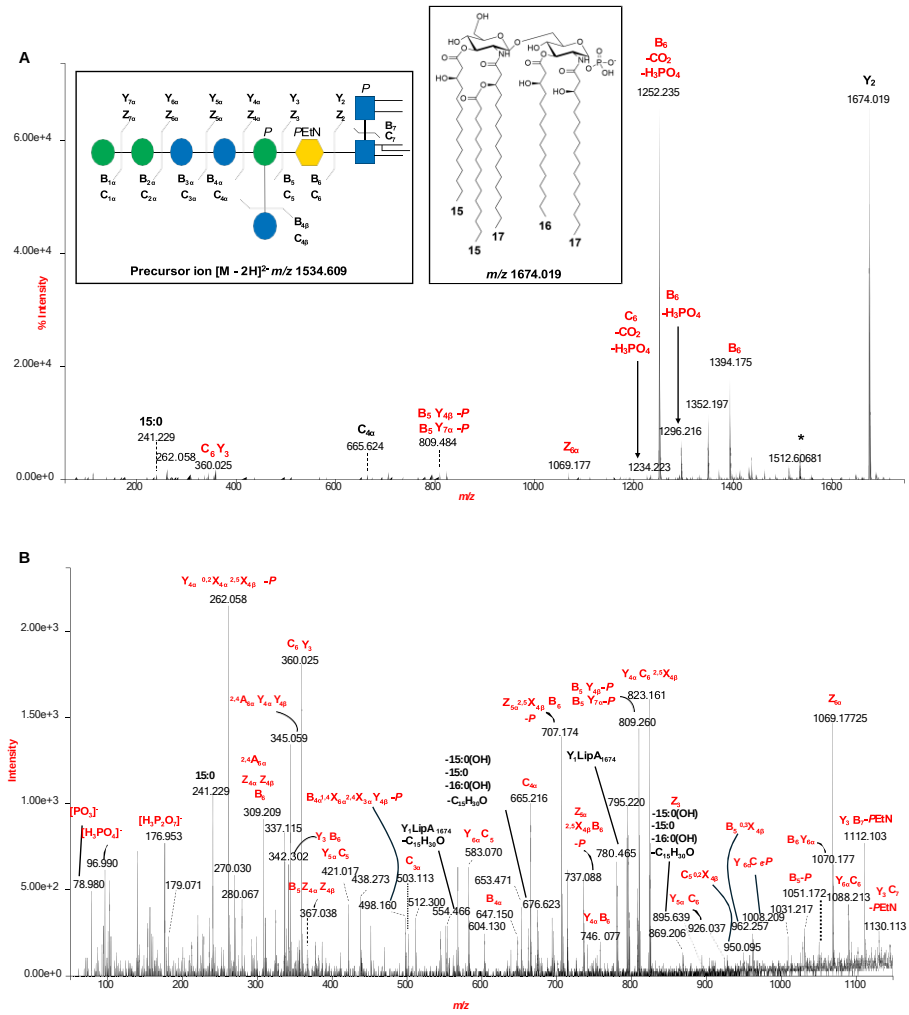

Figure 5.5: (A) Zoom of the negative-ion MS/MS spectrum of $[M-2H]^{2-}$ precursor ion at m/z 1534.609 (3070.582 Da) corresponding to full R-LPS composed of mono-phosphorylated penta-acylated lipid A (m/z 1674.019, Y2 fragment ion) and core OS (m/z 1394.175, B6 fragment ion). (B) Magnified view of the m/z range 50-1150. Spectra are the result of the bisection of the R-LPS which yielded fragment ions derived from core OS, lipid A as well as hybrid ones containing both lipid and sugar moieties. Fragment ions related to the lipid A moiety are shown in black, while those originating from the saccharide portion are highlighted in red. Lack of $C_{15}H_{30}O$ is related to a six-membered ring-based rearrangement due to an enamine to imine tautomerization that can occur when the N-linked chains (in this case 17:0(3-OH)) do not carry secondary fatty acids, i.e. they have a free 3-OH group. The

proposed structure for the oligosaccharide species was drawn using the Symbol Nomenclature for Glycans (SNFG). The nomenclature of glycan fragment ions generated from the cleavage of a glycosidic bond is also reported. Symbols legend: blue circle: glucose; green circle: mannose; blue square: glucosamine; yellow hexagon: Kdo; P and PEtN stand for phosphate and 2-aminoethyl phosphate.

5.5 Analysis in silico of S. copri DSM 18205 R-LPS Biosynthesis

To rationalize the unusual structural features revealed by MS and NMR, we next examined the genome of *S. copri* DSM 18205 to identify loci potentially involved in R-LPS biosynthesis. The convergence of genomic and chemical evidence in fact could provide a coherent framework for LPS biosynthesis and offers insights into how gut symbionts may fine-tune their LPS architecture to shape host-microbe interactions. Most of the predicted LPS biosynthesis-related proteins were encoded within operons, which collectively contain 82 proteins, including both LPS-related and unrelated ones. For these, annotated Pfam domains [77]were identified and visualized. These operons include genes involved in the nine conserved steps of lipid A biosynthesis, [38]as well as several operons encoding enzymes responsible for lipid A modification, Kdo biosynthesis, and glycosyltransferase activities. Through this analysis, we confirmed that the *S. copri* genome encodes only one secondary acyltransferase, consistent with the absence of hexa-acylated lipid A species and in agreement with previous observation in other Bacteroidetes [78]. Moreover, we identified two homologs of the lpxA gene in *S. copri* (LK433_RS06380 and LK433_RS13255), whereas in *E. coli* this gene is typically present as a single, essential copy for lipid A biosynthesis [79]. The presence of two lpxA homologs in *S. copri* is particularly intriguing, given that LpxA functions as a homotrimer and serves as a “molecular ruler” whose acyl chain length selectivity directly shapes the structure of the lipid A domain [80]Notably, the two *S. copri* LpxA homologs retain the catalytic residues and characteristic acyltransferase domains, yet share only ~45% sequence identity with each other.

Structural modelling using AlphaFold3[81], [82] predicted the formation of stable homotrimeric complexes for each isoform, whereas heterotrimeric assemblies appeared less favorable due to weaker interface stability. This duality, also observed in other Bacteroidetes, may represent an evolutionary adaptation to broaden the substrate range. The presence of functionally distinct LpxA variants could thus account for the incorporation of different acyl chains at the 3-OH position of glucosamine, providing a plausible molecular basis for the lipid A microheterogeneity observed in MS analyses and directly linking sequence variation to chemical diversity. While based on predictive analyses, the functional implications of these insights merit further experimental investigation. Following the identification of candidate R-LPS biosynthetic genes, we mapped their corresponding operons and identified two putative operons likely involved in core OS biosynthesis. These regions encode multiple glycosyltransferases, spanning GT2, GT4, GT32, GT90, and GT113 families, consistent with the diverse sugar residues identified by NMR and MS. Likewise, we identified genes likely involved in non-carbohydrate modifications of the R-LPS (like phosphate and PEtN addition in the case of *S. copri*) such as genes homologous to eptA and eptB (LK433_RS03400 and LK433_RS06640) for PEtN modifications of lipid A and Kdo, while two additional genes (LK433_RS10260 and LK433_RS10015), related to lpxE/F/T, may regulate lipid A phosphorylation through phosphate addition or removal [83], [84]. Taken together, the genetic repertoire mirrors the unusual structural complexity of *S. copri* R-LPS revealed experimentally, including PEtN-modified Kdo, mannose phosphorylation, and lipid A heterogeneity, thereby reinforcing the tight connection between genome content and chemical phenotype.

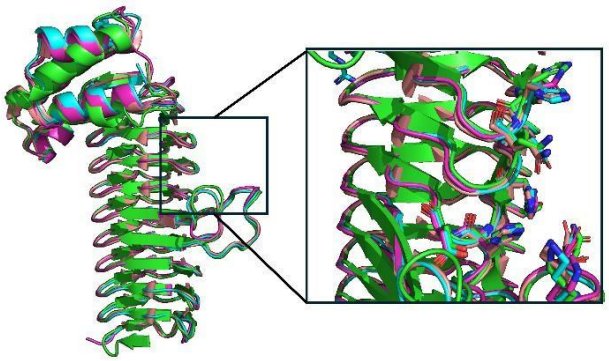

Figure 5.6: The picture shows the three-dimensional model of $ScLpxA_2$ (in magenta) and ScLpxA (in cyan), obtained with AlphaFold3, superimposed on the crystallographic structure of BfLpxA (pink, PDB: 4R36) and that of EcLpxA (green, PDB: 1LXA) using PyMOL. The superposition highlights a strong structural similarity between the proteins, with differences mainly located in the flexible loop regions and α-helical domains. The highly conserved catalytic histidine and other residues involved in the formation of the active site are highlighted.

5.6 S. copri DSM 18205 R-LPS TLR-mediated activation pathway

Intrigued by the novel chemical structure and microheterogeneity of *S. copri* R-LPS, we next evaluated its immunostimulatory potential. Given the well-established role of lipid A and the core OS in modulating host immune responses, functional assays were performed to assess how *S. copri* R-LPS interacts with key pattern recognition receptors (PRRs) of the innate immune system, particularly Toll-like receptors (TLRs). To this end, we first employed a panel of cell-based reporter systems and immune cell lines designed to dissect receptor-specific activation pathways. These included HEK-Blue™ hTLR4 cells, which co-express human TLR4, MD-2, and CD14, enabling the selective detection of TLR4-mediated NF-κB activation, and HEK-Blue™ hTLR2 cells, used to assess potential engagement of the TLR2 pathway. Additionally, differentiated THP-1 cells were employed as a human macrophage-like model to evaluate broader innate immune responses, including cytokine release, in a

more physiologically relevant context. As shown in *Figure 5.7*, a, experiments with HEK-Blue™ hTLR4 cells demonstrated that *S. copri* R-LPS induces TLR4-mediated NF-κB activation, but at significantly lower levels than *E. coli* LPS across all concentrations tested. This indicated that although recognized by TLR4/MD-2/CD14, it signaling capacity is markedly attenuated. Remarkably, pre-incubation with *S. copri* R-LPS reduced NF-κB activation by subsequent *E. coli* LPS challenge, demonstrating an inhibitory effect comparable, though slightly weaker, than that of the known TLR4 antagonist *R. sphaeroides* LPS (*Figure 5.7*). These results suggest that *S. copri* R-LPS can compete with pro-inflammatory LPSs for TLR4 engagement in the gut, thereby modulating the host immune response to stronger LPS stimuli.

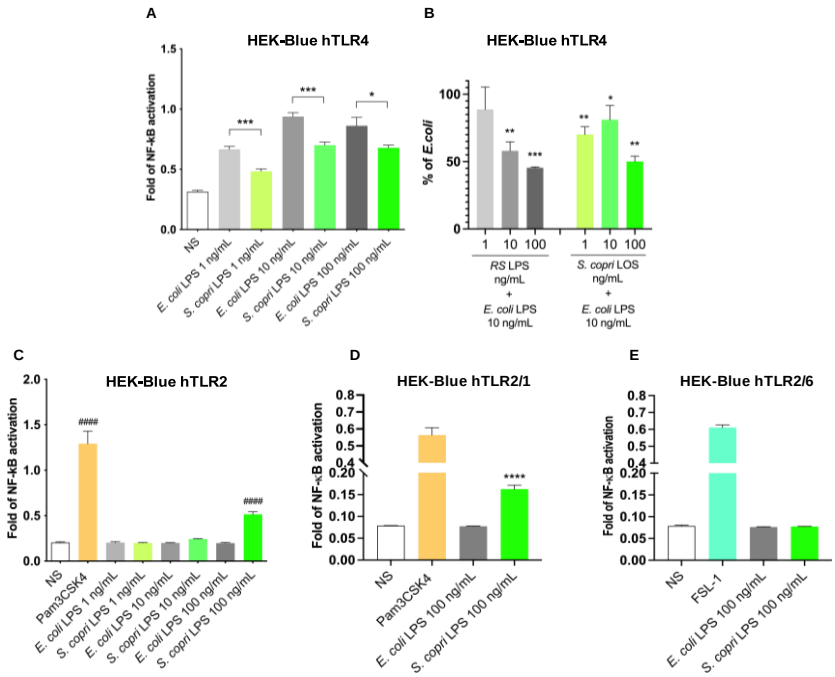

Figure 5.7: NF-kB activation in HEK-Blue cells upon stimulation with *S. copri* R-LPS. Cells were stimulated for 18 hours with either *E. coli* LPS or *S. copri* R-LPS, and NF-kB activation was quantified by Quanti-Blue assay (OD 620 nm). The effects of *S. copri* R-LPS were evaluated on TLR4 (A) and

TLR2 (C). *E. coli* LPS was used as a positive control for TLR4 activation, while treatment with 500 ng/mL of PAM3CSK4 was employed to verify TLR2 activation. Unstimulated (NS) cells were considered as negative control. (B) Competition assay in HEK Blue hTLR4. Cells were pre-treated with either Rhodobacter sphaeroides (RS) LPS or *S. copri* R-LPS (1-10-100 ng/mL) for 4 hours and then stimulated with 10 ng/mL *E. coli* LPS for 16 hours. NF-kB activation is expressed as a percentage relative to stimulation with 10 ng/mL *E. coli* LPS (set as 100%) and shown as mean ± standard deviation. Statistical significance was determined by unpaired t-test between *S. copri* R-LPS and *E. coli* LPS (*p-value < 0.05; **p-value < 0.01; ***p-value < 0.001 vs *E. coli* LPS) (A, B) and vs NS (####p-value < 0.0001 and ****p-value < 0.0001) (C-E).

Consistent with these findings, treatment of differentiated THP-1 cells did not alter their viability and resulted in modest NF-κB activation and significantly lower TNF-α production compared to *E. coli* LPS, further supporting its weak pro-inflammatory potential. Finally, since microbiota-derived LPSs have also been reported to engage TLR2, [85], [86] we examined this pathway and observed that *S. copri* R-LPS activated TLR2 signaling only at higher concentrations (100 ng/mL; *Figure 5.7, c*). As the TLR2 receptor functions as a heterodimer formed with either TLR1 or TLR6, we tested the *S. copri* R-LPS in a comparative analysis using the hTLR2-1 (only TLR2 and TLR1 present) and hTLR2-6 (only TLR2 and TLR6). Interestingly, we observed that *S. copri* R-LPS triggered a modest activation of the TLR2-1 heterodimer and not of the TLR2-6 complex (*Figure 5.7 d, e*).

5.7 Multiparameter Phenotyping of Human PBMCs Using Mass Cytometry upon stimulation with S. copri DSM 18205 R-LPS

To extend the functional implications of *S. copri* R-LPS chemical peculiarities, we then assessed its effects on PBMCs, which include a varied population of immune

cells mainly composed of lymphocytes (T cells, B cells, NK cells), monocytes and dendritic cells [87]. PBMCs represent an ex vivo model of the human immune system, enabling the evaluation of complex multicellular immune responses, beyond those observed in engineered cell lines[87]. To evaluate this response, we measured the production of key cytokines, including TNF-α, IL-6 and IL-10 following stimulation with *S. copri* R-LPS. These experiments were conducted using the ELLA platform (Bio-Techne), an automated microfluidic-based immunoassay system that allows highly sensitive and multiplexed analysis. Overall, *S. copri* R-LPS induced a milder pro-inflammatory cytokine profile compared to *E. coli* LPS, with significantly lower levels of TNF-α and IL-6, suggesting a reduced stimulatory capacity on primary immune cells. Likewise, the release of IL-10 was weaker than that observed in response to *E. coli* LPS at both concentrations tested. Of note, *S. copri* R-LPS was able to induce measurable but moderate cytokine responses in PBMCs, with the most pronounced differences emerging at lower concentration (1 ng/mL). Given these findings and the desire to better understand the subtle immunomodulatory effects of *S. copri* R-LPS at physiologically relevant low concentrations, we employed mass cytometry (CyTOF) for an in-depth characterization of immune cell phenotypes upon stimulation with chemically distinct LPSs. CyTOF, in fact, enables the simultaneous measurement of multiple surface markers, making it ideal to detect fine alterations in complex immune cell populations. Using this highly sensitive approach, we analyzed PBMC responses to *S. copri* and *E. coli* LPS at low concentrations (0.01 and 0.1 ng/mL), with the aim of uncovering differential capacities to elicit immune activation. We clustered the major immune populations of PBMCs obtained from six healthy donors based on their expression of key surface markers, and as shown in the global UMAP representation (*Figure 5.8, a*), the most prominent effects of LPS treatments were observed in the monocyte compartment. This was further supported by subset-specific analysis. In fact, as shown in *Figure 5.8 a, b*, both treatments did not induce detectable changes in the $CD3^+/CD3^-$ cell ratio nor were significant effects detected on the $CD4^+$ or $CD8^+$ T cell populations. Similarly, innate immune cells, such as NK

and dendritic cells, appeared unaffected. In contrast, a consistent reduction of monocyte subset $CD45^{+}CD3^{-}CD14^{+}$ was already detectable after treatment with only 0.01 ng/mL of *E. coli* LPS (*Figure 5.8 , panel f*).This finding aligns with the well-established role of pro-inflammatory LPSs in driving monocyte activation and their differentiation into antigen-presenting cells, a process typically related to CD14 downregulation [88]. Intriguingly and in contrast, treatment with 0.01 ng/mL of *S. copri* R-LPS led to a modest, non-significant decrease in CD14 surface expression (*Figure 5.8, panel f*). Notably, the differential effect between the two LPSs became less pronounced at the higher concentration of 0.1 ng/mL, at which both treatments led to a comparable reduction in CD14 expression. These results suggest that *E. coli* LPS is more potent than *S. copri* R-LPS in the early triggering of innate immune responses and on the shifts within monocyte cell subsets. To further explore these differential responses and their relevance in immune activation, we analyzed in depth the major monocyte subsets currently known. Monocytes in fact are typically classified into three main populations based on CD14 and CD16 surface expression:[89] classical ($CD14^{++}CD16^{-}$), intermediate ($CD14^{++}CD16^{+}$), and non-classical ($CD14^{+}CD16^{+}$). Classical monocytes are primarily involved in homeostatic and regulatory functions, intermediate monocytes are associated with inflammatory responses, and non-classical monocytes specialize in patrolling and tissue surveillance [90], [91]. In our analysis, both *S. copri* and *E. coli* LPS mainly impacted $CD16^{+}$ monocyte subsets, including both the intermediate and non-classical populations. In contrast, the CD16- monocytes were minimally affected, particularly at the lower dose. Importantly, other $CD16^{+}$ cell types, such as NK cells ($CD56^{+}CD16^{+}$), remain unaltered upon LPS treatment. This indicates that the observed changes are not merely dependent on CD16 expression alone, but rather on the specific co-expression of CD14 and CD16 (*Figure 5.8, a*). Numerous studies have linked the maturation of $CD16^{+}$ monocyte subsets to a more inflammatory antigen-presenting cell phenotype, in contrast to the more regulatory profile observed for classical monocytes [92], [93]. Our data further support this observation as the CD14+CD16+ monocytes also

express elevated levels of activation markers typically related to inflammation as CD11c, TLR4, and HLA-DR (*Figure 5.9, a, b*) [94]. As shown in *Figure 5.8 c, d*, the milder effect of *S. copri* R-LPS is particularly evident within this specific monocyte subset. Overall, these findings confirm that the immune system differently responds to the two chemically different LPSs even at very low doses. The pro-inflammatory *E. coli* LPS, even at minimal concentrations, immediately triggers innate immune activation, leading to a reorganization of immune functions that favor pro-inflammatory responses. In contrast, the microbiota-derived *S. copri* LPS does not induce the "down-regulation" of the CD14+CD16+ population. At lower concentrations, this immune homeostasis is only mildly affected, suggesting the existence of a sort of "tolerability threshold", rooted in its different chemical composition. The stability in CD14+CD16+ population provides strong evidence of this tolerance, as these cells play a central role in immune surveillance. Upon higher LPS concentrations, innate immune alert mechanisms are activated, triggering a response characteristic of early host defense.

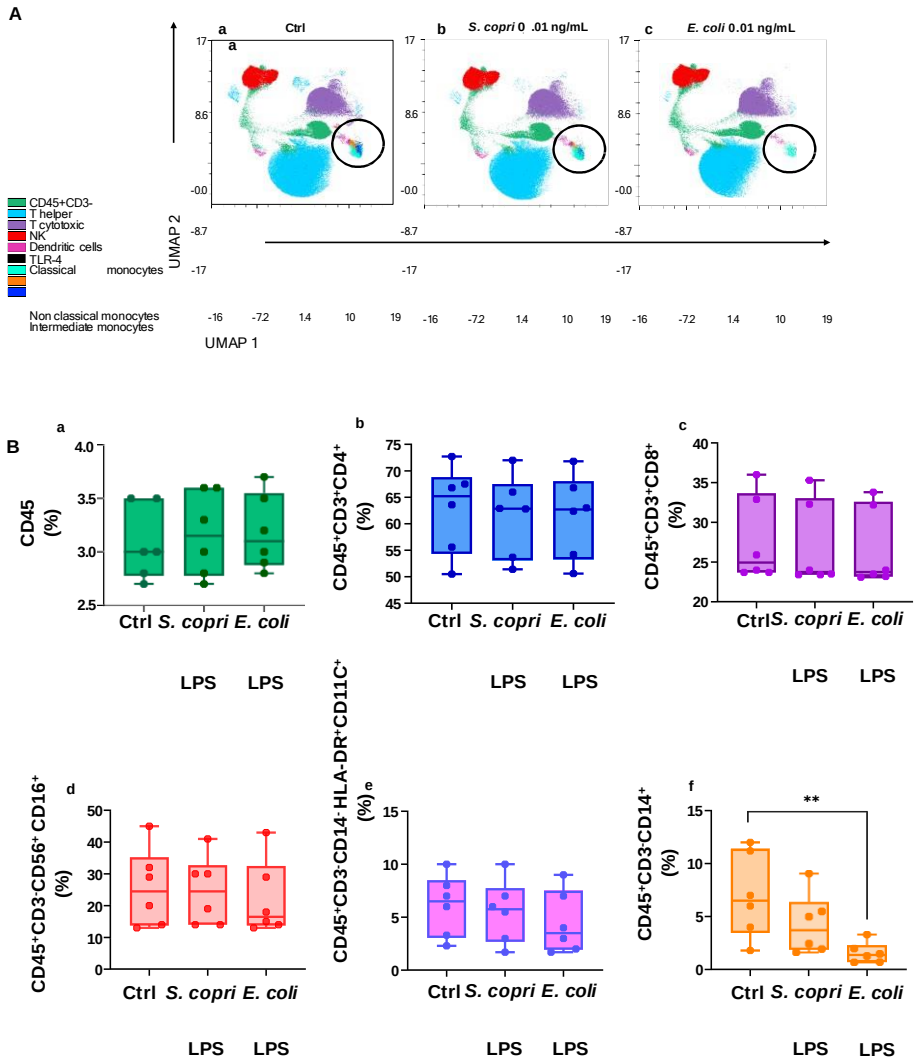

Figure 5.8: PBMCs immunophenotyping. (A) UMAP representation of the main PBMCs populations obtained with CyTOF analysis. Clustering was performed on live cells singlets after quality control and marker selection showed in gating strategy. Graphs represent the untreated control (plot a), PBMCs treated with *S. copri* R-LPS 0.01 ng/ml (plot b) and with *E. coli* LPS 0.01 ng/mL (plot c). (B) Graphic representation of the main PBMCs subpopulations identified with CyTOF analysis: (a) CD3+/CD3- ratio; (b) T helper, (c) T cytotoxic, (d) natural killer, (e) dendritic cells, (f) monocytes. Graphs represent the

mean +/- standard deviation of 6 samples. Statistical analysis was performed by Friedman test with Dunn's post hoc correction. **p-value< 0.01.

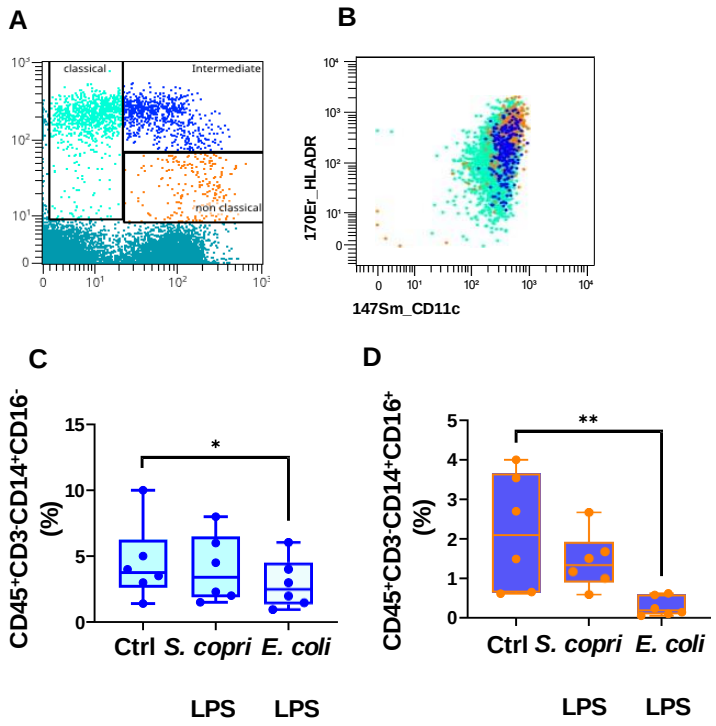

Figure 5.9: Monocytes subsets: (A) Graphic representation of the main monocyte phenotypes: in the Up/Left square the light green population represents the classical monocytes subset (CD14++ CD16-); in the Up/Right square the blue population represents the CD14++CD16+ cells known as intermediate monocytes; in the Low/Right square the orange population represents the CD14+CD16+ subset called non-classical monocytes. (B) Graphical representation of HLA-DR and CD11c expression levels across the three monocyte subsets; non-classical (blu) and intermediate (orange) monocytes display the highest expression levels of both markers. (C) Mean % of CD45+CD14+CD16- (D) Mean % of CD45+CD14+CD16+ monocytes expression of the 6 experiments conducted; Statistical analysis was performed by Friedman test with Dunn's post hoc correction. **p-value< 0.01.

5.8 Conclusion

The *Segatella* genus, especially *S. copri* (formerly *Prevotella copri*), is prevalent in

the gut microbiota of non-Westernized populations [95]. Its impact on health remains

debated, with both beneficial and detrimental roles proposed. Decoding the chemical and immunological characteristics of *S. copri* LPS may clarify this "Segatella paradox" and help distinguish features underlying beneficial versus pathogenic host interactions. Using high-resolution mass spectrometry, NMR spectroscopy, and immune phenotyping, *S. copri* R-LPS was shown to differ markedly from typical enterobacterial LPS in structure and immune activity [27], [96].

Structurally, *S. copri* LPS exhibits a rough phenotype, lacking the O-antigen and possessing a core OS mainly composed of glucose and mannose branched from a Kdo residue modified at O-4 by PEtN. Unlike enterobacteria, where L-*glycero*-D-*manno*-heptose is conserved, *S. copri* features α-mannose as the first sugar linked to Kdo, consistent with other Bacteroidetes [97], [98], [99]. A distinctive α-1,2-linked terminal di-mannose at the non-reducing end, common in diverse microbes, may interact with C-type lectins such as DC-SIGN, acting as an "immunological flag" that modulates immune responses independently or alongside TLR4 signaling [100], [101].

The lipid A domain exhibits extensive heterogeneity, predominantly *mono*-phosphorylated tetra- and penta-acylated forms, with minor *bis*-phosphorylated variants. This contrasts with related species like *P. intermedia* and *P. denticola*, which show simpler, more uniform lipid A profiles [98], [102]. Genomic analyses revealed multiple glycosyltransferases and lipid A-modifying enzymes, including two LpxA isoforms predicted by AlphaFold3, potentially explaining lipid A structural diversity and its role in fine-tuning host immunity.

Functionally, *S. copri* R-LPS showed attenuated TLR4 agonism, limited engagement of TLR2 and TLR2/1, and weak NF-κB activation with minimal TNF-α production in macrophage-like THP-1 cells compared to *E. coli* LPS. It also inhibited *E. coli* LPS-induced TLR4 activation, suggesting competitive receptor binding without strong signaling. In PBMCs, it induced modest cytokine responses and selectively preserved $CD14^{+}CD16^{+}$ monocytes, subsets critical for immune surveillance and inflammation

resolution, contrasting with their depletion by *E. coli* LPS. **This profile suggests *S. copri* R-LPS fosters immune tolerance while retaining capacity to modulate immunity if needed.** These findings highlight the unique chemical and immunological nature of *S. copri* R-LPS and support its role in shaping balanced host-microbiota interactions. By linking LPS structure to immune outcomes, this work advances understanding of gut microbial molecules as mediators of host communication and suggests potential for microbiota-inspired immunomodulatory therapies.

References

[75] T. C. A. Hitch *et al.*, "A taxonomic note on the genus Prevotella: Description of four novel genera and emended description of the genera Hallella and Xylanibacter," *Syst Appl Microbiol*, vol. 45, no. 6, p. 126354, Nov. 2022, doi: 10.1016/j.syapm.2022.126354.

[76] B. Domon and C. E. Costello, "A systematic nomenclature for carbohydrate fragmentations in FAB-MS/MS spectra of glycoconjugates," *Glycoconj J*, vol. 5, no. 4, pp. 397–409, 1988, doi: 10.1007/BF01049915.

[77] J. Mistry *et al.*, "Pfam: The protein families database in 2021," *Nucleic Acids Res*, vol. 49, no. D1, pp. D412–D419, Jan. 2021, doi: 10.1093/nar/gkaa913.

[78] A. N. Jacobson, B. P. Choudhury, and M. A. Fischbach, "The Biosynthesis of Lipooligosaccharide from *Bacteroides thetaiotaomicron*," *mBio*, vol. 9, no. 2, May 2018, doi: 10.1128/mBio.02289-17.

[79] S. M. Galloway and C. R. Raetz, "A mutant of Escherichia coli defective in the first step of endotoxin biosynthesis.," *J Biol Chem*, vol. 265, no. 11, pp. 6394–402, Apr. 1990.

[80] A. H. Williams and C. R. H. Raetz, “Structural basis for the acyl chain selectivity and mechanism of UDP- *N* -acetylglucosamine acyltransferase,” *Proceedings of the National Academy of Sciences*, vol. 104, no. 34, pp. 13543–13550, Aug. 2007, doi: 10.1073/pnas.0705833104.

[81] J. Abramson *et al.*, “Accurate structure prediction of biomolecular interactions with AlphaFold 3,” *Nature*, vol. 630, no. 8016, pp. 493–500, Jun. 2024, doi: 10.1038/s41586-024-07487-w.

[82] D. Álvarez-Salmoral, R. Borza, R. Xie, R. P. Joosten, M. L. Hekkelman, and A. Perrakis, “AlphaBridge: tools for the analysis of predicted macromolecular complexes,” Oct. 26, 2024. doi: 10.1101/2024.10.23.619601.

[83] J. S. Lam, V. L. Taylor, S. T. Islam, Y. Hao, and D. Kocíncová, “Genetic and Functional Diversity of Pseudomonas aeruginosa Lipopolysaccharide,” *Front Microbiol*, vol. 2, 2011, doi: 10.3389/fmicb.2011.00118.

[84] D. E. Heinrichs, M. A. Monteiro, M. B. Perry, and C. Whitfield, “The Assembly System for the Lipopolysaccharide R2 Core-type ofEscherichia coli Is a Hybrid of Those Found inEscherichia coli K-12 and Salmonella enterica,” *Journal of Biological Chemistry*, vol. 273, no. 15, pp. 8849–8859, Apr. 1998, doi: 10.1074/jbc.273.15.8849.

[85] P. Garcia-Vello *et al.*, “The lipooligosaccharide of the gut symbiont Akkermansia muciniphila exhibits a remarkable structure and TLR signaling capacity,” *Nat Commun*, vol. 15, no. 1, p. 8411, Sep. 2024, doi: 10.1038/s41467-024-52683-x.

[86] F. Di Lorenzo *et al.*, “Pairing *Bacteroides vulgatus* LPS Structure with Its Immunomodulatory Effects on Human Cellular Models,” *ACS Cent Sci*, vol. 6, no. 9, pp. 1602–1616, Sep. 2020, doi: 10.1021/acscentsci.0c00791.

[87] K. Verhoeckx *et al.*, Eds., *The Impact of Food Bioactives on Health*. Cham: Springer International Publishing, 2015. doi: 10.1007/978-3-319-16104-4.

[88] I. Zanoni *et al.*, “CD14 Controls the LPS-Induced Endocytosis of Toll-like Receptor 4,” *Cell*, vol. 147, no. 4, pp. 868–880, Nov. 2011, doi: 10.1016/j.cell.2011.09.051.

[89] G. D. Thomas *et al.*, “Human Blood Monocyte Subsets,” *Arterioscler Thromb Vasc Biol*, vol. 37, no. 8, pp. 1548–1558, Aug. 2017, doi: 10.1161/ATVBAHA.117.309145.

[90] Y. Iwahashi, Y. Ishida, N. Mukaida, and T. Kondo, “Pathophysiological Roles of the CX3CL1-CX3CR1 Axis in Renal Disease, Cardiovascular Disease, and Cancer.,” *Int J Mol Sci*, vol. 26, no. 11, Jun. 2025, doi: 10.3390/ijms26115352.

[91] K. L. Wong *et al.*, “Gene expression profiling reveals the defining features of the classical, intermediate, and nonclassical human monocyte subsets,” *Blood*, vol. 118, no. 5, pp. e16–e31, Aug. 2011, doi: 10.1182/blood-2010-12-326355.

[92] P. Vishnyakova *et al.*, “The response of two polar monocyte subsets to inflammation,” *Biomedicine & Pharmacotherapy*, vol. 139, p. 111614, Jul. 2021, doi: 10.1016/j.biopha.2021.111614.

[93] H. Zhong *et al.*, “CD16+ monocytes control T-cell subset development in immune thrombocytopenia.,” *Blood*, vol. 120, no. 16, pp. 3326–35, Oct. 2012, doi: 10.1182/blood-2012-06-434605.

[94] S. R. Aguilar-Ruiz *et al.*, “Human CD16+ and CD16– monocyte subsets display unique effector properties in inflammatory conditions in vivo,” *J Leukoc Biol*, vol. 90, no. 6, pp. 1119–1131, Sep. 2011, doi: 10.1189/jlb.0111022.

[95] M. Valles-Colomer *et al.*, “The person-to-person transmission landscape of the gut and oral microbiomes,” *Nature*, vol. 614, no. 7946, pp. 125–135, Feb. 2023, doi: 10.1038/s41586-022-05620-1.

[96] F. Di Lorenzo, C. De Castro, A. Silipo, and A. Molinaro, “Lipopolysaccharide structures of Gram-negative populations in the gut microbiota and effects on host

interactions," *FEMS Microbiol Rev*, vol. 43, no. 3, pp. 257–272, May 2019, doi: 10.1093/femsre/fuz002.

[97] M. D. Pither *et al.*, "Bacteroides thetaiotaomicron rough-type lipopolysaccharide: The chemical structure and the immunological activity," *Carbohydr Polym*, vol. 297, p. 120040, Dec. 2022, doi: 10.1016/j.carbpol.2022.120040.

[98] F. Di Lorenzo *et al.*, "*Prevotella denticola* Lipopolysaccharide from a Cystic Fibrosis Isolate Possesses a Unique Chemical Structure," *European J Org Chem*, vol. 2016, no. 9, pp. 1732–1738, Mar. 2016, doi: 10.1002/ejoc.201600037.

[99] O. Holst, "The structures of core regions from enterobacterial lipopolysaccharides â€“ an update," *FEMS Microbiol Lett*, vol. 271, no. 1, pp. 3–11, Jun. 2007, doi: 10.1111/j.1574-6968.2007.00708.x.

[100] M. D. Pither *et al.*, "Deciphering the Chemical Language of the Immunomodulatory Properties of *Veillonella parvula* Lipopolysaccharide," *Angewandte Chemie International Edition*, vol. 63, no. 17, Apr. 2024, doi: 10.1002/anie.202401541.

[101] F. Nieto-Fabregat *et al.*, "Atomic-Level Dissection of DC-SIGN Recognition of *Bacteroides vulgatus* LPS Epitopes," *JACS Au*, vol. 4, no. 2, pp. 697–712, Feb. 2024, doi: 10.1021/jacsau.3c00748.

[102] M. Hashimoto, Y. Asai, R. Tamai, T. Jinno, K. Umatani, and T. Ogawa, "Chemical structure and immunobiological activity of lipid A from *Prevotella intermedia* ATCC 25611 lipopolysaccharide," *FEBS Lett*, vol. 543, no. 1–3, pp. 98–102, May 2003, doi: 10.1016/S0014-5793(03)00414-9.

Chapter VI
Phocaiocola vulgatus

Phocaeicola vulgatus is a key member of the human gut microbiota, involved in complex interactions within the intestinal environment. In this study, carried out in collaboration with Professor Laurie Comstock (University of Chicago), we analyzed the structure of LPS from several *P. vulgatus* strains mutated into the LPS biosynthetic pathway with the final goal of defining the key epitopes involved in the binding with key antibacterial toxins produced by the bacterium (BcpT and BSAP-3).

6.1 Introduction

The human gut microbiota is currently the focus of extensive research due to its crucial role in supporting various health-related functions and its involvement in multiple pathological processes. *Phocaeicola vulgatus* (formerly *Bacteroides vulgatus*) is among the most abundant species in the gut microbiota [103], with members of this order establishing stable colonization of the human intestine. In industrialized populations in particular, this bacterium is commonly found within the same individual in the form of multiple, genetically distinct strains [103]. Overall, gut microbiota represents a highly complex and dynamic ecosystem. Despite growing interest, we are still in the early stages of understanding the mechanisms that regulate intestinal homeostasis, as well as the microbiota's resilience to external disturbances and its interactions during colonization processes. Gut symbionts such as *P. vulgatus* have strains and have evolved sophisticated strategies to compete within the intestinal environment [103]. Among these, the production of

antibacterial toxins, and the corresponding resistance mechanisms, represents a key competitive strategy that enhances bacterial fitness by enabling them bacteria to secure space and resources within the microbial community [103]. These bacterial toxins act as essential tools in both inter- and intraspecies competition, promoting colonization by certain strains at the expense of others. In parallel, bacteria have developed defensive strategies to protect themselves against the toxins produced by competitors. Recent studies on the *Phocaeicola* genus have identified several antibacterial toxins produced by *P. vulgatus* and its closely related species *P. dorei*, including BcpT and BSAP-3. These toxins selectively bind to glycan regions of the bacterial lipopolysaccharide (LPS), which they use as molecular receptors to exert their cytotoxic effects [103].

Focusing on the BcpT toxin specifically, it is encoded by a small, mobile plasmid found exclusively in *P. vulgatus* and *P. dorei*. Its activation mechanism involves proteolytic cleavage at two distinct sites within the protein, mediated by specific bacterial proteases [103]. Once activated, BcpT recognizes the glycan core of LPS, as its receptor, highlighting a close relationship between glycan structure and bacterial susceptibility to the toxin [103]. However, the exact regions of the LPS that serve as receptors for BcpT and BSAP-3—as well as the genetic modifications that confer resistance to these toxins—have yet to be fully elucidated. Some bacterial strains can rapidly trigger a defensive response through a sigma/anti-sigma regulatory system (EcfO/Reo) [103], which senses outer membrane stress and induces protective gene expression. Of note, upon activation by toxin binding, this system drives the transcription of genes involved in the synthesis of modified LPS molecules, which in turn may hinder toxin binding to its ligand. In this context Therefore, lipopolysaccharides **LPS are not only central to host–microbe interactions but also play a key role in shaping microbial antagonism and competition within the gut**.

It is important to note that previous studies conducted by Prof. Di Lorenzo have elucidated the complete structure of the LPS from a *P. vulgatus* strain isolated from the mouse intestine (strain *mpk*) [86]. Building on this work, my primary objective has been to define and compare the structure of the LPS from a wild-type *P. vulgatus* strain isolated from humans (provided by Prof. Comstock) with that of the previously published murine isolate. Following this, I focused on analyzing structural mutations in the LPS. To this end, I also examined five mutants, resolving the structure of their LPS core oligosaccharides using chemical analyses and NMR spectroscopy. It is important to note that previous studies conducted by Prof. Di Lorenzo have disclosed the full structure of the LPS from a *P. vulgatus* strain isolated from mouse intestine (strain *mpk*). For this reason, my aim has been first to define and compare the structure of the *P. vulgatus* wild-type strain human isolate and compare it with the one previasouly published for murine isolate. Then on the analysis of LPS structural mutations. Therefore, I examined one wild-type strain and five mutants derived from it, by resolving the structure of their LPS core OS through NMR spectroscopy. These analyses aim to provide a foundation for future investigations into how structural modifications in LPS affect recognition by antibacterial toxins. Ultimately, this work will contribute to a deeper understanding of the central role of LPS as a strategic point of communication between bacteria and the host, as well as its importance in determining microbial fitness within the highly competitive environment of the human gut.

6.2 Results and Discussion

In the present chapter, we report the structural characterization of the LPSs from a total of five strains of *Phocaeicola vulgatus*: one wild-type human isolate (*PVCL10T00C06*, referred to as *WT*), and four mutants derived from this: *ΔM0N98_0427*, *ΔM0N98_0428-29*, *PVCL09T03C04*, and *ΔAntisigma*. The primary objective of this study was to identify LPS regions that may act as molecular targets

for the antibacterial toxins BSAP-3 and BcpT. The LPS was extracted from lyophilized bacterial cells using an optimized protocol designed to ensure high purity. The extraction process, which will be described in full detail in Chapter XI, paragraph 11.2 included multiple purification steps involving enzymatic hydrolysis, dialysis, molecular size exclusion chromatography, and ultracentrifugation. Purity levels were assessed by SDS-PAGE followed by silver staining. Following purification, all LPS samples underwent monosaccharide derivatization followed by GC-MS analysis to support NMR data interpretation. Deacylation was then performed, and an aliquot of the purified, deacylated LPS from the *WT* human isolate and from each of the five mutant strains was analyzed by via 1D and 2D NMR spectroscopy. The *WT* human isolate was directly compared with the murine isolate *Bacteroides P. vulgatus* mpk, previously caracterized by Di Lorenzo *et al.* (2020). Remarkably, the core oligosaccharide (*OS*) structure of the human-derived *PVCL10T00C06* strain was found to be identical to that of the murine strain. This structural overlap validated the use of the previously published glycan architecture as a reference for analyzing the human *WT* and its mutants. The NMR analysis employed a comprehensive set of experiments including: ^{1}H NMR, ^{13}C HSQC, DQF-COSY, TOCSY, NOESY, ROESY, ^{1}H,^{13}C HMBC, and ^{31}P and ^{1}H,^{31}P HSQC. Spin systems corresponding to individual sugar residues were assigned based on scalar connectivity observed in DQF-COSY and TOCSY spectra. ^{13}C chemical shifts were identified using HSQC, while the anomeric configuration of each sugar unit was determined by NOE contacts and $^{3}J_{\text{H-1,H-2}}$ coupling constants. Relative stereochemistry was inferred from vicinal $^{3}J_{\text{H,H}}$ values. Further structural detail was confirmed through inter-residual NOEs (NOESY, ROESY) and long-range correlations in the HMBC spectra. The position of phosphate groups within the glycan structure was elucidated via ^{31}P and ^{1}H,^{31}P HSQC experiments. For the *WT* strain, the following anomeric signals and assignments were identified in the *Figure 6.1 and Table 6.1*. In the ^{1}H NMR spectrum, eleven anomeric signals corresponding to eleven spin systems (**A**–**L**) were identified. The Kdo unit (**K**) was confirmed by

its characteristic methylene signals at δ^{H} 1.69 and 2.73 ppm. All sugar residues—, except for residue **D**—, were found in the pyranose form, while **D** was identified as a β-galactofuranose, based on ^{13}C chemical shifts and HMBC correlations. Spin systems **A** and **B** were assigned to α- and β-GlcN units of the lipid A backbone. The positions of phosphate groups were confirmed through ^{31}P and $^{1}H,^{31}P$ HSQC experiments. Rhamnopyranose residues were attributed to spin systems **C**, **G**, and **I**; their configurations were defined through $^{3}J^{H_1,H_2}$ coupling constants and NOE data. Residues **E** and **H** were identified as α-fucopyranose (α-Fucp) and β-galactopyranose (β-Galp), respectively. Residue **F** was assigned to a β-glucopyranose (β-Glcp), and **L** to a β-mannopyranose (β-Manp). The structural features and linkage positions of each residue were clarified using a combination of scalar couplings, NOESY, ROESY, and HMBC spectra. The repeating unit of the O-antigen was composed of residues **I** and **L**, with **I** (α-RhaOC) linked to **L** (β-Manp) via (→3) and (←4) glycosidic linkages.

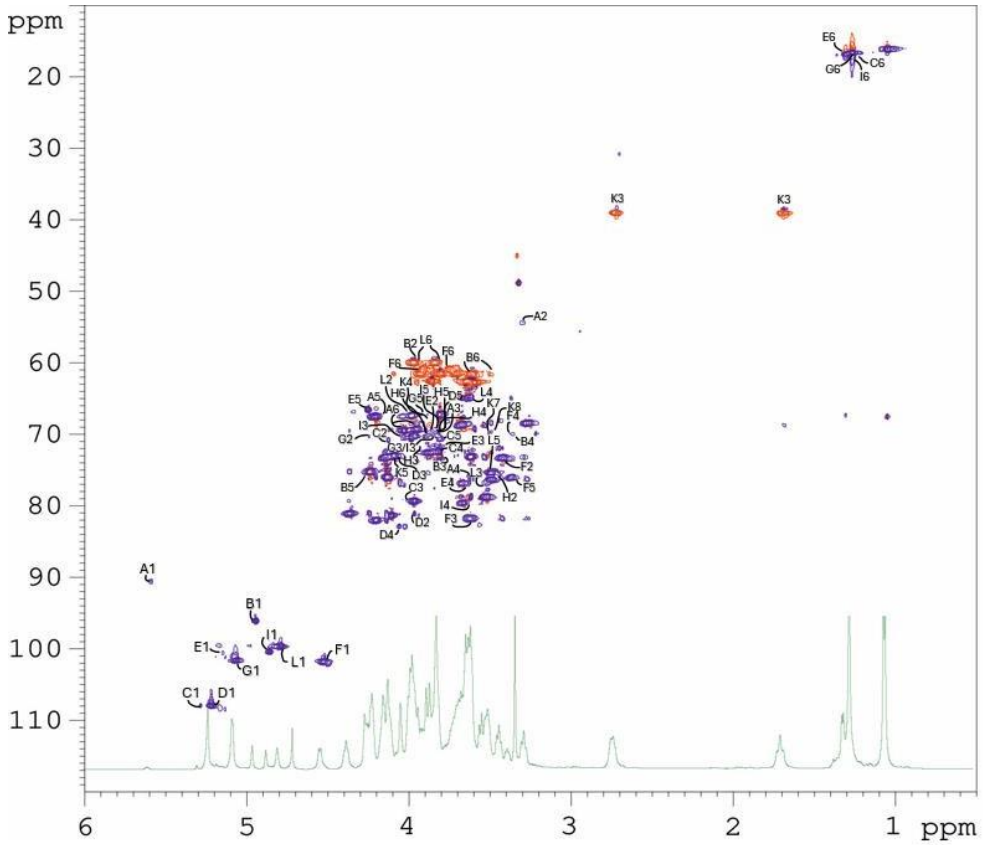

Figure 6.1: Structural characterization of deacylated LPS from *P. vulgatus PVCL10T00C06* by NMR (600 MHz, 298 K, in D_2O). ^1H (in green) and ^1H, ^{13}C HSQC spectra (positive in blue, negative in/ red) of the saccharide moiety obtained after complete deacylation of the LPS. Main one-bond heteronuclear correlations and assigned chemical shifts are indicated.

		Chemical Shift						
		1	2	3	4	5	6	7
	A, 6-α-GlcpN	5.50	3.20	3.85	3.63	4.21	4.21/3.94	
		90.4	54.5	69.7	73.2	67.7	68.9	
	B, 6-β-GlcpN	4.86	3.98	3.81	3.37	4.25	3.61/3.49	
		96.1	59.4	72.5	70.0	75.3	61.6	
	C, 3,4-α-Rhap (α-Rhal)	5.14	4.14	4.03	3.85	3.85	1.26	
		107.9	69.7	79.1	75.5	67.3	16.7	
	D, t-β-Galf	5.08	3.94	4.03	4.03	3.81	3.61	
		108.5	81.2	77.2	82.9	70.7	62.3	
	E, t-α-Fucp	5.12	3.94	3.80	3.63	4.25	1.13	
		101.1	69.2	71.5	73.3	66.6	16.9	
	F, 3-β-Glcp	4.48	3.42	3.63	3.35	3.35	3.92/3.74	
		102.3	73.4	81.9	70.0	76.0	60.9	
	G, t-α-Rhap (α-RhaII)	4.99	4.25	3.85	3.42	3.95	1.26	
		01.34	70.3	69.6	72.0	67.4	16.8	
	H, 2,6-β-Galp	4.72	3.44	3.77	3.81	3.72	3.93	
		ND	76.3	72.5	69.2	70.8	69.5	
	I, 4-α-Rhap (α-RhaOC)	4.78	4.25	3.95	3.66	3.76	1.26	
		100.4	70.6	70.2	79.7	67.3	17.3	
	L, 3-β-Manp	4.73	4.04	3.54	3.61	3.49	3.97/3.84	
		100.5	67.6	76.8	65.0	76.4	60.1	
	K, 5-α-Kdop			2.73/1.69	4.14	4.03	3.49	3.51
				39.1	67.5	73.0	69.72	70.3

Table 6.1: Chemical shifts (δ, ppm) of the proton (^1H) and carbon (^13C) nuclei assigned to the saccharide residues of the deacylated LPS from *Phocaeicola vulgatus PVCL10T00C06.*

The same analytical methodology was applied to the remaining mutants, and all structures were defined and sketched in *Figure 6.2*

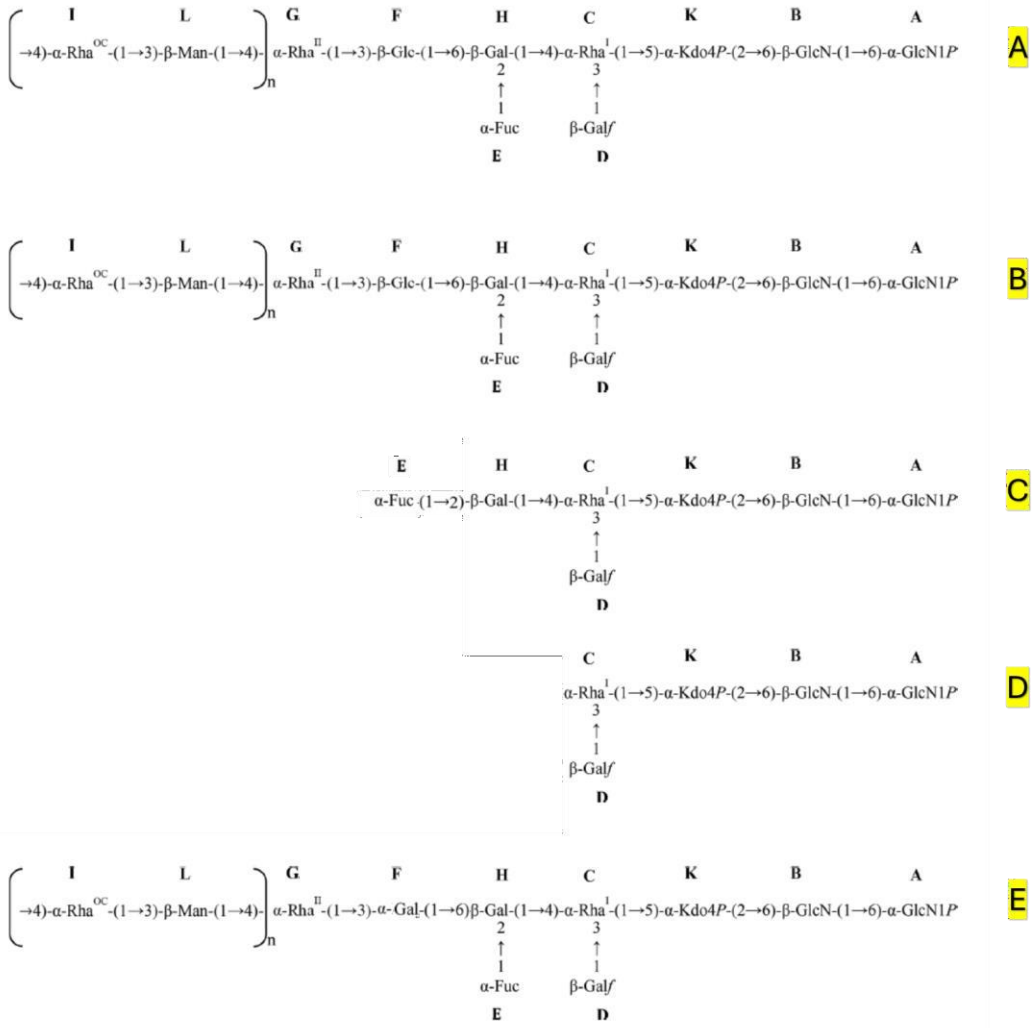

Figure 6.2: Structural comparison of deacylated LPS from *Phocaeicola vulgatus* wild-type **A)** *PVCL10T00C06* and mutants **D)** *ΔM0N98_0427* **C)** ΔM0N98_0428-29 **B)** *ΔAntisigma*, and **E)** *PVCL09T03C04*) by NMR spectroscopy ^{1}H and $^{1}H,^{13}C$-HSQC NMR spectra (600 MHz, 298 K, in D_2O).

Specifically, the analysis focused on two out of four mutants that were confirmed that two out of four mutants to possess a structure shorter than that of the wild-type (WT), namely *ΔM0N98_0427* and *ΔM0N98_0428-29*. The mutant *PVCL09T03C04* was confirmed to carry a substitution of only one sugar unit: more precisely, the F monosaccharide (β-Glc) is replaced by an α-Gal residue. Finally, the *ΔAntisigma* mutant exhibits a structure characterized by an increased number of repeating disaccharide units forming the O-antigen of the LPS portion. The two mutants that differ from the WT due to them with a shorter structure, as previously mentioned, are *ΔM0N98_0427* (*Figure 6.3 and Table 6.2*) and *ΔM0N98_0428-29* (*Figure 6.4 and Table 6.3*). These are composed of a total of five spin systems (**A**, **B**, **C**, **D**, and **K**) and seven spin systems (**A**, **B**, **C**, **D**, **E**, **H**, and **K**), respectively. The details of the assignments and chemical shifts are provided in the corresponding figures reporting HSQC spectra.

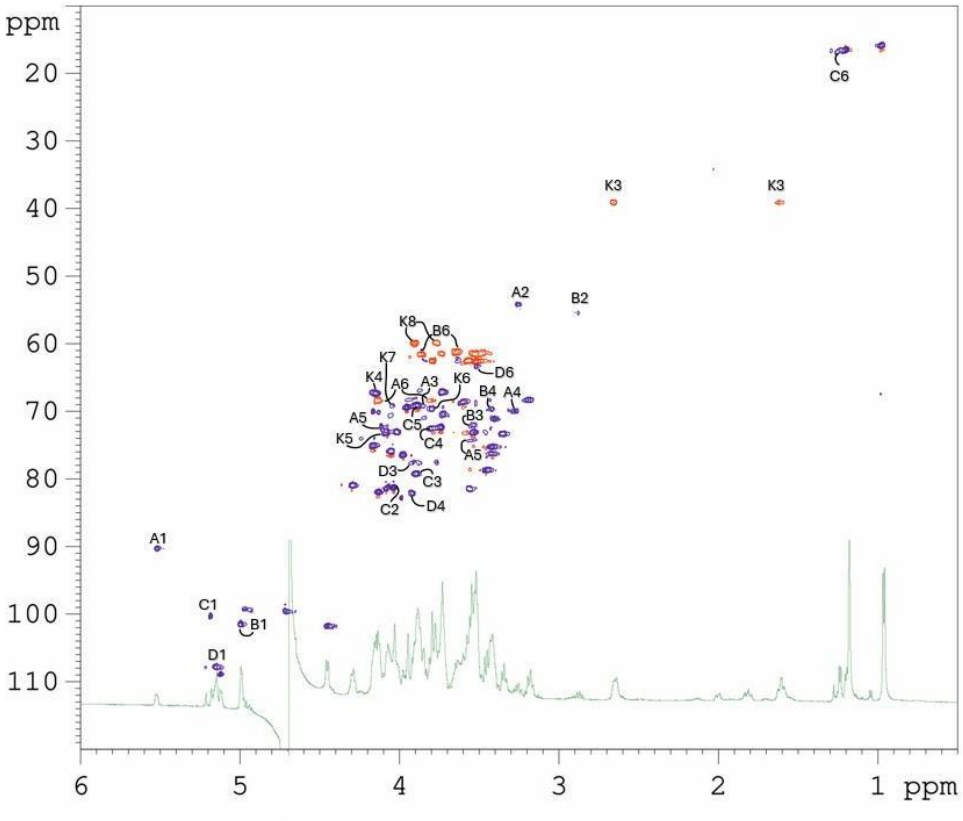

Figure 6.3: Structural characterization of deacylated LPS from *P. vulgatus ΔM0N98_0427* by NMR (600 MHz, 298 K, in D_2O). ^1H (in green) and ^1H, ^{13}C HSQC spectra (positive in blue, negative in/ red) of the saccharide moiety obtained after complete deacylation of the LPS. Main one-bond heteronuclear correlations and assigned chemical shifts are indicated.

	Chemical Shift							
	1	2	3	4	5	6	7	8
A, 6-α-GlcpN	5.51	3.25	3.81	3.26	4.08	4.12/3.81		
	90.3	54.2	69.8	69.2	73.0	68.5		
B, 6-β-GlcpN	4.97	2.89	3.53	3.42	3.53	3.87/3.72		
	99.1	54.8	72.0	69.7	74.3	61.5		
C, 3,4-α-Rhap (α-Rhal)	5.18	4.03	3.89	3.79	3.89	1.25		
	100.3	81.3	79.3	72.5	69.1	16.9		
D, t-β-Galf	5.14	4.08	3.92	3.91	3.72	3.56		
	107.9	81.6	77.8	82.2	70.3	63.3		
K, 5-α-Kdop			1.61/2.65	4.15	4.08	3.72	4.05	3.91/3.76
			39.2	67.3	73.1	70.4	70.6	59.9

Table 6.2: Chemical shifts (δ, ppm) of the proton (^{1}H) and carbon (^{13}C) nuclei assigned to the saccharide residues of the deacylated LPS from *Phocaeicola vulgatus ΔM0N98_0427*

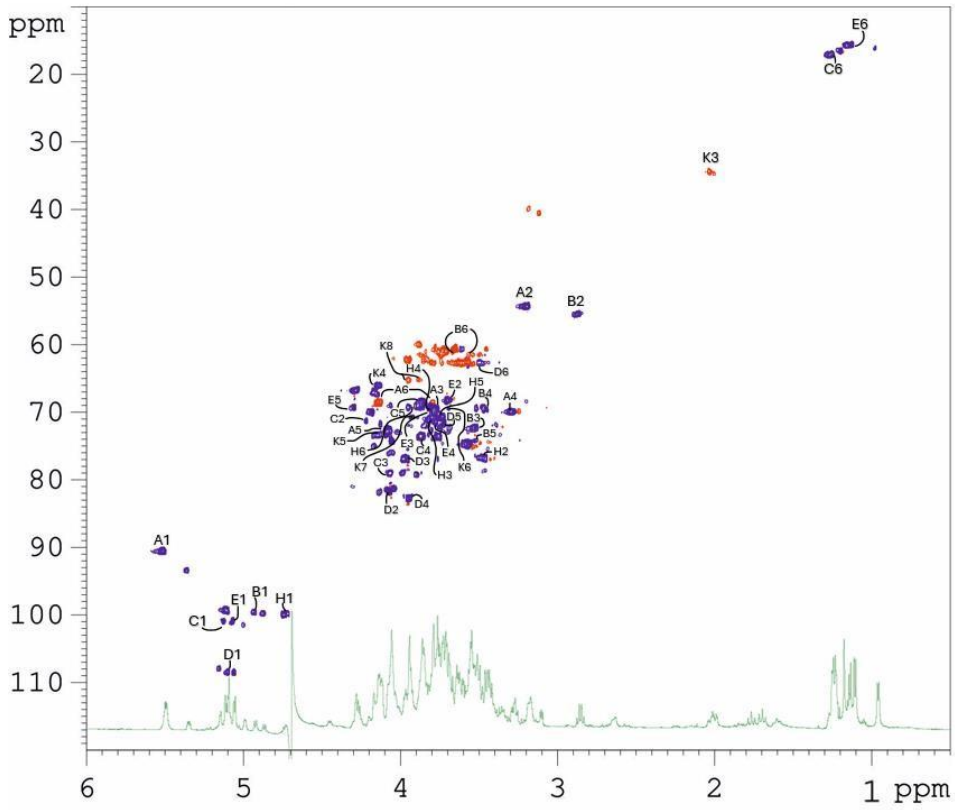

Figure 6.4: Structural characterization of deacylated LPS from *P. vulgatus ΔM0N98_0428-29* by NMR (600 MHz, 298 K, in D_2O). ^1H (in green) and ^1H, ^{13}C HSQC spectra (positive in blue, negative in and red) of the saccharide moiety obtained after complete deacylation of the LPS. Main one-bond heteronuclear correlations and assigned chemical shifts are indicated.

	Chemical Shift							
	1	2	3	4	5	6	7	8
A, 6-α-GlcpN	5.51	3.19	3.80	3.28	4.08	4.12/3.79		
	90.6	54.4	69.2	70.0	73.1	68.4		
B, 6-β-GlcpN	4.93	2.87	3.50	3.44	3.86	3.62/3.47		
	99.6	55.5	72.3	69.7	68.7	61.3		
C, 3,4-α-Rhap (α-Rhal)	5.12	4.17	4.06	3.86	3.86	1.24		
	99.4	70.0	79.0	73.6	68.7	17.1		
D, t-β-Galf	5.09	4.06	3.95	3.94	3.73	3.56		
	108.5	81.7	77.0	82.8	70.6	62.8		
E, t-α-Fucp	5.06	3.69	3.77	3.77	4.29	1.12		
	101.0	68.3	71.5	73.0	69.3	15.64		
H, 2,6-β-Galp	4.73	3.45	3.77	3.77	3.73	3.95		
	100.0	76.9	71.46	69.7	70.7	69.4		
K, 5-α-Kdop			ND/2.02	4.15	4.13	3.69	3.91	3.95/3.88
			34.5	67.3	73.4	69.7	70.8	65.33

Table 6.3: Chemical shifts (δ, ppm) of the proton (^1H) and carbon (^{13}C) nuclei assigned to the saccharide residues of the deacylated LPS from *Phocaeicola vulgatus ΔM0N98_0428-29*

Unlike the previously analyzed strains, where variations involved the length of the sugar chains, as previously mentioned, the mutant *PVCL09T03C04 Figure 6.4* and *Table 5.4* shows a change in sugar composition: an α-Gal residue replaces the typical β-Glc residue found in the other strains. Although functional results are still pending, this variation could significantly affect the interaction between LPS and bacterial protein toxins, opening new hypotheses about the specific role of this monosaccharide in toxin recognition and neutralization.

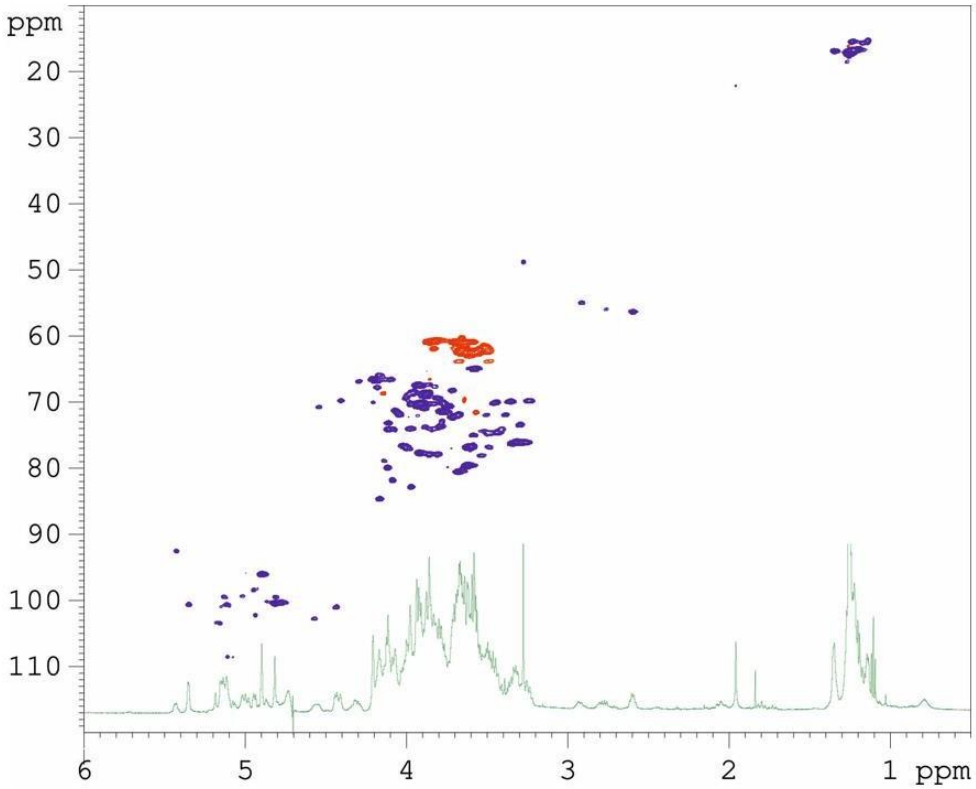

Figure 6.5: Structural characterization of deacylated LPS from *P. vulgatus PVCL09T03C04* by NMR (600 MHz, 298 K, in D_2O). ^1H (in green) and ^1H, ^{13}C HSQC spectra (positive in blue, negative in red) of the saccharide moiety obtained after complete deacylation of the LPS. Main one-bond heteronuclear correlations and assigned chemical shifts are indicated.The signals related to the sole sugar residue different from the WT structure has been reported.

Regarding the last mutant, *ΔAntisigma*, structural investigation was carried out following the same approach as for the other strains. However, unlike the previously analyzed mutants, *ΔAntisigma*in this case this mutant exhibits exhibited an LPS significantly longer not only than the other mutants but also than compared to the wild-type WT strain. This increased length is attributable to a greater number of O-antigen repeating units, which in this case consist of a disaccharide composed of α-

Rha (1→3) β-Man. To identify and quantify these repeating units, the deacylated LPS of *ΔAntisigma* was analyzezd by high-performance liquid chromatography (HPLC) (*Figure 6.5*). Before comparing the molecular weight of the WT strain *PVCL10T00C06* with that of *ΔAntisigma*, a calibration curve was established by injecting four dextran standards of known molecular weight. Following this, the deacylated LPS samples from both *PVCL10T00C06* the WT and *ΔAntisigma* were injected, and their molecular weights were estimated based on their retention times. The LPS of from the WT *PVCL10T00C06* was found to have a molecular weight of approximately 6,047 Da, while that of *ΔAntisigma* was approximately 10,036 Da. By subtracting the molecular weight of the WT LPS from that of the *ΔAntisigma* mutant (10,036 Da – 6,047 Da), the additional mass attributable to the extra repeating units was calculated to be 3,989 Da. Given that each O-antigen repeating unit—, composed of α-Rha and β-Man—, has an approximate molecular weight of 308 Da, it was estimated that *ΔAntisigma* carries approximately 13 additional disaccharide units relative to the WT strain (3,989 / 308 ≈ 12.95).

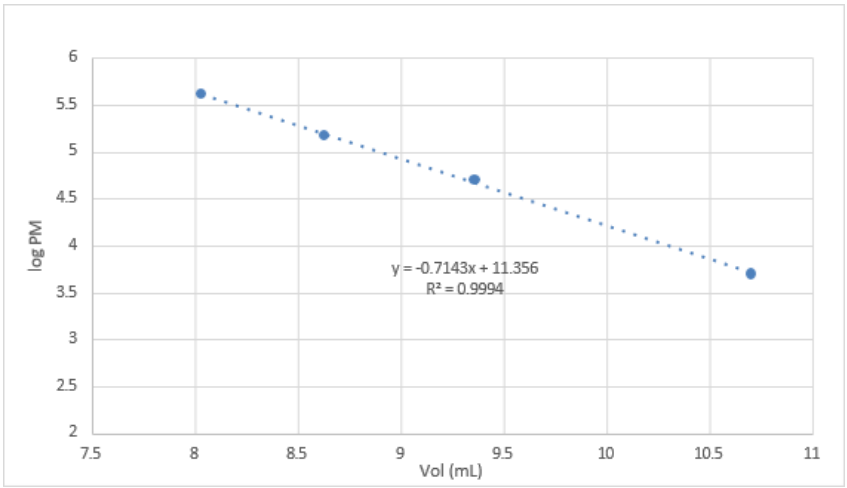

Figure 6.6: Calibration curve obtained from four dextran standards used to estimate the molecular weight of deacylated LPS from WT and *ΔAntisigma* strains

6.3 Conclusions and future perspective

The results obtained so far confirm the critical importance of LPS structure in determining the susceptibility or resistance of *Phocaeicola vulgatus* strains to bacterial toxins such as BcpT and BSAP-3. Variations in LPS sugar chain composition and length, as well as the presence or substitution of specific monosaccharide units, are key factors in modulating toxin recognition. This once again highlights the relevance of LPS structural diversity and how a tight structure–function relationship is fundamental to understanding the defensive strategies adopted by these bacteria within the competitive gut environment. Focusing specifically on the mutants whose structures have been resolved and described in this section, the first two mutants—, *ΔM0N98_0427* and *ΔM0N98_0428-29*—, were found to be shorter than the original wild-type strain *PVCL10T00C06* (human isolate). Despite their conserved sugar composition, the reduced length of these mutants may impair toxin recognition, potentially offering early insight into the concept of a "minimal recognition length" required for effective toxin–LPS interaction. It remains to be clarified whether the key determinant of recognition lies solely in the composition of the LPS saccharide chain at the core oligosaccharide level, or whether it may also be influenced by the overall chain length, which could sterically hinder the toxin's access to its receptor. For this reason, resolving the structure of the third mutant, *ΔAntisigma*, becomes was critically important. Due to its significantly extended O-antigen, this mutant offers a valuable model for investigating how polysaccharide chain elongation may interfere with toxin binding and influence evasion from immune responses or other antimicrobial factors. Similarly, the substitution of β-Glc with an α-Gal residue in another mutant suggests may offer the unique opportunity to unveail the minimal structural change necessary to impair the toxin binding that even subtle structural changes can substantially affect molecular recognition. From an applied perspective, a deeper understanding

of these molecular interactions opens promising therapeutic opportunities. Targeting the toxin–LPS recognition system or exploiting the tightly regulated proteolytic activation of bacterial toxins, could pave the way for the development of novel antimicrobial strategies that selectively modulate gut microbiota composition and function. Additionally, the ability to engineer LPS structures could be harnessed to design innovative immunomodulatory agents capable of influencing immune responses without triggering excessive inflammation. The project is still ongoing, and the goal is to expand structural analysis to a broader set of mutants and to deepen functional investigations in *in vitro* models, in collaboration with Professor L. Comstock, is to testevaluating the binding of specific toxins to these structurally diverse *P. vulgatus* LPS the emerging hypotheses and to further clarify the molecular mechanisms underlying resistance and susceptibility to *P. vulgatus*-derived antibacterial toxins. In the long term, the integration of structural, functional, and genomic approaches may offer a comprehensive understanding of microbial adaptation and competition strategies within the human gut, with important implications for human health and the development of innovative therapies.

References

[86] F. Di Lorenzo *et al.*, "Pairing *Bacteroides vulgatus* LPS Structure with Its Immunomodulatory Effects on Human Cellular Models," *ACS Cent Sci*, vol. 6, no. 9, pp. 1602–1616, Sep. 2020, doi: 10.1021/acscentsci.0c00791.

[103] J. C. Evans *et al.*, "A proteolytically activated antimicrobial toxin encoded on a mobile plasmid of Bacteroidales induces a protective response.," *Nat Commun*, vol. 13, no. 1, p. 4258, Jul. 2022, doi: 10.1038/s41467-022-31925-w.

Chapter VII

The chemistry of gut microbiome-derived lipopolysaccharides impacts on the occurrence of food allergy in the pediatric age

This study has been published in

Frontiers in Molecular Biosciences 2023 Oct 13:10:1266293 doi: 0.3389/fmolb.2023.1266293.

Premise: This chapter investigates the emerging connection between gut microbiota and the onset of food allergies in children, a topic gaining significant attention in biomedical research. Uniquely, **this study analyses Lipid A directly extracted from fecal samples**, offering a novel glimpse into the microbial landscape of pediatric patients with food allergies compared to healthy controls. The aim is to identify distinct molecular "fingerprints" of Lipid A that correlate with health or disease states, potentially paving the way for new diagnostic and preventive strategies in food allergy management.

7.1 Introduction

In recent decades, the incidence of food allergies has risen sharply, with a particularly concerning increase observed in children. This trend has drawn significant attention from the scientific community, which has long been investigating the role of the gut microbiota in immune-related conditions. Central to this discussion is intestinal homeostasis, a key regulator of overall physiological balance. Numerous studies have

shown that intestinal dysbiosis can impair immune system development, especially during early life, and contribute to the onset of allergic diseases [104].

The precise mechanisms connecting microbiota and food allergies remain unclear, but bacterial components like LPS are believed to influence immune responses both locally and systemically. The MATFA project (Microbiome as Potential Target for Innovative Preventive and Therapeutic Strategies for Food Allergy), led by Prof. Berni Canani at the University of Naples Federico II, found that children with food allergies from Campania exhibited an increased abundance of *Ruminococcus gnavus*, a Gram-positive bacterium [105], and a decreased presence of *Bacteroides*, a Gram- negative genus [105]. This finding presents an apparent paradox: *Bacteroides* spp., being Gram-negative, produce LPS, typically considered pro-inflammatory. However, as discussed in previous chapters, the immunostimulatory potential of LPS depends heavily on the structural features of its lipid A and inner core residues [106]. Notably, *Bacteroides* strains, which may constitute up to 40% of the human gut microbiota, produce LPS with chemical structures distinct from canonical inflammatory forms.

Building on these insights, the following section presents the results of a study aimed at identifying a molecular "fingerprint" associated with the gut microbial profile of healthy versus allergic pediatric subjects. **Central to this investigation is a pioneering protocol that enabled, for the first time, the direct analysis of lipid A from biological material, specifically, fecal samples.**

7.2 Structural features of GM-derived LPS are different in FA children vs. healthy controls

From the subjects population analyzed in the previous MATFA study [105] we randomly selected stool samples of 10 children with FA and 10 healthy controls (CT)

already evaluated for microbiome structure and functions. The samples were processed as previously described to obtain fecal supernatants [105], [107]. Supernatants then underwent a modified enzyme-hot phenol/water extraction procedure followed by several steps of purification and "re-purification" to exclude the co-presence of immunostimulatory contaminants, such as lipoproteins, lipopeptides and phospholipids, as previously described [57], [108]. Surprisingly, we observed that the amount of LPS in the stool samples from FA patients was remarkably lower if compared with what observed in stool samples from CT. Purified fecal LPSs from 6 FA (FA6, 11, 21, 22, 26, 28) and 6−ΔΔCT (CT3, 10, 12, 20, 22, 25) children, chosen among those that resulted in the highest yield, were then checked via SDS-PAGE after silver nitrate gel staining (*Figure 7.1*). This analysis clearly highlighted that all CT children displayed a similar LPS profile, as proven by the polydisperse banding pattern (ladder-like pattern) due to the occurrence of LPS molecules with a different number of repeating units in the O-antigen moiety. By contrast, a rather diverse electrophoretic profile was observed for FA children derived LPS, with the presence of both LPS (Lanes 1 and 5, *Figure 7.1*) and LOS (Lanes 2–4 and 6, *Figure 7.1*), i.e., LPS devoid of the O-antigen repeating unit. No contaminating proteins/lipoproteins in the isolated fecal LPS extracts were detected (*Figure 7.1*, D). The analysis of LPS carbohydrate and fatty acid content could provide clues on the LPS itself and about its source. Therefore, monosaccharides composing fecal LPS extracts were inspected and reported in *(Figure 7.2*, *7.3).* Remarkably, no heptose residues were detected in all fecal LPS extracts from the stool samples of the CT children, which were instead clearly observed in most of the LPS extracts collected by the stool samples of FA patients. These results agree with the high abundance of Bacteroides-derived LPS in CT fecal samples (see below) as the absence of heptoses in the LPS of Bacteroides species is considered a hallmark of these bacteria [96]. By contrast, the presence of heptoses in FA fecal LPS suggested the presence of LPS from Gamma-proteobacteria, and possibly from the Enterobacteriaceae family whose blooming in the human gut typically leads to the instauration and persistence of an

inflammatory state [27], [96]. Likewise, fatty acid compositional analyses disclosed the presence of the typical pattern of Bacteroides LPS in CT fecal LPS [78], [109], [110], [111] whereas 12:0, 14:0, 14:0(3-OH) fatty acids were also identified in some FA fecal LPS, which might be considered instead a signature of Gammaproteobacteria [96]

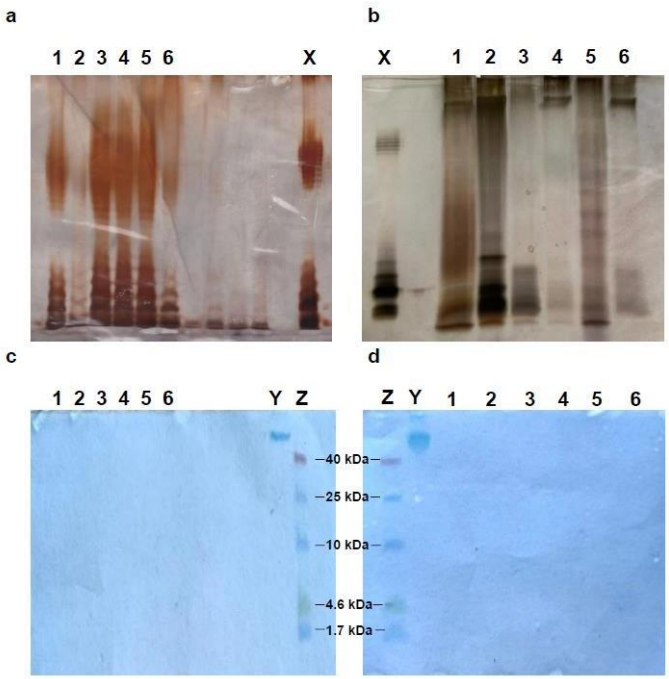

Figure 7.1: Representation of an electrophoretic run in 12.5% SDS polyacrylamide with **a)** silver staining and **b)** Comassie blue. The samples in the run are six LPS extracted from fecal supernatants of CT (a, c) and FA (b, d). In the **a)** staining LPS of *E. coli* O127:B8 (line X) was used as control, in the **b)** SDS-PAGE stained with Comassie Blue was used bovine serum albumin (BSA) (line Y) and BLUeye Prestained Protein Ladder (line Z)

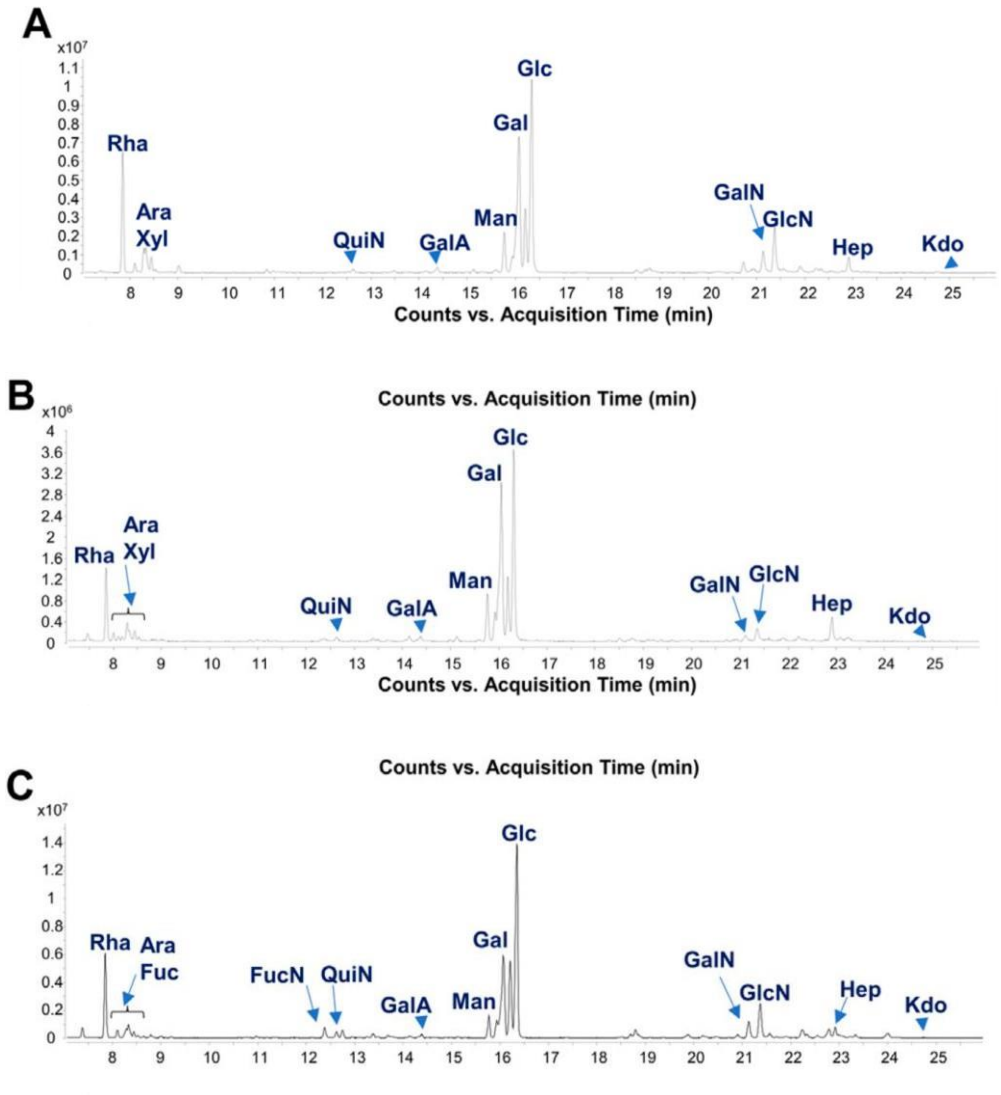

Figure 7.2 Representation of the GC-MS chromatogram recorded after methanolysis followed by acetylation of the samples made on LPS samples isolated from fecal material of patients with food FA. The chromatograms recorded belong to subjects FA6, FA26 and FA21.

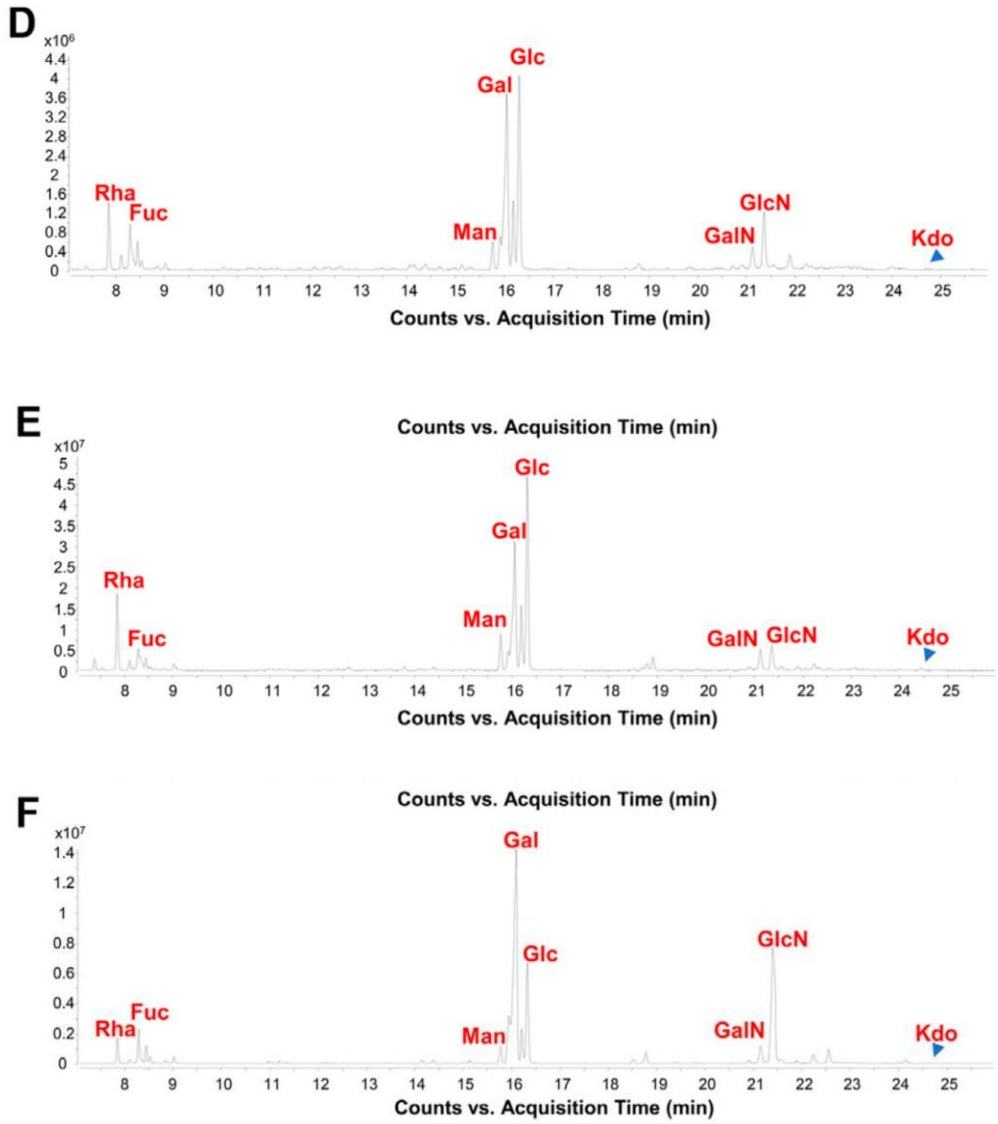

Figure 7.3 Representation of the GC-MS chromatogram recorded after methanolysis followed by acetylation of the samples made on LPS samples isolated from fecal material of control patients (CT). The chromatograms recorded belong to subjects CT3, CT12 and CT22.

7.3 GM-derived lipid A mass spectral profiles are diverse between FA children and healthy controls

Lipid A is the primary immunostimulatory part of an LPS, as it is recognized by the immunity receptor complex Toll-like receptor 4 (TLR4)/Myeloid differentiation factor-2 (MD-2), leading to the production of pro-inflammatory mediators that initiate and shape the immune response [27]. However, the activation of the TLR4/MD-2-dependent response is greatly dependent on the chemical structure of the lipid A [112], [113], [114]. In order to enable a rapid profiling of lipid A from feces and therefore to take a glance at the fecal LPS immunostimulatory potential, we have conceived an adaptation of a micro-scale lipid A isolation procedure [115], in order to extract the lipid A directly from an aliquot of each fecal supernatant. All the fecal lipid A mixtures (CT Lipid A and FA Lipid A) were inspected by negative and positive-ion MALDI-TOF MS and MS/MS. Reflectron MALDI-TOF MS spectra, recorded in negative-ion polarity, of all CT Lipid A and FA Lipid A are reported in *Figures 7.4, 7.6*. Strikingly, MALDI-TOF MS spectra of all CT Lipid A were almost identical, indicating the occurrence of a predominant lipid A type in feces of healthy pediatric donors. Noteworthy, all CT Lipid A had masses with a m/z ratio of <1720, which is consistent with the presence of hypoacylated lipid A species, that is lipid A expressing less than six acyl chains. Moreover, it was possible to promptly associate these peaks to Bacteroides-derived lipid A as in all MS spectra (*Figure 7.4*) two main clusters of peaks were detected and matched with [M-H]− mono-phosphorylated penta-acylated (at about m/z 1,659) and tetra-acylated lipid A species (at about m/z 1,419), in agreement with previous studies on Bacteroides sp. lipid A [78], [110], [111], [116], [117] Moreover, each of these groups of peaks was characterized by the occurrence of mass differences of 14 amu (a–CH2– unit) that is diagnostic of the presence of lipid A species differing in the acyl chain length, also in accordance to the wellknown length heterogeneity of fatty acids decorating *Bacteroides* sp. lipid A [78], [86], [110], [111], [117]. To confirm this structural hypothesis, a detailed negative-ion MS/MS analysis has been conducted on several ion peaks (*Figure 7.5*) that allowed to determine the location of the phosphate group and the acyl moieties with the respect to the disaccharide backbone. Briefly, the main peak at m/z 1,659 observed in most

of the MS spectra was assigned to a mixture of at least four isomers all consistent with penta-acylated lipid A species made up of the typical glucosamine disaccharide backbone carrying one phosphate on the reducing glucosamine unit and bearing 17:0(3- OH) and/or 16:0(3-OH), and 17:0(3-OH), 16:0(3-OH) and/or 15: 0(3-OH) as primary amide- and ester-bound acyl chains respectively, and one secondary 15:0 unit, with the latter present as acyloxyacylamide of the nonreducing glucosamine. The minor peak at m/z 1,419 was assigned to a mono-phosphorylated tetraacylated lipid A species lacking in the primary O-linked acyl moiety of the nonreducing glucosamine. Overall MS and MS/MS data of the CT Lipid A were consistent with the isolation and presence of almost exclusively lipid A, and therefore of LPS, belonging to Bacteroides sp., which was in agreement with our previous metagenomic analyses [105]. By contrast, a remarkable difference and a high heterogeneity of components was found in MALDI-TOF MS spectra of FA Lipid A in which the identification of a common trend was not straightforward. As shown in *Figure 7.6*, although clusters of peaks attributable to *Bacteroidesderived* lipid A (at about m/z 1,659 and m/z 1,419) could still be detected in most of the cases, several key differences compared to CT Lipid A spectra were immediately apparent. Briefly, i) the majority of MS spectra displayed a lower signal-to-noise ratios compared to CT counterparts; ii) a significant reduction in the intensity of peaks assigned to monophosphorylated penta-acylated lipid A species was observed in some spectra together with an increment in the intensity of peaks ascribed to mono-phosphorylated tetra-acylated ones; iii) in some spectra, masses with a m/z ratio of >1,720 were detected. This latter characteristic was investigated further as it was considered an indication of the presence of bis-phosphorylated and/or hexa-acylated lipid A species, and therefore of potentiallymore pro-inflammatory LPSs. A negative-ion MS/MS analysis has been performed and allowed to establish the structure of several lipid A not detected in CT feces (*Figure 7.7*). Choosing as examples MS spectra of patients FA21 and FA28, it was possible to identify bis-phosphorylated penta-acylated lipid A (at m/z 1753.6 and m/z 1795.6) (*Figures 7.7 A, B*), and a *Proteobacteria*-like

bisphosphorylated hexa-acylated lipid A (at m/z 1796.9) *(Figure 7.7 C*). Finally, another common trait amongst FA Lipid A MALDI-TOF MS spectra was the occurrence of a cluster of peaks at about m/z 1261.3, which was assigned to bis-phosphorylated tri-acylated lipid A species devoid of the primary ester bound acyl chains and of the secondary acyl substituent(s) (*Figure 7.7 D*).

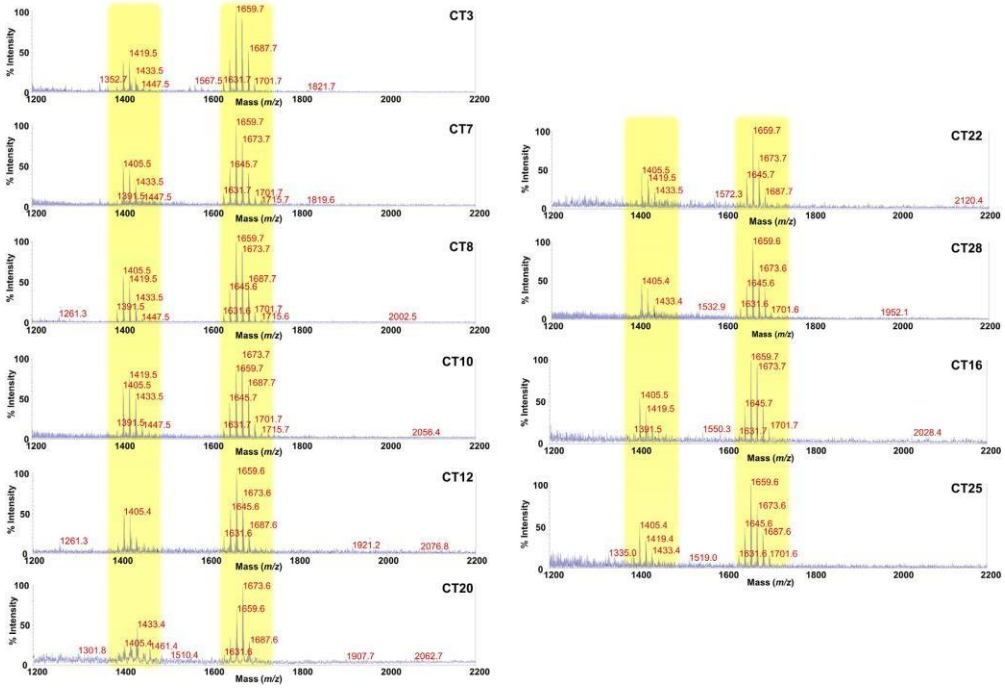

Figure 7.4: MALDI-MS spectrum chromatogram of the Lipid A mixture extracted from fecal supernatants of controls (CT). The MALDI-TOF MS spectra of Reflectron were recorded with negative ionic polarity using THAP as matrix. Yellow squares in the image highlight the clusters of peaks attributed to tetra-monophosphorylated (m/z 1.419) and penta-acylated (m/z 1.659) Lipid A species belonging to the genus Bacteroides.

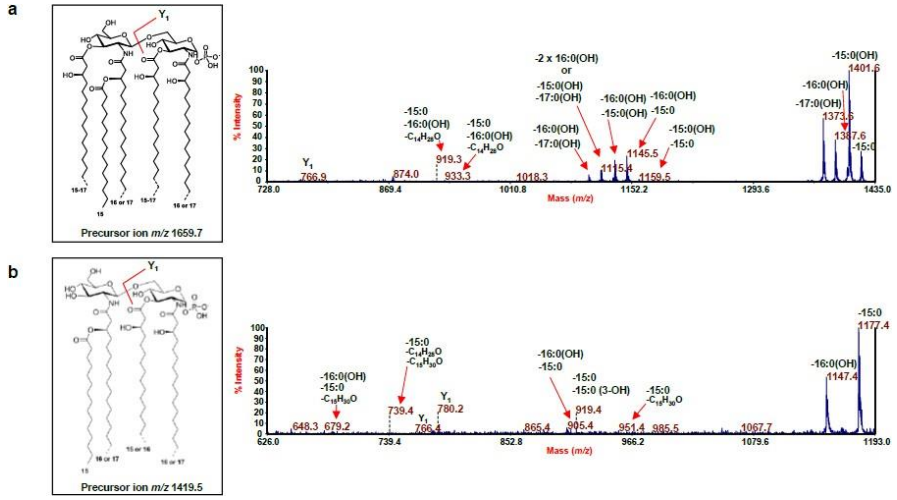

Figure 7.5 MALDI MS/MS spectrum of precursor ions at m/z 1659.7 (a) and m/z 1419.5 (b), representative ionic peaks of the cluster attributed to the penta-acylated and tetra-acylated monophosphorylated species of lipid A, found in all MALDI-TOF analyses of CTs. The fragment assignment is shown in the graph, together with the hypothesis of the structure of Lipid A. The analysis made on the Y ions - created after cleavage of the glycosidic bond - was crucial for the location of the phosphate group and acyl chains bound to the reducing glucosamine. Peaks were observed due to the loss of C15H30O (226 u.m.) and C14H28O (212 u.m.), linked to a rearrangement of the N-linked 3-OH acyl chains with a free hydroxyl group. The absence of fragments resulting from the loss of an entire hydroxylated acyl chain with a 15:0 moiety indicates that it is bound as a substituent to the amide group of the non-reducing glucosamine residue. The acyl chains in lipid A are shown as linear for illustrative purposes only; the dotted lines reflect the variability in their length.

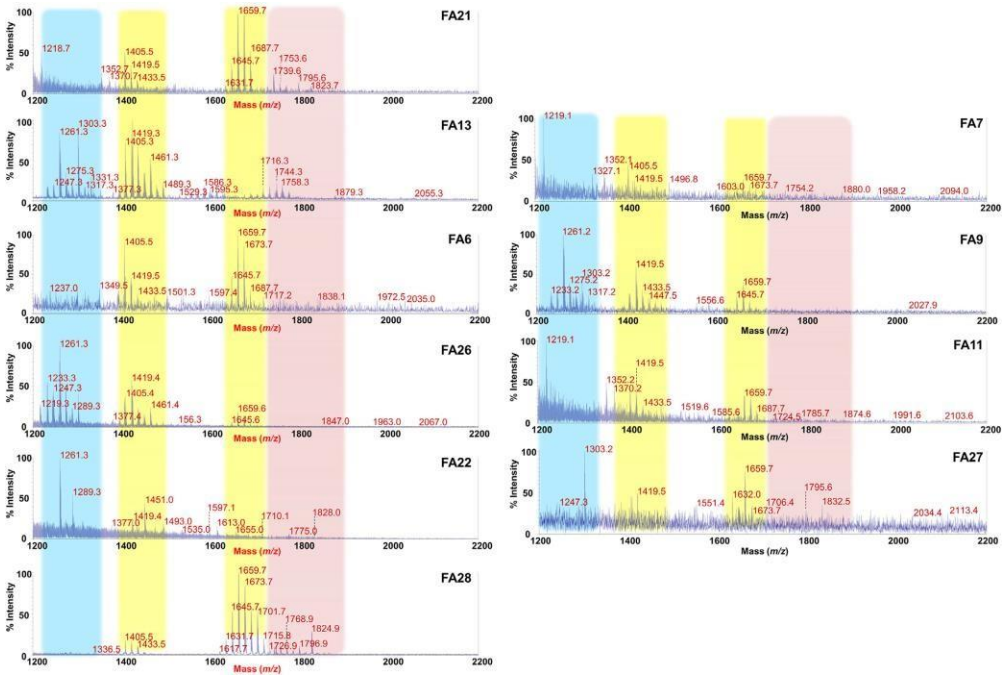

Figure 7.6 MALDI-TOF MS mass spectrum of the Lipid A mixture extracted from fecal supernatants of food allergy (FA) patients. MS spectra were recorded with negative ionic polarity using THAP as matrix. The pink boxes show peaks attributable to families of bacteria known to be pro-inflammatory, i.e. bisphosphorylated and/or hexa-acylated species. The blue box shows the cluster related to tri-acylated bisphosphorylated Lipid A species.

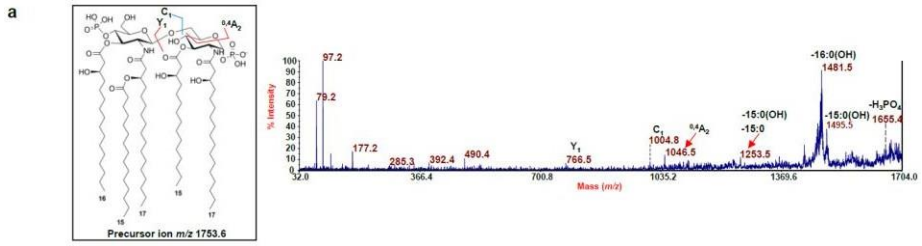

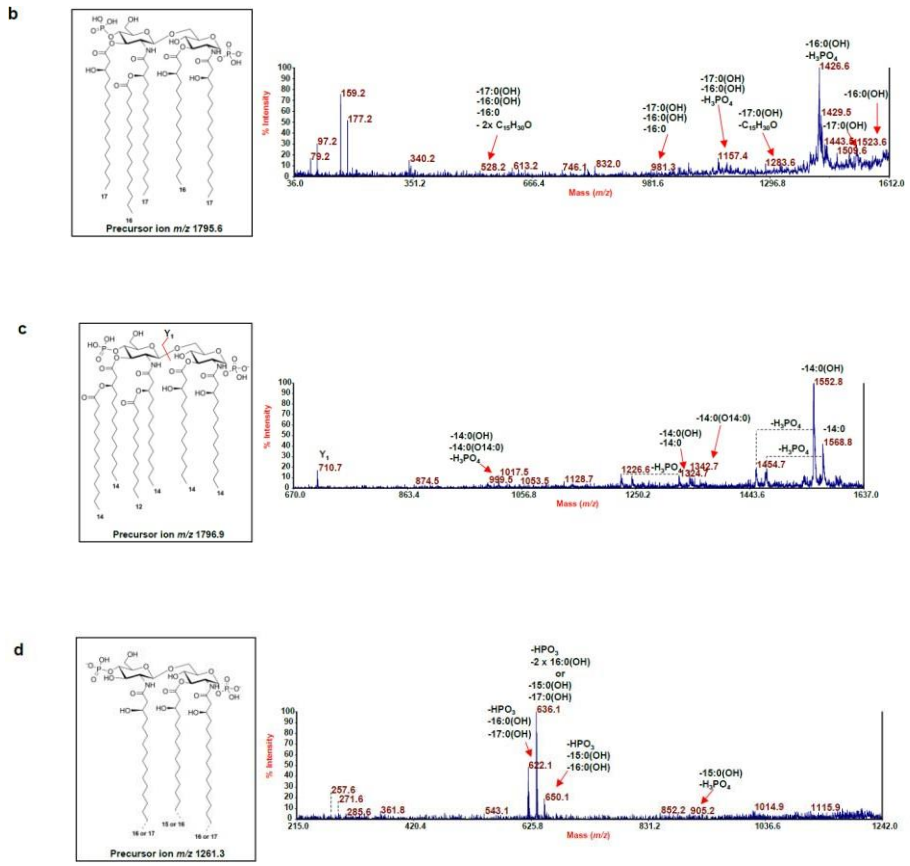

Figure 7.7: The MALDI MS/MS spectra in negative ion mode of the precursors at m/z 1753.6, 1795.6 and 1796.9 represent the characteristic peaks of a family of bis-phosphorylated A-lipids, detected exclusively in the feces of FA subjects. The spectrum at m/z 1261.3 represents tri-acylated bis-phosphorylated A-lipids. The graphs show the main fragments and the proposed structure, shown in the inset. The dotted lines represent the variability in the length of the fatty acid chains. Also visible are peaks resulting from the loss of C15H30O (226 u.m.), caused by a rearrangement in the N-linked 3-OH acyl chains with a free hydroxyl group.

7.4 GM-derived LPS and lipid A from FA children elicited a Th2 response

The LPS released by gut microbes can act locally and, after crossing the gut barrier and entering circulation, also systemically [118]. In the frame of allergic diseases, LPS was shown to either promote or prevent T helper 2 (Th2) cell allergic responses [119], [120], [121], [122], but the underlying mechanism(s) remain unclear. To provide a causal relationship between the presence of a specific LPS/lipid A chemistry and a potential ability in eliciting an allergic response, we tested fecal LPSs from CT and FA children, as well as FA and CT lipid A along with their related fecal supernatants on PBMCs from healthy paediatric donors. We chose PBMCs as they are a valuable tool in food research to perform studies within the FA field [123], [124],
[125] but also because they contain LPS responsive cells similar to those present in the gut, thus representing a common proxy for mucosal leukocytes [126], [127]. Remarkably, only stimulation with lipid A and LPS obtained from FA patients induced an increased production of the Th2 cytokines IL-4 and IL-13 (*Figure 7.8 panels A, B*).

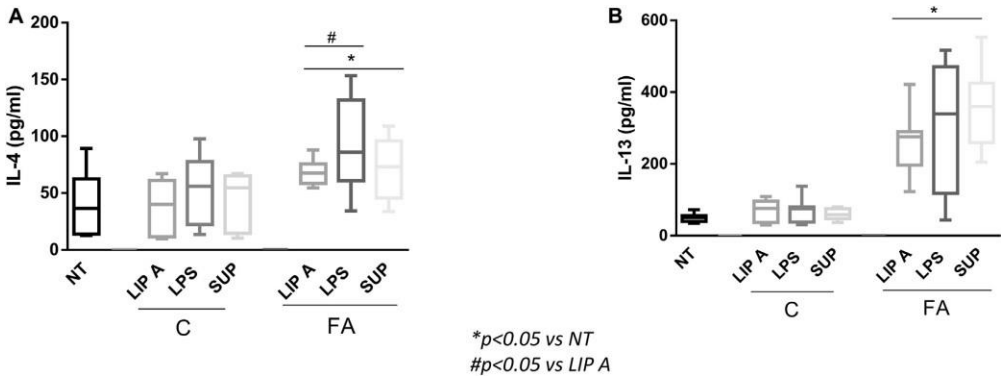

Figure 7.8 Representation of the histogram of data from the assay done with Lipid A (LIP A) fecal supernatants (SUP) from allergy sufferers (FA). the results show that the components described above induce a pro-allergic Th2-type response in PBMC cells. After 24 hours of exposure to 100 µg/mL of each component, a significant increase in IL-4 (A) and IL-13 (B) production was observed. The tests were performed in duplicate on three separate samples. Data are expressed as mean ± standard

deviation. *p < 0.05 vs untreated cells; #p < 0.05 vs LIP A (one-way ANOVA with Tukey's post-hoc test).

7.5 GM-derived LPS and lipid A from healthy children activated immune tolerance mechanisms from FA children

To explore the effects of fecal lipid A and LPS on themain drivers of immune tolerance, we investigated regulatory T cells (Tregs) and IL-10 production in PBMCs from healthy children stimulated with lipid A, LPS and fecal supernatants. We observed that lipid A, LPS and fecal supernatants from CT elicited a significant increase of CD4+/CD25+/ FoxP3+ cells (*Figure 7.9*). This effect significantly correlated with the production of the tolerogenic cytokine IL-10 ($r = 0.9668$, $p < 0.001$). This effect paralleled with a significant increase in the production of the tolerogenic cytokine IL-10. No modulation was observed upon stimulation with lipid A, LPS and fecal supernatants from FA children (*Figure 7.10*).

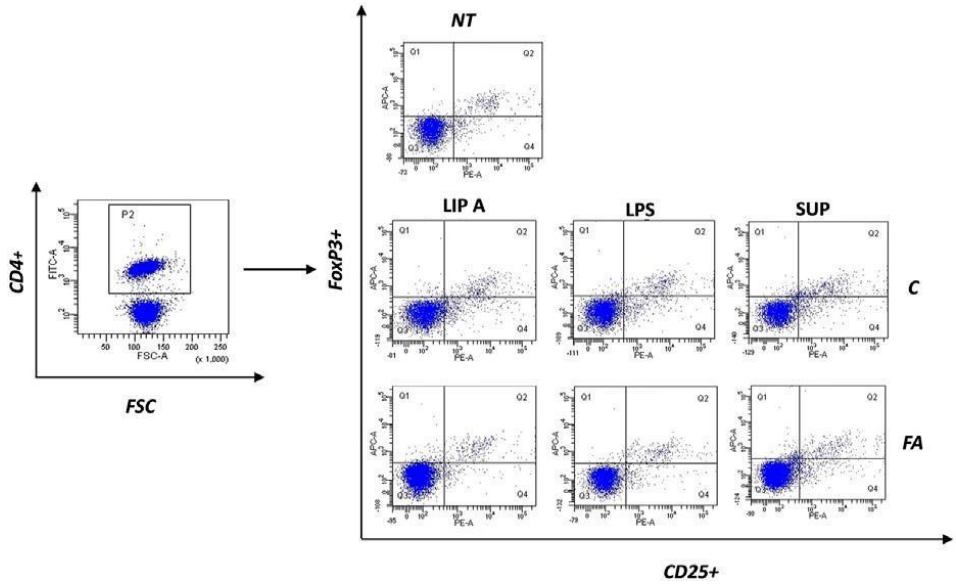

Figure 7.9 Fecal Lipid A (LIP A), LPS and supernatants (SUP) from healthy children (C) activate immune tolerance mechanisms. PBMCs from healthy children (n = 3) were treated for 3 days with 100 μg/mL LIP A, LPS and SUP. After stimulation, cells were analyzed by cytofluorimetry and supernatants collected for cytokine evaluation. In figure it's shown the representative dot plots show a significant increase in the CD4+/CD25+/FoxP3+ regulatory T population after 24 hours of treatment.

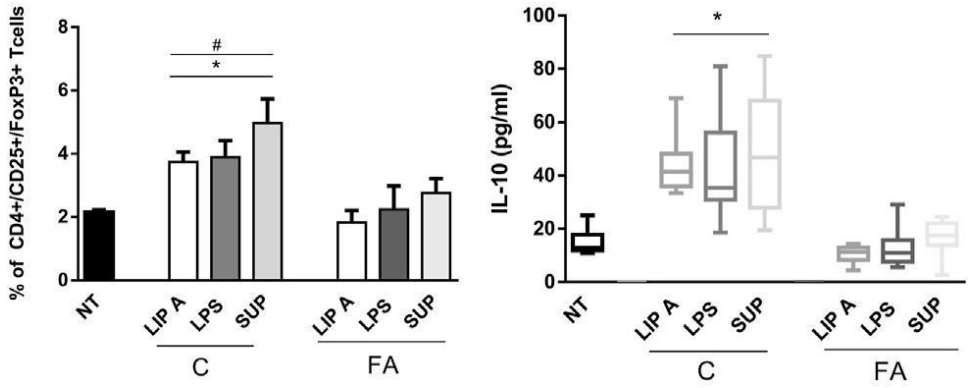

Figure 7.10 In parallel, a significant increase in IL-10 production by PBMCs was noted. Each treatment was performed in duplicate on three separate samples. Results are expressed as mean ± standard deviation. *p < 0.05 compared to untreated cells (NT); #p < 0.05 compared to LIP A (one-way ANOVA with Tukey's post-hoc test).

7.6 GM-derived LPS from healthy children activated non-classical monocytes and IL-12 production

It has been demonstrated that LPS can promote or suppress Th2 cell sensitization depending on activation of classical and nonclassical monocytes [128]. These cells control the capacity of dendritic cells to produce IL-12, which in turn led to the

suppression of the Th2 cell differentiation program in allergenspecific T cells [129]. In order to evaluate the potential ability of fecal lipid A and LPS derived from healthy controls in reducing the allergic response, we assessed nonclassical monocytes and IL-12 production in PBMCs from healthy children. Notably, the exposure to CT LPS and fecal supernatants significantly increased CD14+/CD16++ cells number compared to FA lipid A, LPS and fecal supernatants (*Figure 7.11 panel A*). Concomitantly, IL-12 release resulted in a significant increase after stimulation with CT LPS and fecal supernatants (*Figure 7.11, panel B*).

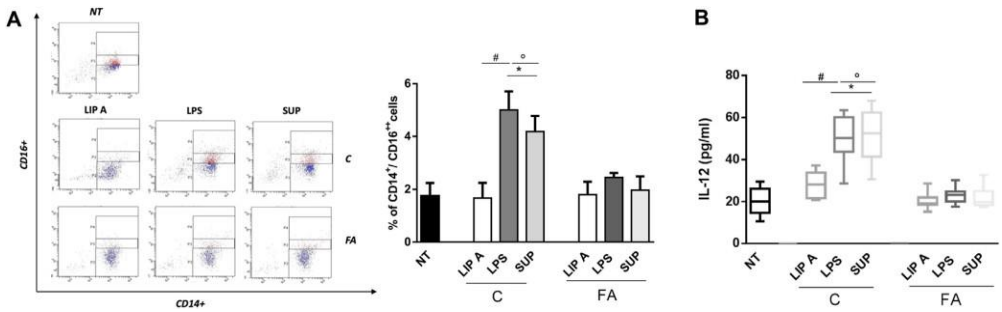

Figure 7.11 Fecal LPS and supernatants (SUP) from healthy children (C) activate non-classical monocytes (CD14+/CD16++) and stimulate IL-12 production, helping to inhibit the Th2-type immune response. PBMCs of healthy children (n = 3) were treated for 3 days with 100 µg/mL LIP A, LPS and SUP. After 24 h, LPS and SUP induced a significant increase in CD14+/CD16++ cells and IL-12 secretion, whereas LIP A showed no relevant effects. Each treatment was performed in duplicate on three separate samples. Data are reported as mean ± standard deviation. *p < 0.05 vs untreated cells (NT); #p < 0.05 vs LIP A; °p < 0.05 vs LPS (one-way ANOVA with Tukey's post-hoc test).

7.7 Discussion

Over recent decades, the prevalence of food allergies (FA) in pediatric populations has increased significantly, with substantial implications for child health, healthcare

systems, and society as a whole [104], [122]. As previously discussed, growing evidence suggests that the gut microbiota plays a pivotal role in modulating the onset of food allergies. However, the specific bacterial taxa and molecular mechanisms involved remain incompletely understood, adding complexity to this emerging field.

In this study, we sought to clarify mechanisms underlying the induction or suppression of allergic inflammation by analyzing LPS and lipid A directly extracted from stool samples of healthy children and FA patients. Structural characterization via MALDI-TOF MS revealed distinct chemical differences between the lipid A profiles of control (CT) and FA subjects. Lipid A from CT samples exhibited a conserved pattern, predominantly composed of mono-phosphorylated tetra- and penta-acylated species typically associated with *Bacteroides* spp. In contrast, FA samples showed a heterogeneous lipid A profile, enriched in bis-phosphorylated and hexa-acylated species known for their pro-inflammatory potential. Additionally, MALDI-TOF spectra from FA subjects displayed a lower signal-to-noise ratio, consistent with a reduced abundance of Gram-negative bacteria in their gut microbiota. This was further supported by the lower LPS extraction yield from FA stool samples compared to CT samples.

These findings underscore significant structural differences in microbiota-derived LPS between healthy and allergic children and suggest that LPS chemistry may serve as a biomarker for diagnosing and stratifying pediatric food allergy risk. Moreover, this study introduced an innovative approach by bypassing traditional bacterial isolation and cultivation methods. Instead, LPS and lipid A were directly analyzed from biological samples and tested on PBMCs.

Functional assays demonstrated that LPS and lipid A from CT samples promoted the production of the tolerogenic cytokine IL-10 and supported the expansion of regulatory T cells (Tregs) [130], [131], which are essential for maintaining immune tolerance. Exposure to CT-derived LPS also increased the frequency of non-classical monocytes, a population known to secrete GM-CSF. This cytokine modulates LPS

activity by promoting monocyte differentiation into dendritic cells capable of producing IL-12, thereby counteracting allergic inflammation [132]. These results suggest that immune tolerance is mediated not only by IL-12 but also by the synergistic effects of Treg expansion and IL-10 release [128], [130].

Importantly, our data also revealed that the carbohydrate portion of LPS contributes significantly to its immunomodulatory properties, as complete LPS molecules elicited a stronger tolerogenic response than lipid A alone. These observations reinforce the concept that specific structural variants of LPS can exert either pro-allergic or tolerogenic effects. Therefore, targeted structural modulation of LPS may represent a promising strategy for preventing and treating allergic diseases, paving the way for more personalized and effective therapeutic interventions.

References

[104] O. I. Iweala and C. R. Nagler, "The Microbiome and Food Allergy," *Annu Rev Immunol*, vol. 37, no. 1, pp. 377–403, Apr. 2019, doi: 10.1146/annurev-immunol-042718-041621.

[105] F. De Filippis *et al.*, "Specific gut microbiome signatures and the associated pro-inflamatory functions are linked to pediatric allergy and acquisition of immune tolerance," *Nat Commun*, vol. 12, no. 1, p. 5958, Oct. 2021, doi: 10.1038/s41467-021-26266-z.

[106] P. Garcia-Vello, F. Di Lorenzo, D. Zucchetta, A. Zamyatina, C. De Castro, and A. Molinaro, "Lipopolysaccharide lipid A: A promising molecule for new immunity-based therapies and antibiotics," *Pharmacol Ther*, vol. 230, p. 107970, Feb. 2022, doi: 10.1016/j.pharmthera.2021.107970.

[107] J. R. Marchesi *et al.*, “Rapid and Noninvasive Metabonomic Characterization of Inflammatory Bowel Disease,” *J Proteome Res*, vol. 6, no. 2, pp. 546–551, Feb. 2007, doi: 10.1021/pr060470d.

[108] M. Hirschfeld, Y. Ma, J. H. Weis, S. N. Vogel, and J. J. Weis, “Cutting Edge: Repurification of Lipopolysaccharide Eliminates Signaling Through Both Human and Murine Toll-Like Receptor 2,” *The Journal of Immunology*, vol. 165, no. 2, pp. 618–622, Jul. 2000, doi: 10.4049/jimmunol.165.2.618.

[109] F. Di Lorenzo, F. Crisafi, V. La Cono, M. M. Yakimov, A. Molinaro, and A. Silipo, “The Structure of the Lipid A of Gram-Negative Cold-Adapted Bacteria Isolated from Antarctic Environments,” *Mar Drugs*, vol. 18, no. 12, p. 592, Nov. 2020, doi: 10.3390/md18120592.

[110] A. WEINTRAUB, U. ZÄHRINGER, H. WOLLENWEBER, U. SEYDEL, and E. Th. RIETSCHEL, “Structural characterization of the lipid A component of *Bacteroides fragilis* strain NCTC 9343 lipopolysaccharide,” *Eur J Biochem*, vol. 183, no. 2, pp. 425–431, Aug. 1989, doi: 10.1111/j.1432-1033.1989.tb14945.x.

[111] T. Vatanen *et al.*, “Variation in Microbiome LPS Immunogenicity Contributes to Autoimmunity in Humans,” *Cell*, vol. 165, no. 4, pp. 842–853, May 2016, doi: 10.1016/j.cell.2016.04.007.

[112] A. Molinaro *et al.*, “Chemistry of Lipid A: At the Heart of Innate Immunity,” *Chemistry – A European Journal*, vol. 21, no. 2, pp. 500–519, Jan. 2015, doi: 10.1002/chem.201403923.

[113] F. Di Lorenzo *et al.*, “Activation of Human Toll-like Receptor 4 (TLR4)·Myeloid Differentiation Factor 2 (MD-2) by Hypoacylated Lipopolysaccharide from a Clinical Isolate of Burkholderia cenocepacia,” *Journal of Biological Chemistry*, vol. 290, no. 35, pp. 21305–21319, Aug. 2015, doi: 10.1074/jbc.M115.649087.

[114] F. Di Lorenzo *et al.*, "Chemistry and Biology of the Potent Endotoxin from a *Burkholderia dolosa* Clinical Isolate from a Cystic Fibrosis Patient," *ChemBioChem*, vol. 14, no. 9, pp. 1105–1115, Jun. 2013, doi: 10.1002/cbic.201300062.

[115] A. El Hamidi, A. Tirsoaga, A. Novikov, A. Hussein, and M. Caroff, "Microextraction of bacterial lipid A: easy and rapid method for mass spectrometric characterization," *J Lipid Res*, vol. 46, no. 8, pp. 1773–1778, Aug. 2005, doi: 10.1194/jlr.D500014-JLR200.

[116] F. Di Lorenzo, K. A. Duda, R. Lanzetta, A. Silipo, C. De Castro, and A. Molinaro, "A Journey from Structure to Function of Bacterial Lipopolysaccharides," *Chem Rev*, vol. 122, no. 20, pp. 15767–15821, Oct. 2022, doi: 10.1021/acs.chemrev.0c01321.

[117] M. D. Pither *et al.*, "Structural determination of the lipid A from the deep-sea bacterium Zunongwangia profunda SM-A87: a small-scale approach," *Glycoconj J*, vol. 39, no. 5, pp. 565–578, Oct. 2022, doi: 10.1007/s10719-022-10076-6.

[118] A. E. Mohr, M. Crawford, P. Jasbi, S. Fessler, and K. L. Sweazea, "Lipopolysaccharide and the gut microbiota: considering structural variation," *FEBS Lett*, vol. 596, no. 7, pp. 849–875, Apr. 2022, doi: 10.1002/1873-3468.14328.

[119] J. Bortolatto *et al.*, "Toll-like receptor 4 agonists adsorbed to aluminium hydroxide adjuvant attenuate ovalbumin-specific allergic airway disease: role of MyD88 adaptor molecule and interleukin-12/interferon-γ axis," *Clinical & Experimental Allergy*, vol. 38, no. 10, pp. 1668–1679, Oct. 2008, doi: 10.1111/j.1365-2222.2008.03036.x.

[120] Y.-K. Kim *et al.*, "Airway Exposure Levels of Lipopolysaccharide Determine Type 1 versus Type 2 Experimental Asthma," *The Journal of Immunology*, vol. 178, no. 8, pp. 5375–5382, Apr. 2007, doi: 10.4049/jimmunol.178.8.5375.

[121] C. Delayre-Orthez, F. De Blay, N. Frossard, and F. Pons, "Dose-dependent effects of endotoxins on allergen sensitization and challenge in the mouse," *Clinical &*

Experimental Allergy, vol. 34, no. 11, pp. 1789–1795, Nov. 2004, doi: 10.1111/j.1365-2222.2004.02082.x.

[122] M. Eisenstein, "Microbial ambassadors against food allergies," *Nature*, vol. 588, no. 7836, pp. S11–S13, Dec. 2020, doi: 10.1038/d41586-020-02781-9.

[123] L. Paparo *et al.*, "Tolerogenic Effect Elicited by Protein Fraction Derived From Different Formulas for Dietary Treatment of Cow's Milk Allergy in Human Cells," *Front Immunol*, vol. 11, Feb. 2021, doi: 10.3389/fimmu.2020.604075.

[124] K. Verhoeckx *et al.*, Eds., *The Impact of Food Bioactives on Health*. Cham: Springer International Publishing, 2015. doi: 10.1007/978-3-319-16104-4.

[125] L. Drago, E. De Vecchi, A. Gabrieli, R. De Grandi, and M. Toscano, "Immunomodulatory Effects of *Lactobacillus salivarius* LS01 and *Bifidobacterium breve* BR03, Alone and in Combination, on Peripheral Blood Mononuclear Cells of Allergic Asthmatics," *Allergy Asthma Immunol Res*, vol. 7, no. 4, p. 409, 2015, doi: 10.4168/aair.2015.7.4.409.

[126] H. Sokol *et al.*, "*Faecalibacterium prausnitzii* is an anti-inflammatory commensal bacterium identified by gut microbiota analysis of Crohn disease patients," *Proceedings of the National Academy of Sciences*, vol. 105, no. 43, pp. 16731–16736, Oct. 2008, doi: 10.1073/pnas.0804812105.

[127] A. Ardeshir *et al.*, "Breast-fed and bottle-fed infant rhesus macaques develop distinct gut microbiotas and immune systems," *Sci Transl Med*, vol. 6, no. 252, Sep. 2014, doi: 10.1126/scitranslmed.3008791.

[128] K. Kaur *et al.*, "GM-CSF production by non-classical monocytes controls antagonistic LPS-driven functions in allergic inflammation," *Cell Rep*, vol. 37, no. 13, p. 110178, Dec. 2021, doi: 10.1016/j.celrep.2021.110178.

[129] H. Bachus *et al.*, "Impaired Tumor-Necrosis-Factor-α-driven Dendritic Cell Activation Limits Lipopolysaccharide-Induced Protection from Allergic

Inflammation in Infants," *Immunity*, vol. 50, no. 1, pp. 225-240.e4, Jan. 2019, doi: 10.1016/j.immuni.2018.11.012.

[130] S. Sakaguchi, T. Yamaguchi, T. Nomura, and M. Ono, "Regulatory T Cells and Immune Tolerance," *Cell*, vol. 133, no. 5, pp. 775–787, May 2008, doi: 10.1016/j.cell.2008.05.009.

[131] B. R. Traxinger, L. E. Richert-Spuhler, and J. M. Lund, "Mucosal tissue regulatory T cells are integral in balancing immunity and tolerance at portals of antigen entry," *Mucosal Immunol*, vol. 15, no. 3, pp. 398–407, Mar. 2022, doi: 10.1038/s41385-021-00471-x.

Chapter VIII
Bacteroides xylanisolvens

8.1 introduction

B. xylanisolvens is a Gram-negative bacterium belonging to the genus *Bacteroides*, primarily known for its active role in the degradation of xylan, [133] a hemicellulosic polysaccharide composed mainly of β-(1→4)-linked xylose units and constitutes a major component of plant cell walls [134]The ability to degrade complex dietary fibers is attributed to specific genetic loci encoding polysaccharide-degrading enzymes such as endo-xylanases Xyn10A/B that cleave hemicellulosic substrates into oligosaccharides and monosaccharides [135]. The end products of these fermentative metabolic pathways include short-chain fatty acids (SCFAs) such as acetate, propionate, and succinate, which are important for the host's energy metabolism and play critical roles in maintaining intestinal homeostasis [136]. Beyond its well-characterized capacity to degrade plant fibers, *B. xylanisolvens* has also demonstrated potential as a biotherapeutic agent. A recent study developed a combined product consisting of strains of *B. xylanisolvens* and *Clostridium butyricum*. This study showed that the combination of these two bacteria was more effective than treatment with either strain alone in improving metabolic syndrome in diet-induced obese mice [137]. Despite being increasingly recognized as a beneficial microbe actively involved in maintaining host homeostasis, the structural characteristics of *B. xylanisolvens* surface molecules, such as LPS, remain largely unexplored. Intrigued by the known benefits of this bacterium, we have initiated the structural resolution of *B. xylanisolvens* LPS.

8.2 Structural Characterization

Following the extraction of LPS from an aliquot of dried *Bacteroides xylanisolvens* cells, an enzymatic hydrolysis and dialysis step was performed to remove residual nucleic acids and proteins resulting from the LPS extraction process. Subsequently, an SDS-PAGE analysis was carried out to assess the degree of purity and to evaluate the nature of the LPS isolated from the cellular material [116], [138]. The 12.5% polyacrylamide gel was stained using silver nitrate. This analysis revealed the appearance of a fast-migrating band, which is consistent with the presence of a rough-type LPS (R-LPS) (*Figure 8.1*).

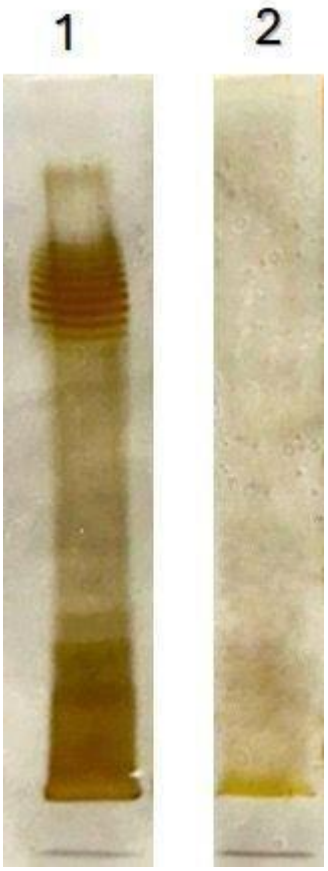

Figure 8.1: 12.5% SDS-PAGE after silver staining of R-LPS extracted from *B. xylanisolvens* cell lysate (lane 2) and *E. coli* positive control (lane 1).

To remove impurities and to separate the R-LPS from any co-extracted capsular polysaccharides potentially associated with the LOS, a series of ultracentrifugation steps was performed. Both the supernatant and the pellet were subsequently analyzed by ^{1}H NMR spectroscopy (*Figure 8.2 A and B*). The ^{1}H NMR spectrum of the supernatant obtained from ultracentrifugation clearly shows the presence of a polysaccharide, which in this context may be considered a contaminant of the sample. In contrast, the ^{1}H NMR spectrum of the corresponding pellet displays an almost undetectable pattern, which can be attributed to the presence of R-LPS. This is consistent with the low solubility of R-LPS molecules, which makes them difficult to detect in analyses carried out in D_2O.

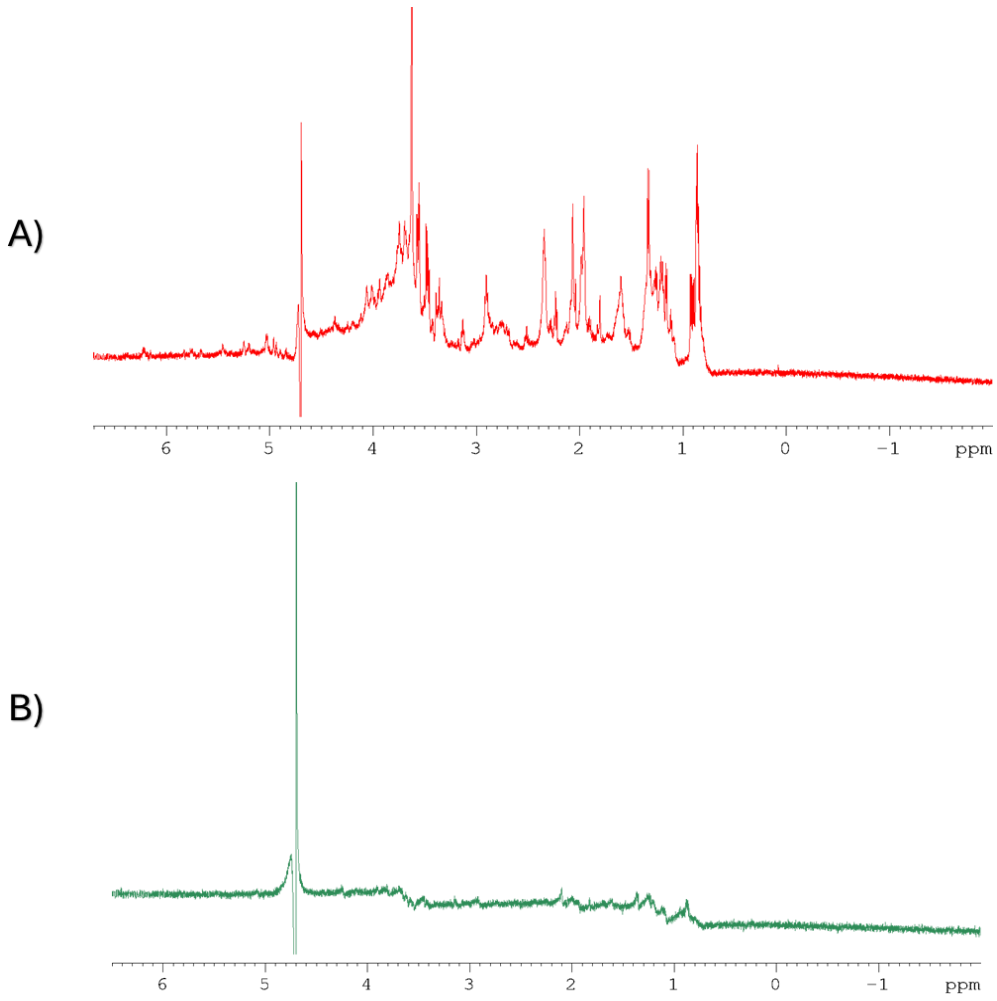

Figure 8.2: ^{1}H NMR spectra of the supernatant (A) and pellet (B) obtained after ultracentrifugation of *B. xylanisolvens* following enzymatic hydrolysis.

8.3 Extraction and compositional analysis

The monosaccharide composition of *B. xylanisolvens* R-LPS was investigated using GC-MS. Derivatization analysis of the monosaccharides revealed the presence of various deoxyhexoses, hexoses and hexosamines and acyl chains of different lengths.

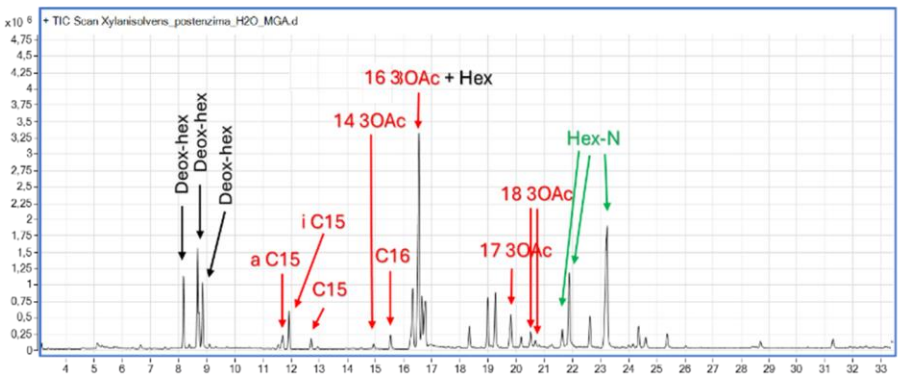

deox-hex	
	8.16
	8.65
	8.82
hex	
	16.31
	16.50
	16.64
	16.74
hex-N	
	21.61
	21.85

Figure 8.3: Results of the compositional analysis of monosaccharides and fatty acids from the R-LPS extracted from *Bacteroides xylanisolvens*, obtained using the acylated methyl glycoside derivatization method, performed on the aqueous phase. The table reports the sugar composition along with the corresponding retention times.

8.4 Structural Investigation of the Core Oligosaccharide

The structural characterization of the core oligosaccharide component of the R-LPS from *B. xylanisolvens* involved a deacylation of the extracted molecule on an aliquot of the sample followed by size-exclusion chromatography using a Sephadex® G-10 column to remove salts from the deacylated sample. The structure of the core oligosaccharide was analyzed by NMR spectroscopy. The ^{1}H and ^{1}H-^{13}C HSQC NMR spectra (*Figure 8.4*) of the deacylated sample revealed the presence of at least 15

anomeric signals, indicating a complex oligosaccharide structure in the R-LPS of *B. xylanisolvens.*

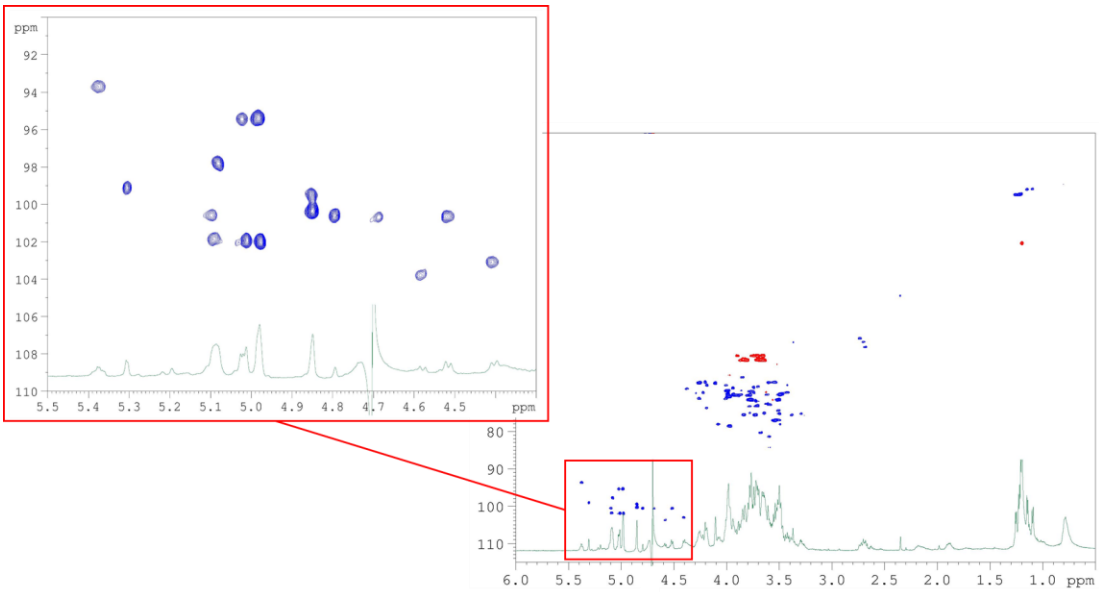

Figure 8.4: Overlay of the ^{1}H (green) and ^{1}H-^{13}C HSQC (blue and red) spectra recorded on the product obtained from the complete deacylation of the R-LPS from *B. xylanisolvens*. On the left, a zoom of the anomeric region is shown.

Subsequently, several two-dimensional NMR experiments (DQF-COSY, TOCSY, NOESY, ROESY, ^{1}H-^{13}C HSQC, ^{1}H-^{13}C HMBC) were recorded. The structural characterization is currently ongoing along with the definition of the immunological properties of purified R-LPS.

8.5 Conclusions and Future Perspectives

This chapter focused on the extraction and preliminary structural characterization of the R-LPS from *B. xylanisolvens*. The resulting NMR data recorded on deacylated R-LPS revealed a high degree of structural complexity, with at least 15 anomeric signals detected in the region between 5.5 and 4.3 ppm. These signals are indicative of a rich and diverse oligosaccharide architecture, potentially featuring interesting and unique structural traits. Future steps in the structural investigation of *B. xylanisolvens* R-LPS will include, in addition to further NMR-based elucidation of the core-OS, mild acid hydrolysis of the enzyme-treated extract followed by sequential purification steps. These will enable subsequent analysis by MALDI-TOF MS, MS/MS, and ESI/MS techniques, to also resolve in parallel the structure of the lipid A component. Such studies will be fundamental to gaining deeper insight into the immunomodulatory potential of *B. xylanisolvens* LPS, particularly considering its emerging role in host metabolic health and intestinal immune homeostasis.

References

[132] K. Kaur *et al.*, "GM-CSF production by non-classical monocytes controls antagonistic LPS-driven functions in allergic inflammation," *Cell Rep*, vol. 37, no. 13, p. 110178, Dec. 2021, doi: 10.1016/j.celrep.2021.110178.

[133] C. Chassard, E. Delmas, P. A. Lawson, and A. Bernalier-Donadille, "Bacteroides xylanisolvens sp. nov., a xylan-degrading bacterium isolated from human faeces," *Int J Syst Evol Microbiol*, vol. 58, no. 4, pp. 1008–1013, Apr. 2008, doi: 10.1099/ijs.0.65504-0.

[134] N. Bhardwaj, B. Kumar, and P. Verma, "A detailed overview of xylanases: an emerging biomolecule for current and future prospective," *Bioresour Bioprocess*, vol. 6, no. 1, p. 40, Dec. 2019, doi: 10.1186/s40643-019-0276-2.

[135] T. Zhao *et al.*, “Degradation of xylan by human gut Bacteroides xylanisolvens XB1A,” *Carbohydr Polym*, vol. 315, p. 121005, Sep. 2023, doi: 10.1016/j.carbpol.2023.121005.

[136] C. Chassard, E. Delmas, P. A. Lawson, and A. Bernalier-Donadille, “Bacteroides xylanisolvens sp. nov., a xylan-degrading bacterium isolated from human faeces,” *Int J Syst Evol Microbiol*, vol. 58, no. 4, pp. 1008–1013, Apr. 2008, doi: 10.1099/ijs.0.65504-0.

[137] S. Qiao *et al.*, “Cross-feeding-based rational design of a probiotic combination of *Bacterides xylanisolvens* and *Clostridium butyricum* therapy for metabolic diseases,” *Gut Microbes*, vol. 17, no. 1, Dec. 2025, doi: 10.1080/19490976.2025.2489765.

Appendix

Chapter IX

Pushing the Boundaries of Structural Heterogeneity with the Lipid A of Marine Bacteria Cellulophaga

This studywas published Chembiochem 2023 May 16;24(10): e202300183.doi: 10.1002/cbic.202300183. Epub 2023 Apr 21.

Premise. The next chapter focuses on the structural analysis of three Lipid A molecules from *Cellulophaga* species: *C. baltica* NNO 15840^T, *C. tyrosinoxydans* EM41^T, and *C. algicola* ACAM 630^T. The Lipid A from these bacteria displayed significant structural diversity, ranging from tetra- to hexa-acylated forms, some containing phosphate groups and sugar residues on the glucosamine backbone. Their immunomodulatory effects have been explored through TLR4 activation assays, shedding light on the connection between structure and immune response.

9.1 Introduction

Marine bacteria inhabit an incredibly diverse range of environments, from surface associations with other organisms to the ocean depths, often facing rapid changes in climate and salinity [139], [140], [141]. To survive these harsh and fluctuating conditions, they adapt primarily by modifying their membranes, especially the LPS component [139], [140]While Lipid A is generally the most conserved part of LPS, marine bacteria exhibit significant alterations in this structure, such as shortened, desaturated, and branched acyl chains, that reinforce their outer membranes against environmental stresses [141]. This chapter presents the MALDI-TOF MS and MS/MS analysis of Lipid A extracted from three *Cellulophaga* species within the phylum *Bacteroidetes*: *C. algicola* ACAM 630^T, isolated from Antarctic algal [142]; *C.*

baltica NNO 15840^T, from brown alga *Fucus serratus* in the North Sea [143]; and *C. tyrosinoxydans* EM41^T, obtained from seawater near Jeju Island, Republic of Korea [144]. These analyses aimed to elucidate structural adaptations linked to marine survival and their potential immunological implications.

9.2 Isolation and Compositional analysis of the LPS from Cellulophaga

LPS was extracted from dried cells of *C. algicola* ACAM 630^T, *C. baltica* NNO 15840^T, and *C. tyrosinoxydans* EM41^T through the hot phenol/water method (Chapter XI, paragraph 11.2). Crude LPS was extensively purified by means of enzymatic digestion, dialysis, ultracentrifugation, and size-exclusion chromatography. The nature and degree of purity were then evaluated by SDS-PAGE followed by silver nitrate gel staining [145]. The gel displayed, for all three bacterial species, a ladder-like pattern typical of an O-antigen-containing LPS (i. e., an S-LPS) (not shown), which was in accordance with previous analyses [146], [147]. A detailed compositional analysis was performed on the three LPSs to establish the fatty acid content. This analysis disclosed an exceptionally heterogenous composition, which entailed also the presence of 2-hydroxylated acyl chains (i. e. 15: 0(2-OH)), and that was qualitatively identical for *C. baltica* NNO 15840^T and *C. tyrosinoxydans* EM41^T while slightly differed for *C. algicola* ACAM 630^T. In particular, a higher degree of unsaturated fatty acids was observed for *C. baltica* NNO 15840^T and *C. tyrosinoxydans* EM41^T compared to *C. algicola* ACAM 630^T. To gain insights into the lipid A structure, an aliquot of each purified LPS underwent a mild acid hydrolysis followed by centrifugation to isolate the lipid A as the water-insoluble precipitate. After purification, the isolated lipid A fractions were analyzed via MALDI-TOF MS and MS/MS, and in parallel, underwent detailed compositional analysis that disclosed the occurrence of D-configured 2-amino-2-deoxy-glucose (glucosamine), as

expected, and mannose, (*Figure 9.1*), which thus indicated the presence of this additional sugar on the lipid A of *Cellulophaga* strains.

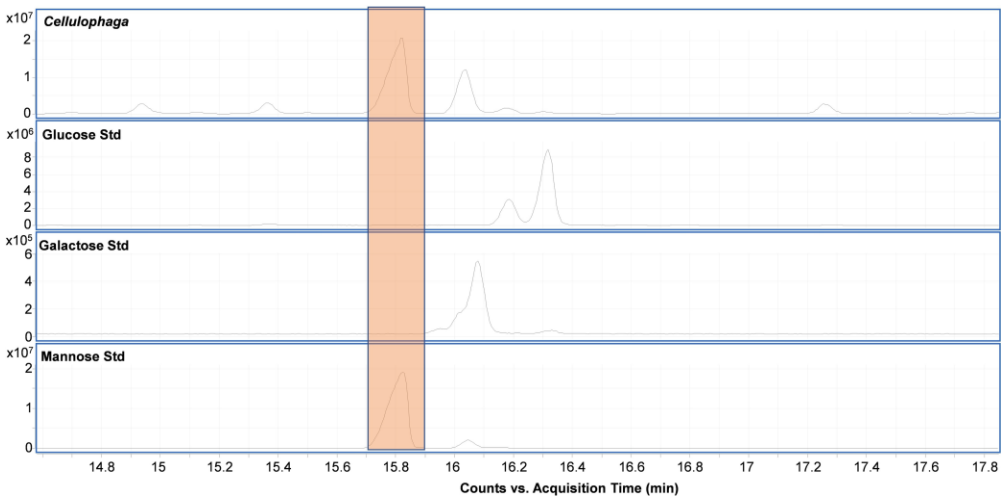

Figure 9.1: (a) Zoomed GC-MS chromatogram of the AMG of the hexose found in all *Cellulophaga* lipid A fractions. (b–d) GC-MS profiles of AMG from glucose (b), galactose (c), and mannose (d) standards. Retention time comparison identifies the unknown hexose as mannose.

9.3 MALDI-TOF MS and MS/MS of lipid A from Cellulophaga strains

Reflectron MALDI-TOF mass spectra, recorded in negative-ion polarity, of *C. algicola* ACAM 630^{T}, *C. baltica* NNO 15840^{T}, and *C. tyrosinoxydans* EM41^{T} lipid A are reported in *Figure 9.2*, while those recorded in positive-ion polarity are in *Figure 9.3*. As shown in *Figure 9.2*, MALDI-TOF MS spectra were similar, and all displayed the occurrence of two main clusters of peaks that matched with [M- H] mono-phosphorylated tetra-acylated (at about m/z 1625) and penta-acylated lipid A species (at about m/z 1849). In addition, in all three MALDI-TOF mass spectra, minor groups of peaks ascribed to tetra- and penta-acylated species that differed in 162 amu were also found and suggested the occurrence of a hexose on the typical lipid A

glucosamine disaccharide backbone, which was in accordance with chemical analyses. Finally, a minor family of peaks was identified at about m/z 2089 and matched with mono-phosphorylated hexaacylated lipid A species carrying the hexose unit (*Figure 9.2*). The complexity and structural heterogeneity of these lipid As were even more palpable due to the presence of peaks differing in 14 amu (a - CH2- unit) for each of the above clusters, which was diagnostic for the presence of lipid A forms that differ in the length of their acyl chain moieties. In addition, peaks also differing in 2 amu, due to the occurrence of unsaturated fatty acids, were also identified and were particularly evident in the MS spectra of C. *baltica* NNO 15840^T and *C. tyrosinoxydans* EM41^T (*Figure 9.2b and 9.2c*), in agreement with compositional analysis. Pushing the boundaries of such an utmost structural variety, a cluster of peaks assigned to bis-phosphorylated penta-acylated lipid A species lacking in the hexose decoration was identified only in the *C. algicola* ACAM 630^T lipid A spectrum (*Figure 9.2a*). In detail, the main peak at m/z 1849.7 detected for *C. algicola* ACAM 630^T and *C. baltica* NNO 15840^T (*Figure 9.2a,b*) was assigned to a penta-acylated lipid A species composed of the typical glucosamine disaccharide backbone substituted by one phosphate and one hexose, and mainly bearing two hydroxyeptadecanoic acids [17 : 0(OH) or i17 :0(OH) or a17: 0(OH)], one hydroxypentadecanoic acid [15 :0(OH) or i15:0(OH) or a15: 0(OH)], one hydroxyhexadecanoic acid [16 : 0(OH)] and one hexadecanoic acid (16 : 0) (*Table 9.1*); whereas the main peak at m/z 1835.7 detected for *C. tyrosinoxydans* EM41^T matched with a mono-phosphorylated lipid A species, decorated by one hexose and carrying one 17: 0(3-OH) [or i17 :0(OH) or a17: 0(OH)], two 16: 0(OH), one 15: 0(OH) [or i15:0(OH) or a15: 0(OH)], and one 16:0 (*Table 9.1*). For the sake of simplicity, hereafter the acyl moieties will be mentioned without indicating their linear or branched nature, taking into consideration that most of them can be also found in their anteiso- and isobranched structures. As for *C. algicola* ACAM 630^T, the peak at m/z 1767.6 was assigned to a bis-phosphorylated penta-acylated lipid A species carrying two 17: 0(OH), one 16: 0(OH), one 15: 0(OH), and one 16:0 (*Table*

9.1). To exclude possible alterations of the lipid A derived by the mild acid treatment, we have also executed a MALDI-TOF MS investigation directly on bacterial pellets following Larrouy-Maumus et al. (2016) protocol [148]. The negative-ion MALDI-TOF mass spectra confirmed the structural hypothesis deduced by analysis of the isolated lipid A fractions (*Figure 9.2*), thus excluding any lack of structural information likely occurring as a consequence of the chemical treatment to isolate the lipid A. A detailed negative-ion MS/MS investigation was executed to unveil the exact location of the lipid A acyl moieties with respect to the glucosamine disaccharide skeleton as well as the position of the phosphate and the hexose residue. In detail, the MS/MS spectrum of the precursor ion at m/z 1849.7 (*Figure 9.4a*) displayed two intense peaks at m/z 1577.6 and m/z 1593.7 that were attributed to ions derived by the loss of a 16: 0(OH) and a 16: 0, respectively. Less intense peaks were observed at m/z 1319.5, m/z 1321.5, and m/z 1335.4 and matched with fragments that originated from the loss of a 15:0(OH) and a 16:0(OH) (for m/z 1319.5), a 16: 0(OH) and a 16:0 (for m/z 1321.5), and a 15: 0(OH) and a 16:0 (for m/z 1335.4) (*Figure 9.4a*). The absence of any peak ascribable to the loss of a whole unit comprising a hydroxylated fatty acid bearing 16:0 as a secondary acyl substituent was a first indication that the latter was present in an acyloxyacyl amide moiety. This structural hypothesis was then corroborated by the observation of the peaks at m/z 675.5 and m/z 449.5 assigned to fragments originating from a rearrangement that only occurs when the Nlinked fatty acids at positions C-2 and C-2' have a free 3-OH group, i. e. they do not bear secondary acyl chains [149]. Indeed, a six-membered ring-based rearrangement that followed an enamine to imine tautomerization enabled the generation of a loss of a $C_{15}H_{30}O$ neutral fragment (226 amu) from each primary amide-linked acyl chain possessing a free 3-OH group. Since such a rearrangement was observed only when 16:0 was absent, the occurrence of the peaks at m/z 675.5 and m/z 449.5 suggested that the 16:0 unit was a secondary acyl substituent of a primary N-linked moiety. Finally, the detection of the Y1 ion [150] (m/z 766.7), derived by the cleavage of the glycosidic linkage of the glucosamine backbone, enabled (i) to locate the phosphate

group on the reducing glucosamine unit that in turn also carried a 17: 0(OH) and a 15: 0(OH), (ii) to establish that the 16:0 was a secondary fatty acid of the nonreducing glucosamine, and also (iii) to place the hexose unit on the same nonreducing glucosamine. Of note, other peaks at m/z 1579.6 and m/z 1591.7 were also identified and matched with ions derived by the loss of one 17:0 and one 15:0(OH) respectively, thus suggesting the co-existence of two isobaric lipid A forms, that is one carrying two 17: 0(OH), one 15: 0(OH), one 16: 0(OH) and one 16: 0, while the other bears two 17: 0(OH), two 15: 0(OH), and one 17: 0. Likewise, the structure of the lipid A species at m/z 1835.7, detected as the main peak in the *C. tyrosinoxydans* EM41^T MS spectrum (*Figure 9.2c*) was also defined, revealing a penta-acylated lipid A carrying two 16: 0(OH), one 17: 0(OH), one 15:0(OH) and one 16: 0. In both cases (*Figure 9.4a and b*), the occurrence of the C1-type ion [150] at m/z 179.2/179.3, originating from the cleavage of the glycosidic linkage between the hexose and the nonreducing glucosamine was a further confirmation of the presence of this additional sugar on the lipid A backbone. Likewise, an ion originated from the sugar ring fragmentation 0,2A1 [150] occurring on the hexose was also assigned to the peak at m/z 119.2/119.3. To unequivocally locate acyl chains with the respect to the glucosamine backbone, it was fundamental to also analyse the three lipid A fractions upon treatment with NH_4OH, which selectively cleaved the acyl and acyloxyacyl esters and left the acyl and acyloxyacyl amides unaffected [151]. Also, in this case the astounding structural heterogeneity of *Cellulophaga* lipid A was immediately apparent and several clusters of peaks were identified (*Figure 9.5*). In particular, the negative-ion MALDI-TOF MS analysis of the NH_4OH treated lipid A was fundamental to disclose the occurrence of hydroxylated secondary acyl substituents on the reducing glucosamine, as proven by the detection of tetra-acylated lipid A as the main species, which were surprisingly still present after NH_4OH treatment. In particular, the peak at m/z 1609.6 (*Figure 9.5a and 9.5b*) was assigned to a tetra-acylated lipid A species carrying one phosphate, one hexose, and bearing two primary N-linked 17: 0(OH), and one 15: 0(OH) and one 17:0 as secondary fatty acids of the reducing and nonreducing glucosamine,

respectively. Tri-acylated lipid A species carrying only amide-linked fatty acids and one secondary acyl chain were also identified at about m/z 1383 and m/z 1369. Finally, lipid A species carrying the sole N-linked acyl chains were detected at m/z 1117.3. The lack of substituents at position 4 of the reducing glucosamine in the penta- acylated lipid A species also enabled to tentatively place the sixth acyl chain in the minor hexa-acetylated lipid A family (cluster at about m/z 2089, *Figure 9.2*) in such a position. However, the location of the sixth acyl chain remained to be confirmed. In addition, due to the detection of 15: 0(2-OH) in the compositional analysis, it might be also speculated that this fatty acid is present as a secondary substituent of the primary N-linked acyl chains of the reducing glucosamine in the pentaacylated lipid A forms, as previously observed for other bacteria experiencing secondary 2- hydroxylation in their lipid A.[152], [153]. Finally, in order to shed light on the actual presence of lipid A species decorated by two phosphate groups, and therefore lacking in the hexose decoration, the precursor ion at m/z 1753.6 was chosen as representative of the cluster ascribed to bis-phosphorylated penta-acylated lipid A species and analyzed by negative-ion MS/MS. The spectrum (*Figure 9.6*) showed an intense peak at m/z 1481.5 that matched with an ion derived by the loss of a 16: 0(OH) unit, while two less intense peaks were detected at m/z 1401.4 and m/z 1655.5 and were assigned to ions originated from the loss of a phosphate group (for m/z 1655.5), or a 16: 0(OH) unit and phosphate (for m/z 1401.4). The observation of the C1-type ion at m/z 1004.8 corroborated the structural hypothesis of the nonreducing glucosamine carrying one phosphate, two 16: 0(OH) and one secondary 16: 0, which in turn was reflected in the occurrence of the peak at m/z 490.4 attributable to a fragment comprising the reducing glucosamine carrying the phosphate and one 17: 0(OH). The combination of data from chemical analyses, MALDITOF MS and MS/MS investigation of lipid A and NH_4OH-treated lipid A allowed the structural determination of the glycolipid anchor of *C. algicola* ACAM 630^T, *C. baltica* NNO 15840^T and *C. tyrosinoxydans* EM41^T LPS. A complex mixture of monophosphorylated tetra- to hexa-acylated lipid A species variously acylated by saturated and unsaturated, branched and unbranched

fatty acids, and also bearing a mannose unit on the nonreducing glucosamine was unveiled for all three LPS. Additionally, *C. algicola* ACAM 630^{T} was found to also synthesize bis-phosphorylated lipid A species, lacking in the mannosylation of the sugar backbone.

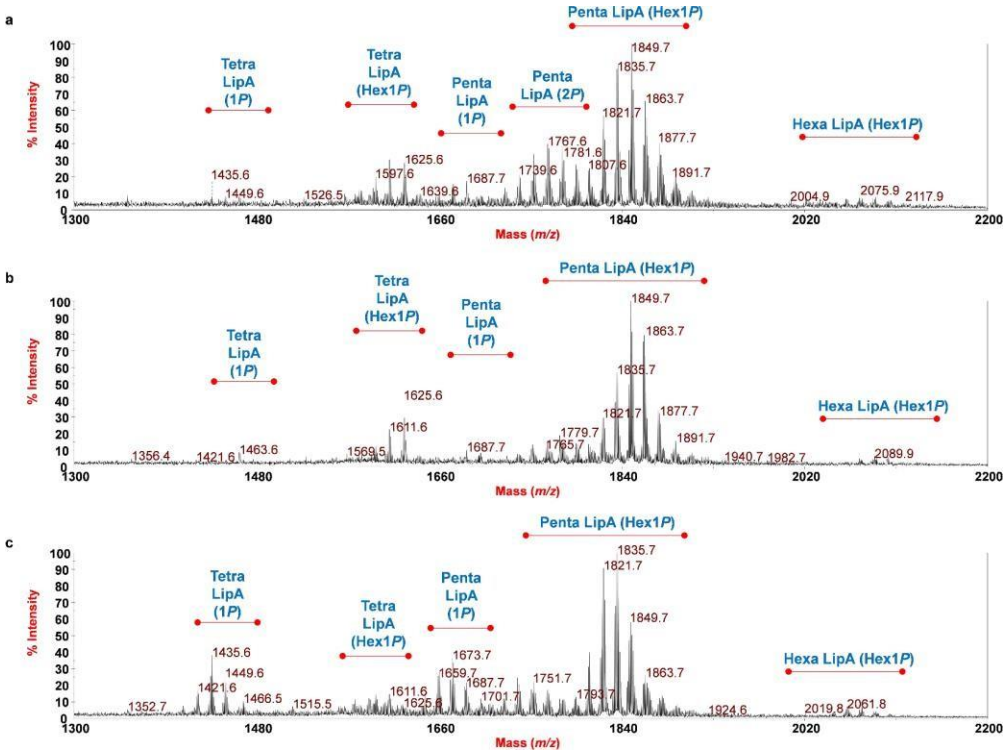

Figure 9.2: (a–c) Negative-mode reflectron MALDI-TOF spectra of lipid A from *C. algicola* ACAM 630^{T} (a), *C. baltica* NNO 15840^{T} (b), and *C. tyrosinoxidans* EM41^{T} (c) after acetate buffer treatment. Lipid A species are labeled as Tetra-, Penta-, or Hexa-Lip A based on acylation. "Hex1P" indicates one phosphate and one hexose (mannose); "1P" and "2P" refer to species with one or two phosphates, lacking or replacing the hexose, respectively.

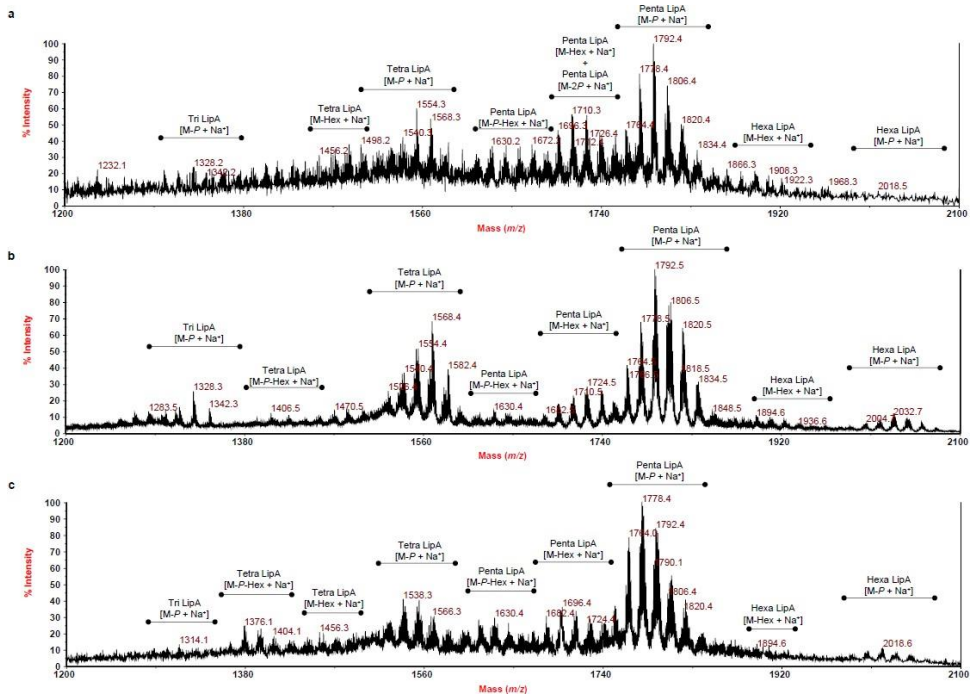

Figure 9.3: Reflectron MALDI-TOF mass spectra, recorded in positive polarity, of lipid A from *C. algicola* ACAM 630^T (**a**), *C. baltica* NNO 15840^T (**b**), and *C. tyrosinoxidans* EM41^T (**c**) obtained after acetate buffer treatment of each LPS fraction. The lipid A species are labelled as Tetra-, Penta- and Hexa- Lip A indicating the degree of acylation.

Table 1. The main ion peaks observed in the MALDI-TOF MS spectra reported in Figures 2 and 4, the predicted masses, and the proposed interpretation of the substituting fatty acids, phosphate (*P*) and hexose (Hex), on the lipid A backbone. The observed masses listed in the table are compared to the calculated monoisotopic mass (predicted mass, Da) of each ion based on the proposed lipid A structures.

Lipid A (Figure 2) Predicted mass (Da)	Observed ion peaks (*m/z*)	Acyl substitution	Proposed composition
2090.5	2089.9	Hexa-acyl	HexN^2, *P*, Hex, [17:0(3-OH)]^2, 15:0(3-OH), 15:0(2-OH), 16:0(3-OH), 16:0
1864.3	1863.7	Hexa-acyl	HexN^2, *P*, Hex, [17:0(3-OH)]^2, 15:0(2-OH), 16:0(3-OH), 17:0
1850.3	1849.7	Penta-acyl	HexN^2, *P*, Hex, [17:0(3-OH)]^2, 15:0(2-OH), 16:0(3-OH), 16:0
1836.3	1835.7	Penta-acyl	HexN^2, *P*, Hex, [16:0(3-OH)]^2, 17:0(3-OH), 15:0(2-OH), 16:0
1782.2	1781.6	Penta-acyl	HexN^2, *P*^{2}, [17:0(3-OH)]^2, 15:0(2-OH), 16:0(3-OH), 17:0
1768.2	1767.6	Penta-acyl	HexN^2, *P*^{2}, [17:0(3-OH)]^2, 15:0(2-OH), 16:0(3-OH), 16:0
1754.2	1753.6	Penta-acyl	HexN^2, *P*^{2}, [16:0(3-OH)]^2, 17:0(3-OH), 15:0(2-OH), 16:0
1688.3	1687.7	Penta-acyl	HexN^2, *P*, [17:0(3-OH)]^2, 15:0(2-OH), 16:0(3-OH), 16:0
1612.1	1611.6	Penta-acyl	HexN^2, *P*, Hex, [17:0(3-OH)]^2, 15:0(2-OH), 16:0(3-OH)
1450.0	1449.6	Tetra-acyl	HexN^2, *P*, [17:0(3-OH)]^2, 15:0(2-OH), 16:0(3-OH)
1436.0	1435.6	Tetra-acyl	HexN^2, *P*, [17:0(3-OH)]^2, 15:0(2-OH), 15:0(3-OH)
NH_4OH treated lipid A (Figure 4)			
1610.1	1609.6	Tetra-acyl	HexN^2, *P*, Hex, [17:0(3-OH)]^2, 15:0(2-OH), 17:0
1596.1	1595.6	Tetra-acyl	HexN^2, *P*, Hex, [17:0(3-OH)]^2, 15:0(2-OH), 16:0
1528.0	1527.5	Tetra-acyl	HexN^2, *P*^{2}, [17:0(3-OH)]^2, 15:0(2-OH), 17:0
1448.0	1447.4	Tetra-acyl	HexN^2, *P*, [17:0(3-OH)]^2, 15:0(2-OH), 17:0
1369.9	1369.5	Tri-acyl	HexN^2, *P*, Hex, [17:0(3-OH)]^2, 17:0
1286.8	1287.3	Tri-acyl	HexN^2, *P*^{2}, [17:0(3-OH)]^2, 17:0
1117.6	1117.3	Di-acyl	HexN^2, *P*, Hex, [17:0(3-OH)]^2

Table 9.1

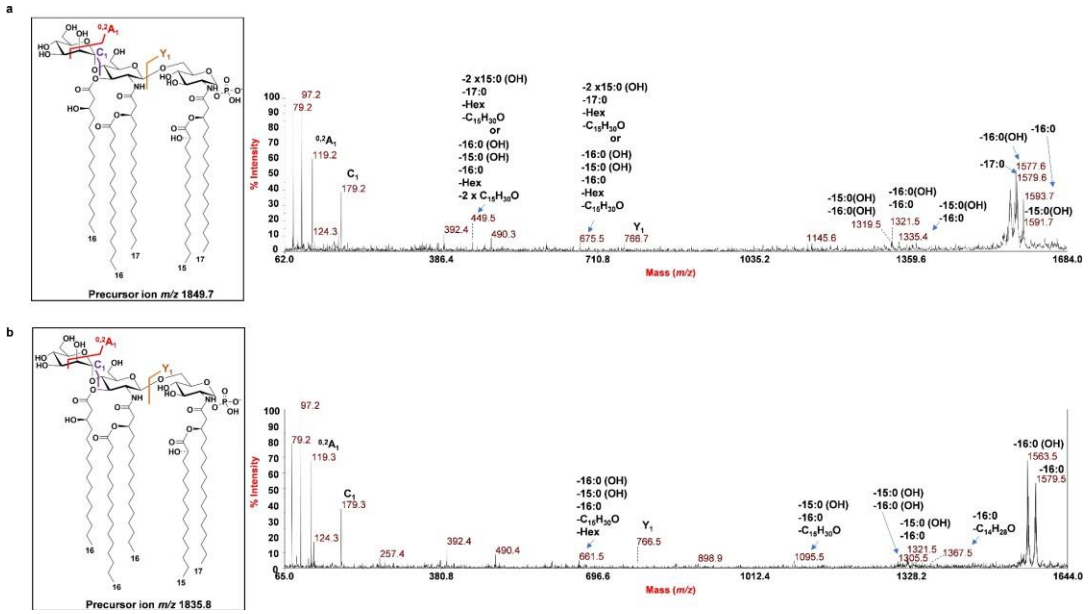

Figure 9.4 Negative-ion MALDI MS/MS spectra of precursor ions at *m/z* 1849.7 (a) and *m/z* 1835.7 (b), representative ion peaks of the cluster ascribed to pentaacylated lipid A species from *C. algicola* ACAM 630^{T}, *C. baltica* NNO 15840^{T}, and *C. tyrosinoxidans* EM41^{T}. The assignment of main fragments is reported in both spectra. Peaks derived by the loss of $C_{15}H_{30}O$ (226 mass units) or $C_{14}H_{28}O$ (212 mass units), due to the rearrangements occurring on amide-linked 3-OH acyl chains having the hydroxyl group free, have been also indicated. The proposed structures for the lipid A species are sketched in the insets, where the representation of acyl chains in their linear form is given for description purposes only. The α-anomeric configuration of the mannose is tentative. For the species detected at *m/z* 1849.7 (a), the main lipid A form has been sketched in the inset nevertheless an additional isobaric species present in minor amount was identified and is composed of two 17: 0(OH), two 15: 0(OH), and one 17: 0.

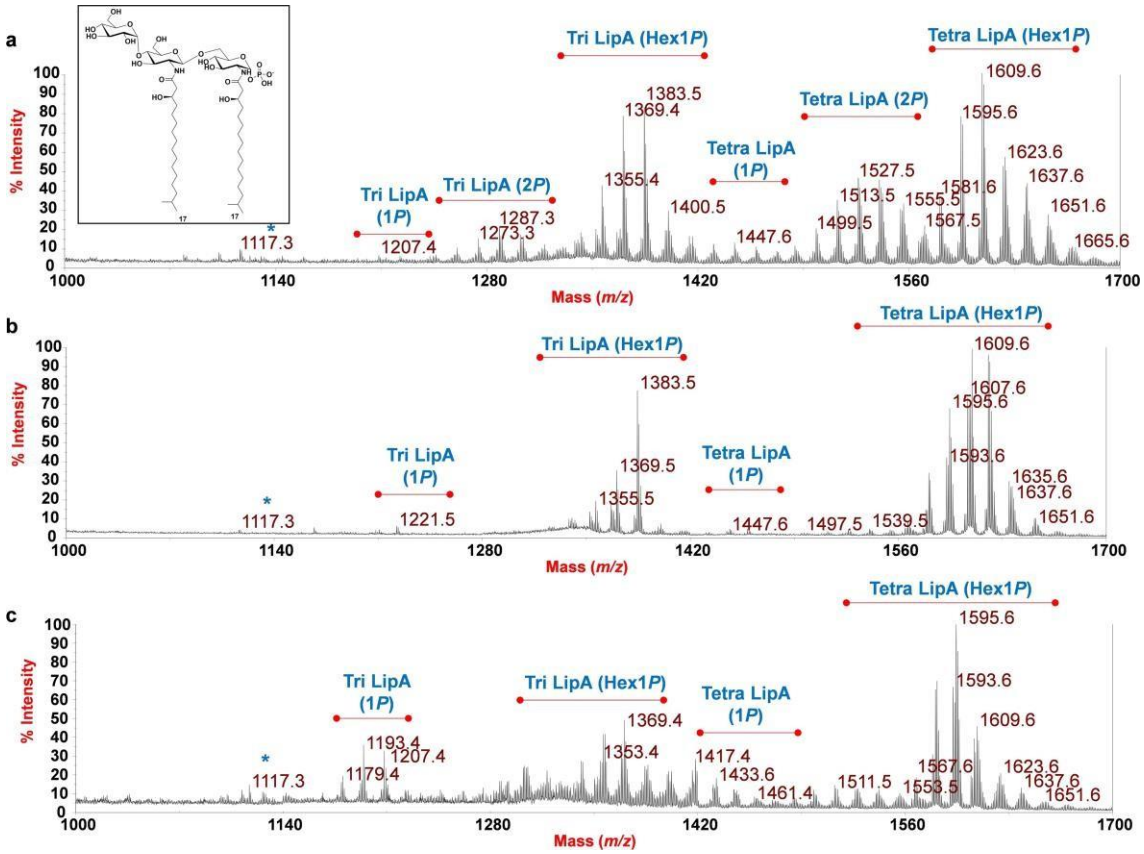

Figure 9.5: Reflectron MALDI- OF mass spectra, recorded in negative polarity, of lipid A from *C. algicola* ACAM 630^{T} (a), *C. baltica* NNO 15840^{T} (b), and *C. tyrosinoxidans* EM41^{T}(c) after treatment with NH_4OH. The lipid A species are labelled as Tri- and Tetra LipA indicating the degree of acylation. "Hex1*P*" indicates the lipid A species carrying one phosphate and one hexose (i. e. mannose) on the glucosamine disaccharide backbone. "1*P*" is indicative of lipid A species lacking in the hexose decoration, while "2*P*" has been used to label lipid A species having a phosphate group in place of the hexose on the nonreducing glucosamine unit. The asterisk indicates the peak that was assigned to the structure sketched in the inset.

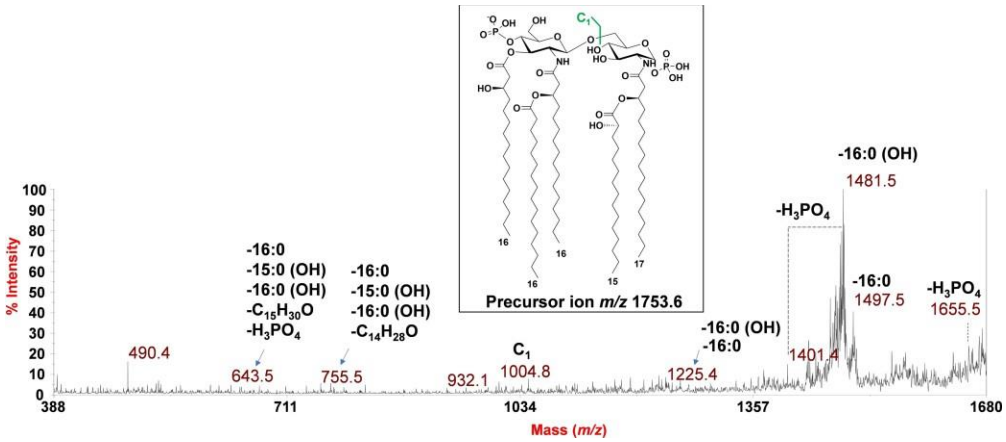

Figure 9.6: Negative-ion MALDI MS/MS spectrum of precursor ion at *m/z* 1753.6, chosen as a representative ion peak of the group ascribed to *bis*phosphorylated penta-acylated lipid A species detected only for *C. algicola* ACAM 630^{T}. The assignment of main fragments is reported. Peaks derived by the loss of $C_{15}H_{30}O$ (226 mass units) or $C_{14}H_{28}O$ (212 mass units) have been also reported. The proposed structure is sketched in the inset, where the representation of acyl chains in their unbranched form is given for description purposes only. The α-anomeric configuration of the mannose is tentative.

9.4 TLR activation by LPS from Cellulophaga

The immunological activity of LPSs from the three *Cellulophaga* species was evaluated in vitro by using HEK-Blue^{TM} hTLR4 cells. Activation of NF-kB was the read-out of this assay. Since HEKBlue^{TM} hTLR4 cells also stably express a secreted embryonic alkaline phosphatase (SEAP) that is produced upon activation of NF-kB, stimulation with a TLR4 ligand activates NF-kB and thereby the production of SEAP, which in turn can be detected in cell culture media by an alkaline phosphatase substrate. Therefore, HEK-Blue hTLR4 cells were stimulated with different concentrations (1, 10, and 100 ng/mL) of *C. algicola* ACAM 630^{T}, *C. baltica* NNO 15840^{T} or *C. tyrosinoxydans* EM41^{T} LPS, while *S. typhimurium* SH 2201 LPS was used as the positive control and at the same concentrations as above. Untreated cells

were evaluated as the negative control. As shown in *Figure 9.7*, a, LPSs from *C. baltica* NNO 15840^T and *C. tyrosinoxydans* EM41^T induced a significantly lower NF-kB activation compared to cells treated with S. typhimurium LPS (*C. baltica* NNO 15840^T and *C. tyrosinoxydans* EM41^T LPS vs. *S. typhimurium* LPS, $p<0.01$ at 1 ng/mL, and $p<0.001$ at 10 ng/mL and 100 ng/mL, *Figure 9.7a*), while no significant difference was observed between LPS of *C. algicola* ACAM 630^T and *S. typhimurium* LPS, thus suggesting that *C. algicola* ACAM 630^T expresses a more immunostimulatory LPS compared to *C. baltica* NNO 15840^T and *C. tyrosinoxydans* EM41^T. In parallel, the lack of any NF-kB activation in HEKBlue ™ Null2™ cells, used to evaluate the effective immunoactivation of *Cellulophaga* LPS via TLR4, indicated that NF-kB activation by all three LPSs was TLR4-dependent. In addition, to further assess the absence of phospholipids/ lipoproteins in LPS preparations, HEK-Blue^{TM} hTLR2 were stimulated with different concentrations (1, 10, and 100 ng/mL) of *C. algicola* ACAM 630^T, *C. baltica* NNO 15840^T or *C. tyrosinoxydans* EM41^T LPS as well as with LPS from *S. typhimurium* and analyzed as above for the HEK-Blue hTLR4 cells stimulation assay. In this experiment, the synthetic triacylated lipopeptide and TLR2 agonist Pam3CSK4 was used as the positive control. As shown in *Figure 9.7b*, no activation of NF-kB was recorded for all the LPSs tested in this latter experiment.

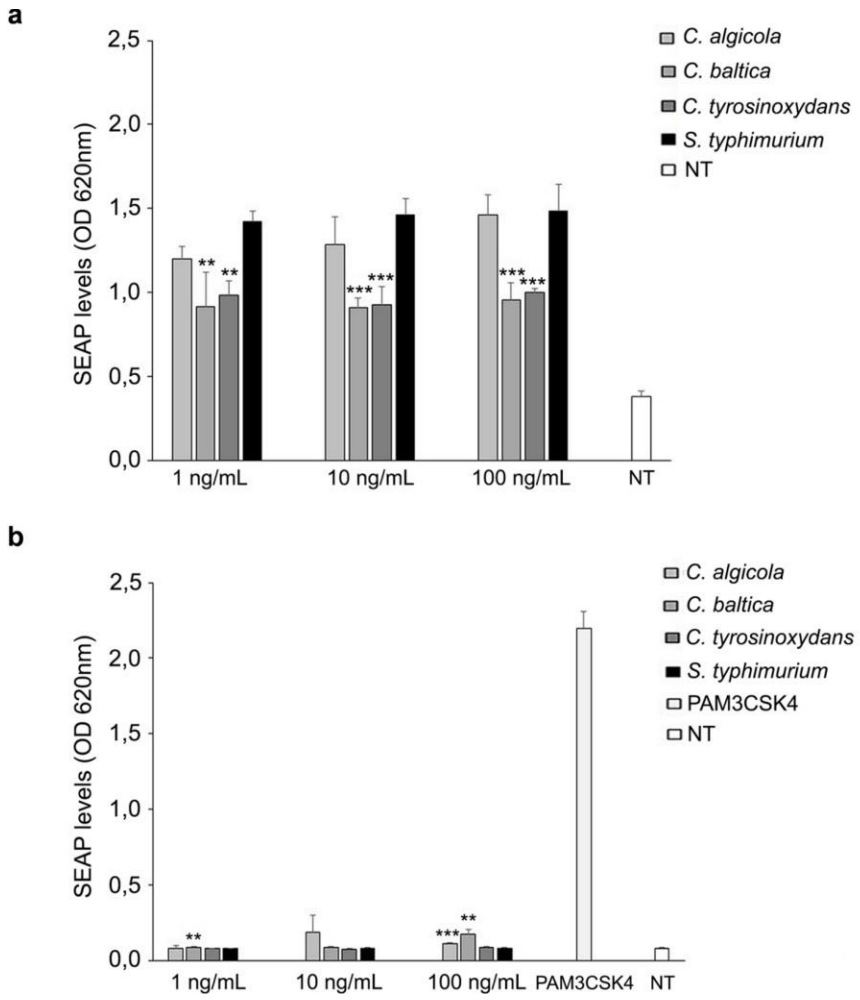

Figure 9.7: Stimulation of HEK Blue™ hTLR4 (a) and hTLR2 (b) cells with LPS from *C. algicola* ACAM 630^T, *C. baltica* NNO 15840^T, and *C. tyrosinoxidans* EM41^T at concentrations of 1, 10, and 100 ng/mL. LPS from *S. typhimurium* SH 2201 served as a positive control. SEAP activity (OD) is shown. Statistically significant differences between *C. baltica* and *C. tyrosinoxidans* LPS and *S. typhimurium* LPS are indicated (**p < 0.01; *p < 0.001, Student's t-test). NT: untreated cells. Data are presented as mean ± SD from three independent experiments performed in triplicate.

9.5 Conclusion

It is well established that bacteria inhabiting aquatic environments often adapt by modifying their membrane composition, particularly the chemical structure of LPS. These alterations are not only chemically intriguing but also biologically significant due to their immunomodulatory properties, which often result in low or even inhibitory inflammatory potential [140], [141], [154]. Numerous pharmaceutical compounds have been inspired by the structural diversity of LPS and Lipid A from marine bacteria, with applications as vaccine adjuvants and anti-sepsis agents [144]. Motivated by this potential, we investigated three *Cellulophaga* species, focusing first on the structural characterization of Lipid A and then on the immunomodulatory activity of their LPS via TLR4 signaling. MALDI-TOF MS analysis revealed pronounced heterogeneity in Lipid A structures, with variations in acyl chain length and number, phosphorylation patterns, and sugar decorations. Consistent with other marine bacteria, these *Cellulophaga* strains predominantly produce hypoacylated and hypophosphorylated Lipid A. In particular, the substitution of phosphate groups with sugars on the glucosamine backbone may confer increased membrane stability in fluctuating marine environments, given the greater strength of glycosidic bonds compared to phosphate esters. Membrane fluidity is further supported by the presence of unsaturated acyl chains [141], as well as fatty acids with odd carbon numbers and branching, features typical of the *Bacteroidetes* phylum [141]. Hydroxylated acyl chains, often found as secondary substituents on the reducing glucosamine, are another recurring trait in *Cellulophaga*.

To assess the immunological relevance of these structural features, we performed TLR4 activation assays using HEK-Blue cells. LPS from *C. baltica* NNO 15840^T and *C. tyrosinoxydans* EM41^T showed reduced activation compared to *Salmonella* LPS, likely due to their hypoacylated and hypophosphorylated Lipid A. Although these species can produce hexa-acylated forms, their 3+3 symmetry around the glucosamine backbone is less immunogenic than the more stimulatory 4+2 configuration [155].

Additionally, the presence of only one phosphate group on the reducing glucosamine further contributes to their low immunostimulatory potency [155]. In contrast, LPS from *C. algicola* ACAM 630^{T} activated TLR4 similarly to *Salmonella* LPS, likely due to the presence of bis-phosphorylated tetra/penta-acylated Lipid A and mono-phosphorylated hexa-acylated variants. These findings underscore the structural complexity of Lipid A in marine bacteria and its impact on immune activation, even among closely related species. Ultimately, this study highlights the potential of environmental bacteria as a source of novel biomolecules for immunomodulatory and therapeutic applications. The structural diversity of LPS and Lipid A in marine organisms offers promising avenues for the development of innovative treatments targeting immune-related diseases.

References

[138] R. Kittelberger and F. Hilbink, "Sensitive silver-staining detection of bacterial lipopolysaccharides in polyacrylamide gels," *J Biochem Biophys Methods*, vol. 26, no. 1, pp. 81–86, Feb. 1993, doi: 10.1016/0165-022X(93)90024-I.

[139] S. Menden-Deuer, J. Rowlett, M. Nursultanov, S. Collins, and T. Rynearson, "Biodiversity of marine microbes is safeguarded by phenotypic heterogeneity in ecological traits," *PLoS One*, vol. 16, no. 8, p. e0254799, Aug. 2021, doi: 10.1371/journal.pone.0254799.

[140] M. Anwar and S. Choi, "Gram-Negative Marine Bacteria: Structural Features of Lipopolysaccharides and Their Relevance for Economically Important Diseases," *Mar Drugs*, vol. 12, no. 5, pp. 2485–2514, Apr. 2014, doi: 10.3390/md12052485.

[141] F. Di Lorenzo, J. Billod, S. Martín-Santamaría, A. Silipo, and A. Molinaro, "Gram-Negative Extremophile Lipopolysaccharides: Promising Source of Inspiration for a New Generation of Endotoxin Antagonists," *European J Org Chem*, vol. 2017, no. 28, pp. 4055–4073, Aug. 2017, doi: 10.1002/ejoc.201700113.

[142] J. P. Bowman, "Description of Cellulophaga algicola sp. nov., isolated from the surfaces of Antarctic algae, and reclassification of Cytophaga uliginosa (ZoBell and Upham 1944) Reichenbach 1989 as Cellulophaga uliginosa comb. nov.," *Int J Syst Evol Microbiol*, vol. 50, no. 5, pp. 1861–1868, Sep. 2000, doi: 10.1099/00207713-50-5-1861.

[143] J. E. Johansen, P. Nielsen, and C. Sjøholm, "Description of Cellulophaga baltica gen. nov., sp. nov. and Cellulophaga fucicola gen. nov., sp. nov. and reclassification of [Cytophaga] lytica to Cellulophaga lytica gen. nov., comb. nov.," *Int J Syst Evol Microbiol*, vol. 49, no. 3, pp. 1231–1240, Jul. 1999, doi: 10.1099/00207713-49-3-1231.

[144] Y. Tanaka *et al.*, "Marine-derived microbes and molecules for drug discovery," *Inflamm Regen*, vol. 42, no. 1, p. 18, Jun. 2022, doi: 10.1186/s41232-022-00207-9.

[145] R. Kittelberger and F. Hilbink, "Sensitive silver-staining detection of bacterial lipopolysaccharides in polyacrylamide gels," *J Biochem Biophys Methods*, vol. 26, no. 1, pp. 81–86, Feb. 1993, doi: 10.1016/0165-022X(93)90024-I.

[146] A. V. Perepelov *et al.*, "A similarity in the O-acetylation pattern of the O-antigens of Shigellaflexneri types 1a, 1b, and 2a," *Carbohydr Res*, vol. 344, no. 5, pp. 687–692, Mar. 2009, doi: 10.1016/j.carres.2009.01.004.

[147] N. Graham, J. G. Robson, and J. Nachmias, "Grating summation in fovea and periphery.," *Vision Res*, vol. 18, no. 7, pp. 815–25, 1978, doi: 10.1016/0042-6989(78)90122-0.

[148] R. C. D. Furniss *et al.*, “Detection of Colistin Resistance in Escherichia coli by Use of the MALDI Biotyper Sirius Mass Spectrometry System,” *J Clin Microbiol*, vol. 57, no. 12, Dec. 2019, doi: 10.1128/JCM.01427-19.

[149] F. Di Lorenzo *et al.*, “The Lipid A from *Rhodopseudomonas palustris* Strain BisA53 LPS Possesses a Unique Structure and Low Immunostimulant Properties,” *Chemistry – A European Journal*, vol. 23, no. 15, pp. 3637–3647, Mar. 2017, doi: 10.1002/chem.201604379.

[150] B. Domon and C. E. Costello, “A systematic nomenclature for carbohydrate fragmentations in FAB-MS/MS spectra of glycoconjugates,” *Glycoconj J*, vol. 5, no. 4, pp. 397–409, 1988, doi: 10.1007/BF01049915.

[151] A. Silipo, R. Lanzetta, A. Amoresano, M. Parrilli, and A. Molinaro, “Ammonium hydroxide hydrolysis,” *J Lipid Res*, vol. 43, no. 12, pp. 2188–2195, Dec. 2002, doi: 10.1194/jlr.D200021-JLR200.

[152] J. J. . Barchi, *Comprehensive glycoscience edited-in-chief, Joseph J. Barchi, Jr.* Elsevier, 2021.

[153] L. MacDonald *et al.*, “Polymyxin Resistance and Heteroresistance Are Common in Clinical Isolates of *Achromobacter* Species and Correlate with Modifications of the Lipid A Moiety of Lipopolysaccharide,” *Microbiol Spectr*, vol. 11, no. 1, Feb. 2023, doi: 10.1128/spectrum.03729-22.

[154] L. Zaffaroni and F. Peri, “Recent Advances on Toll-Like Receptor 4 Modulation: New Therapeutic Perspectives,” *Future Med Chem*, vol. 10, no. 4, pp. 461–476, Feb. 2018, doi: 10.4155/fmc-2017-0172.

Chapter X

Cold-Adapted Lipid A from Polaribacter sp. SM1127: A Study of Structural Heterogeneity and Immunostimulatory Properties

This studywas published in Chembiochem 2025 Apr 21;26(12): e202500100.
doi: 10.1002/cbic.202500100

Premise. *Polaribacter* sp. SM1172 is a Gram-negative marine bacterium isolated from Arctic Laminaria algae, where it plays a key role in degrading biopolymers within the ecosystem. Notably, its exopolysaccharides possess promising biotechnological properties, including antioxidant activity and wound healing potential. This chapter presents the characterization of Lipid A highlighting significant structural heterogeneity revealed through mass spectrometry. This diversity likely reflects adaptive modifications enabling the bacterium to thrive in extreme Arctic conditions. Immunological assays further demonstrate that its Lipid A induces only minimal activation of NF-κB signaling pathways, suggesting potential applications of these bacterial components as immunomodulatory agents or vaccine adjuvants.

10.1 Introduction

The genus *Polaribacter*, part of the *Flavobacteriaceae* family, comprises Gram-negative marine bacteria renowned for their ability to thrive in cold, nutrient-poor

environments. These organisms play a crucial role in the degradation of biopolymers such as proteins and polysaccharides [156], [157]. The strain examined in this study, *Polaribacter* sp. SM1127, was isolated from *Laminaria*, a brown macroalga found along Arctic coastlines. Its enzymatic capacity to break down compounds like laminarin and fucoidan enables colonization of algal surfaces and contributes to carbon and nutrient cycling [156]. Recent interest has focused on the bacterium's exopolysaccharide (EPS), which exhibits antioxidant properties, moisture retention, and wound-healing potential, traits that underscore its biotechnological relevance [158]. *Polaribacter* sp. survives extreme Arctic conditions through various molecular adaptations, particularly modifications to its membrane composition. Central to this adaptation is the LPS, which undergoes structural changes to enhance membrane stability and protect against cold-induced stress [116]. These alterations include variations in glycan and lipid components, such as changes in sugar residues, acylation patterns of Lipid A, and incorporation of alternative substituents, all of which influence the membrane's physical and immunological properties [116].

To deepen our understanding of microbial adaptation to Arctic environments and to explore the structure–function relationships of LPS and EPS, we have defined both the structure and immunological properties of LPS isolated from *Polaribacter* sp. SM1127 with the ultimate goal of identifying novel molecules for immunotherapeutic or adjuvant applications.

10.2 Isolation and Chemical Analyses of the LPS from Polaribacter sp. SM1127

To isolate and characterize the lipid A from *Polaribacter* sp. SM1127 LPS, two approaches were employed (*Figure 10.1*). First, an aliquot of ethanol precipitation product (EPS-EtOH) containing both EPS and bacterial cell remnants underwent mild acid hydrolysis with acetate buffer, followed by centrifugation to isolate the lipid A in the waterinsoluble fraction ($LipA_{abh}$). In the second approach, EPS-EtOH was ultracentrifuged to separate bacterial cells (which formed the precipitate) from the

EPS (found in the supernatant). Both fractions were then lyophilized and enzymatically digested. The precipitate from ultracentrifugation (UCF_{pc}) was analyzed by sodium dodecyl sulphate–polyacrylamide gel electrophoresis (SDS–PAGE) with silver nitrate staining, which confirmed the presence of LPS in this fraction and indicated its "rough" nature, as evidenced by a gel band typical of low-molecular-mass R-LPS, lacking the O-antigen (*Figure 10.2*). Following the removal of phospholipids using sequential chloroform–methanol and chloroform–methanol–water washes, UCF_{pc} underwent a smallscale extraction procedure to isolate the lipid A fraction ($LipA_{sse}$). Both $LipA_{sse}$ and $LipA_{abh}$ were then subjected to compositional analysis to determine their fatty acid and monosaccharide content. In particular, aliquots of $LipA_{sse}$ and $LipA_{abh}$ underwent methanolysis, followed by acetylation to analyse the fatty acids as methyl esters and to identify the sugar components of the lipid A backbone. The analysis revealed an extremely heterogeneous fatty acid composition, which was qualitatively similar for both $LipA_{sse}$ and $LipA_{abh}$ (*Table 10.1*), and as expected showed the occurrence of the acetylated methyl glycoside derivative of 2-amino-2- deoxy-D-glucose (D-glucosamine). This, along with the fatty acid analysis, provided crucial information for the elucidation of the lipid A structure, which was achieved by matrix-assisted laser desorption/ionization - time of flight (MALDI-TOF) mass spectrometry (MS) and MS/MS analysis of both $LipA_{sse}$ and $LipA_{abh}$.

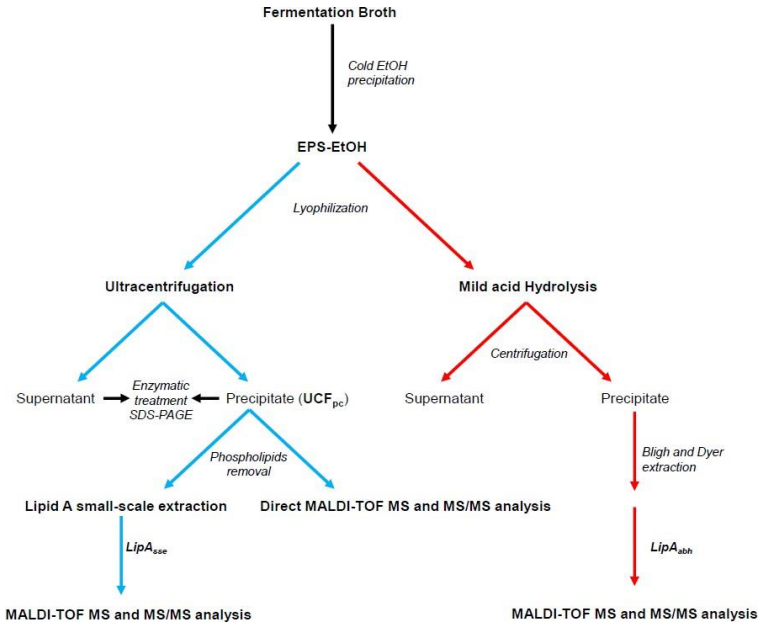

Figure 10.1: A diagram illustrating the methodology used to extract, identify, and characterize the lipid A from *Polaribacter* sp. SM1127, beginning with the crude ethanol-precipitate (*EPS-EtOH*) that was initially collected for isolating the EPS.

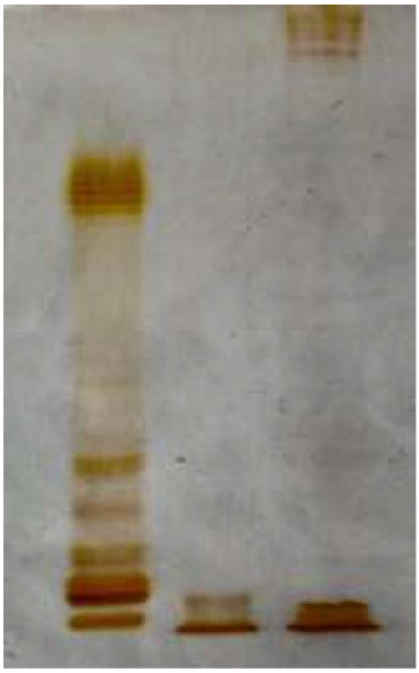

Figure 10.2*:* SDS-PAGE with silver staining shows R-LPS from *Polaribacter* sp. SM1127 (Lane 2) after enzymatic digestion. Lane 3 contains crude EPS with two distinct bands: upper (EPS) and lower (R-LPS). Lane 1 shows S-LPS from *E. coli* O111:B4 as a reference.

Table 1. Fatty acid content of $LipA_{sse}$ and $LipA_{abh}$ isolated from *Polaribacter* sp. SM1127.

Fatty acid component[a)]
*i*13:0
13:0
*i*14:0
14:0
14:0(3-OH)
*i*15:1
*i*15:0
15:0 (*a*15:0)
15:1
15:0
*i*15:0(3-OH)
*a*15:0(3-OH)
15:0(3-OH)
16:1
16:0
*i*16:0(3-OH)
16:0(3-OH)
*a*17:1
17:1
17:0
*a*17:0(3-OH)

[a)]Both lipid A fractions showed the same fatty acid composition. All 3-hydroxy fatty acids displayed an (*R*) configuration. The position of the double bond or the stereochemistry of the unsaturated acyl chains remain to be identified. The stereochemistry of anteiso-branched acyl chains is tentatively given as (*S*) being predominant in bacteria; however, it remains to be confirmed. "*i*" stands for iso and "*a*" stands for anteiso.

Table 10.1

10.3 MALDI-TOF MS and MS/MS Analysis of the Lipid A Isolated from Polaribacter sp. SM1127

Reflectron MALDI-TOF mass spectra, acquired in negative ion mode, for both $LipA_{sse}$ and $LipA_{abh}$ are shown in *Figure 10.3*. The spectra were nearly identical, confirming the effectiveness of the methods used to isolate lipid A directly from EPS- EtOH. In both MS spectra, two major groups of peaks in ≈1:1 ratio were identified, corresponding to deprotonated [M─H] monophosphorylated penta-acylated (around

m/z 1588) and tetraacylated lipid A species (around m/z 1348/1392). The high structural variability in *Polaribacter* sp. SM1127 lipid A was evident, as proven by the presence of peaks differing by 14 amu, indicative of variations in the length of the acyl chains. Additional complexity was observed due to the presence of unsaturated fatty acids, which caused peaks to differ by 2 amu. As an example, in the m/z range of 1560.7–1644.7 (*Figure 10.3*), the peak at m/z 1602.7 was attributed to a penta-acylated lipid A structure consisting of the typical glucosamine disaccharide backbone with a single phosphate group and bearing three 15:0(3-OH) [or i15:0(3-OH) or a15:0(3-OH)], >one 14:0 [or i14:0] and one 17:0 (*Table 10.1 and 10.2*). For the sake of simplicity, hereafter, we will refer to the acyl chains without specifying their branching; however, they may occur in iso- or anteiso- forms, as detailed in the compositional analysis (*Table 10.1*). In the mass region m/z 1334.6–1434.6 (*Figure 10.3*), a heterogenous blend of tetra-acylated lipid A species was identified differing for the acyl chains length and degree of hydroxylation and unsaturation. As example, the peak at m/z 1348.6 was matched with a mono-phosphorylated lipid A species carrying one 15:0(3-OH), one 14:0(3-OH), one 17:0, and one 14:0, while the peak at 1392.6 carries one phosphate and three 15:0(3-OH) and one 17:0 (*Table 10.2*). To locate the phosphate group and acyl chains on the disaccharide backbone, negative-ion MALDI-TOF MS/MS was employed on several peaks. The MS/MS spectrum of the precursor ion at m/z 1602.7 (*Figure 10.4*) showed prominent peaks at m/z 1374.6 and 1332.6, generated by the loss of 14:0 and 17:0, respectively. A less intense peak corresponding to the loss of a 15:0 (3-OH) was also observed at m/z 1344.6. Additional peaks were detected at m/z 1074.5 and 1116.5, resulting from the sequential loss of a primary 15:0(3-OH) and a 17:0(m/z 1074.5) or a 14:0(m/z 1116.5) unit. Since no ions attributable to the loss of a whole unit comprising 15:0(3-OH) and either 14:0 or 17:0 were observed, it was hypothesized that these non-hydroxylated fatty acids were not part of acyloxyacyl moieties. However, the merging of several minor peaks provided additional evidence that guided the positioning of all acyl chains. Specifically, peaks detected at m/z 1134.6 and m/z 1176.6 were matched with

fragments devoid of 17:0 or 14:0, plus 198 amu, respectively. The loss of 198 amu was explained by a rearrangement that can only occur when the N-linked acyl chains do not carry secondary acyl groups, i.e., they have a free 3-OH group. Indeed, an enamine to imine tautomerization followed by six-membered-ring-based rearrangement can produce the loss of a $C_{13}H_{26}O$ neutral fragment (198 amu) from each primary amide-linked 15:0(3-OH) having a free 3-OH group [149]. Since these rearrangements were observed when also 17:0 or 14:0 were absent, one can speculate that both these fatty acids were linked to the two N-linked 15:0(3-OH). However, the observation of the peak at m/z 1404.7, generated by the sole loss of 198 amu, supported the hypothesis that only one of the two fatty acids (17:0 or 14:0) was attached to a primary amide-bound 15:0(3-OH). This was further demonstrated by the detection of the Y-type ion [76] at m/z 738.7, originating from the cleavage of the glycosidic bond between the two glucosamines. This was crucial for placing two 15:0(3-OH) on the reducing glucosamine, along with the phosphate group, and simultaneously locating the 17:0, 14:0, and another 15:0(3-OH) on the nonreducing glucosamine. Finally, the detection of the peak at m/z 978.5, corresponding to the loss of two $C_{13}H_{26}O$ neutral fragments (198 þ 198 amu) plus one 14:0, helped identify the 17:0 as a primary ester-bound fatty acid on the nonreducing glucosamine, with the 14:0 identified as acyloxyacylamide moiety of the same glucosamine. To gain insights into lipid A species displaying unsaturated acyl chains, precursor ion at m/z 1614.6 was chosen as a representative and underwent MS/MS investigation (*Figure 10.5*). This analysis was crucial in bringing to light the intrinsic additional heterogeneity of *Polaribacter* sp. SM1127 lipid A, which was justified by its fatty acid content (*Table 10.1*). Indeed, at least four isobaric lipid A species were assigned to ion at m/z 1614.7 (LA1–LA4, *Figure 10.5*) differing for the length of the acyl chains. Briefly, the spectrum clearly displayed main peaks at m/z 1386.6, m/z 1372.6, m/z 1360.6, m/z 1356.6, m/z 1346.6, and m/z 1342.6 attributed to ions derived by the loss of 14:0, 15:0, 16:1, 15:0(3-OH), 17:1, and 16:0(3-OH), respectively. Four main observations were key to define the structure of each lipid A species: 1) the examination of peaks

matching with fragments originated by the loss of combinations of the aforementioned acyl chains; 2) the detection of ions generated by the loss of acyl chains plus a neutral fragment derived from enamine to imine tautomerization; 3) the assignment of Y-type ions (m/z 738.7 and m/z 752.7) to counterprove the nature of the fatty acids on the reducing glucosamine unit and, specularly, of those on the nonreducing one; 4) the identification of 1,4A2 cross-ring fragmentation [76] derived ions at m/z 1013.3 and m/z 1027.3, which finally confirmed the structural assignments. Overall, the structures identified for precursor ion at m/z 1614.7, summarized in *Figure 10.5*, comprise primary ester-bound 17:1 or 16:1 on the nonreducing glucosamine, primary ester-bound 16:0(3-OH) or 15:0(3-OH) on the reducing unit, primary amide-linked 16:0(3-OH) and/or 15:0(3-OH) on the nonreducing unit while always 15:0(3-OH) was found on the reducing one, and 14:0 or 15:0 as secondary acyl substituents in an acylooxyacylamide moiety of the nonreducing residue. Likewise, the structure of tetra-acylated lipid A species detected at m/z 1348.6 and m/z 1406.6 were also defined (*Figure 10.6*). The analysis of the MS/MS spectrum of the latter precursor ion highlighted once again the existence of two isobaric species differing for the length of the secondary fatty acid decorating the nonreducing glucosamine (14:0 or 15:0) and of the primary N-linked acyl chain on the reducing one [15:0(3-OH) or 16:0(3-OH)]. In conclusion, integrating data from chemical analyses and MS/MS-based structural studies, we show that *Polaribacter* sp. SM1127 synthesizes a remarkably heterogeneous mixture of tetra- and penta-acylated lipid A species. These species feature the typical glucosamine disaccharide backbone decorated by one phosphate on the reducing glucosamine unit and carrying acyl chains of various lengths and branching degree, also experiencing non-hydroxylated and/or unsaturated acyl chains as primary ester-bound moieties of the nonreducing glucosamine.

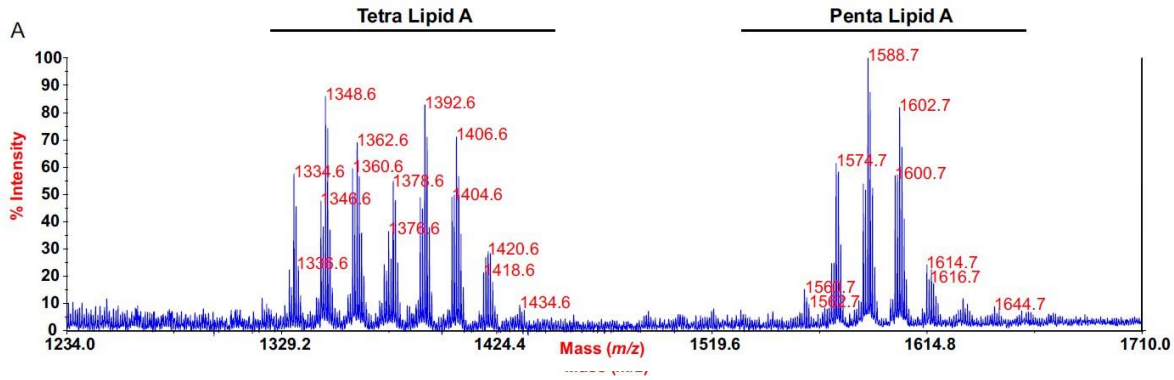

Figure 10.3: Reflectron MALDI-TOF MS spectra, recorded in negative-ion polarity, of A) $LipA_{sse}$ and B) $LipA_{abh}$. Lipid A species are labeled as Tetra LipA and Penta Lipd A based on the degree of acylation

Table 2. Main ion peaks detected in the MALDI-TOF MS spectra reported in Figure 2, the predicted masses, and the proposed interpretation of the fatty acids and phosphate (P) on the lipid a diglucosamine backbone.

Predicted mass [Da][a)]	Observed ion peaks [*m/z*]	Acyl substitution	Proposed composition
1615.18 (LA1)	1614.7 (LA1)	Penta-acyl	$HexN^2$, P, $[16:0(3\text{-}OH)]^2$ [15:0(3-OH)] (16:1) (14:0)
1615.18 (LA2)	1614.7 (LA2)	Penta-acyl	$HexN^2$, P, $[15:0(3\text{-}OH)]^2$ [16:0(3-OH)] (16:1) (15:0)
1615.18 (LA3 and LA4)	1614.7 (LA3 and LA4)	Penta-acyl	$HexN^2$, P, $[15:0(3\text{-}OH)]^2$ [16:0(3-OH)] (17:1) (14:0)
1603.18	1602.7	Penta-acyl	$HexN^2$, P, $[15:0(3\text{-}OH)]^3$ (17:0) (14:0)
1589.18	1588.7	Penta-acyl	$HexN^2$, P, $[15:0(3\text{-}OH)]^2$ [14:0(3-OH)] (17:0) (14:0)
1407.0 (LA1)	1406.6 (LA1)	Tetra-acyl	$HexN^2$, P, $[16:0(3\text{-}OH)]^2$ [17:0(3-OH)] (14:0)
1407.0 (LA2)	1406.6 (LA2)	Tetra-acyl	$HexN^2$, P, [15:0(3-OH)] [16:0(3-OH)] [17:0(3-OH)] (15:0)
1392.96	1392.6	Tetra-acyl	$HexN^2$, P, $[15:0(3\text{-}OH)]^3$ (17:0)
1362.97	1362.6	Tetra-acyl	$HexN^2$, P, $[15:0(3\text{-}OH)]^2$ (17:0) (14:0)
1348.96	1348.6	Tetra-acyl	$HexN^2$, P, [15:0(3-OH)] [14:0(3-OH)] (17:0) (14:0)

[a)]The observed masses are compared to the calculated monoisotopic mass (predicted mass, Da) of each ion based on the proposed lipid A chemical structures.

Table 10.2

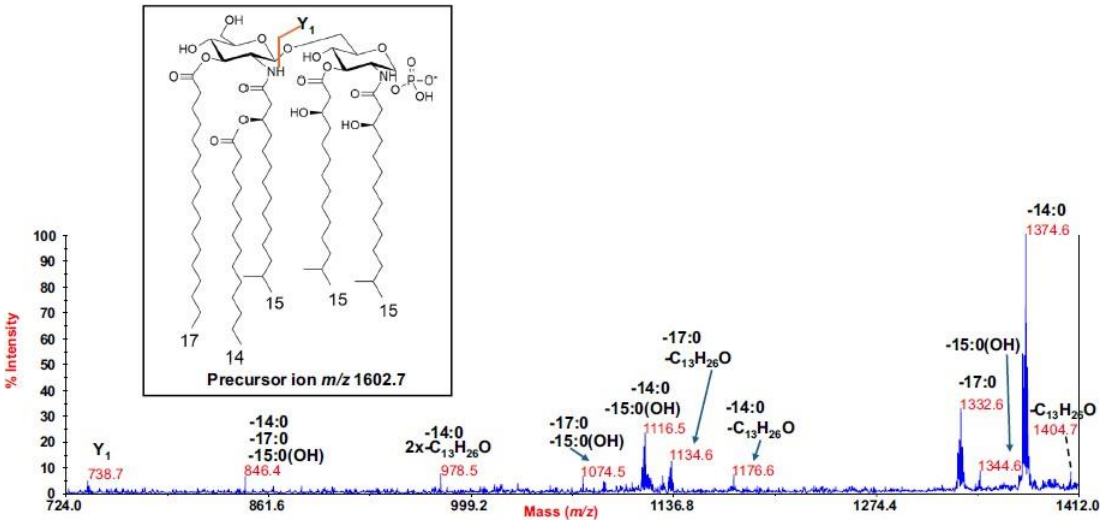

Figure 10.4: Negative-ion MALDI MS/MS spectrum of the m/z 1602.7 ion, representing a mono-phosphorylated, penta-acylated lipid A species from *Polaribacter* sp. SM1127. Key fragment ions are labeled, with a proposed structure shown in the inset. The branched (iso) acyl chains are noted, along with peaks from loss of $C_{13}H_{26}O$ (198 Da) due to N-linked acyl chain rearrangements.

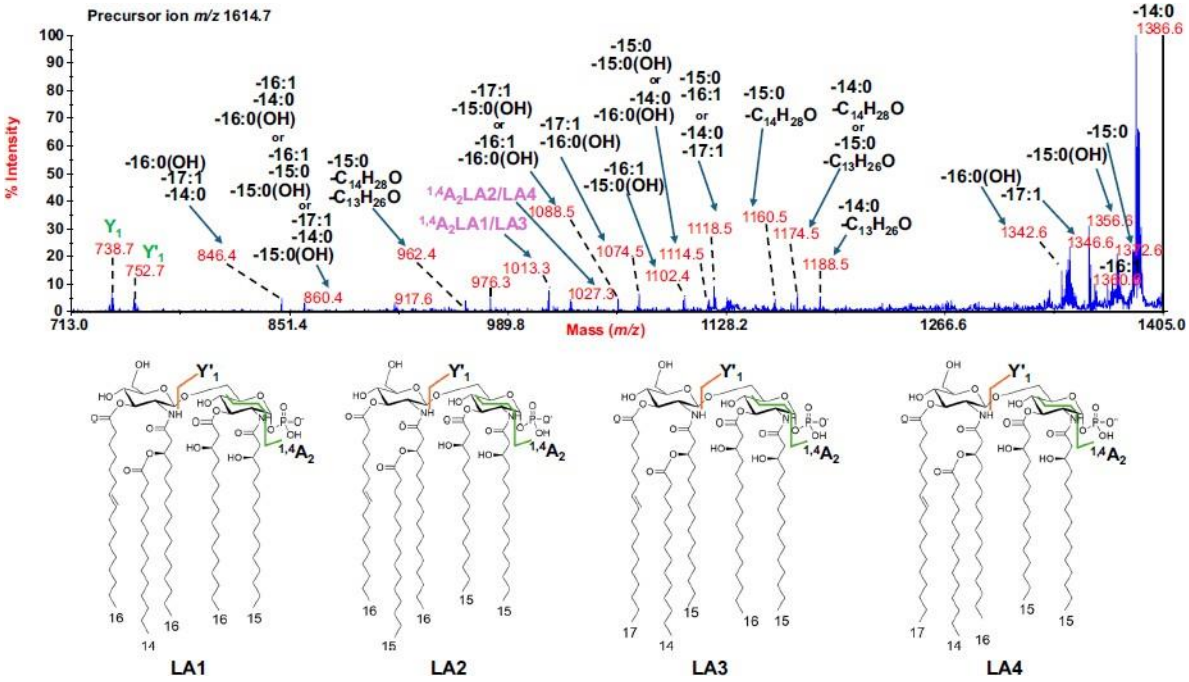

Figure 10.5: Negative-ion MALDI MS/MS spectrum of the m/z 1614.7 ion, representing a mono-phosphorylated, penta-acylated lipid A species detected in *Polaribacter* sp. SM1127 ($LipA_{sse}$ and $LipA_{abh}$). Key fragments are labeled, and four isobaric structures are illustrated below the spectrum, with unbranched fatty acids shown for simplicity. Peaks from the loss of $C_{13}H_{26}O$ (198 Da) and/or $C_{14}H_{28}O$ (212 Da) are also indicated.

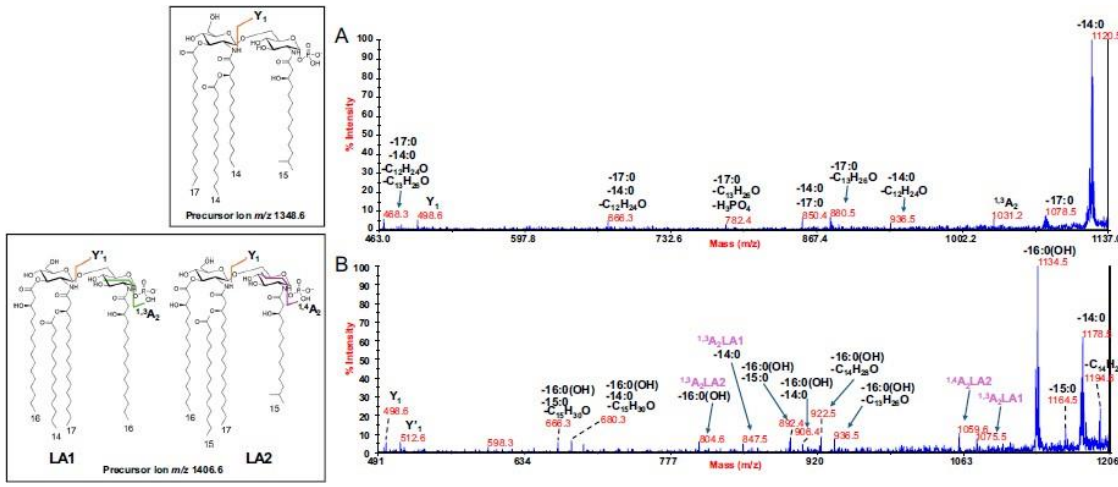

Figure 10.6: Negative-ion MALDI MS/MS spectra of precursor ions at A) m/z 1348.6 and B) m/z 1406.6, chosen as representatives of the heterogeneous cluster ascribed to mono-phosphorylated tetra-acylated lipid A species. In the inset, it is reported the proposed structure, where the iso-branching of the fatty acids is tentative. Peaks originated from the enamine to imine tautomerization and subsequent rearrangement have been also reported.

10.4 Immunostimulatory Properties of Polaribacter sp. SM1127 LPS and EPS

The peculiar structural diversity of *Polaribacter* sp. SM1127 lipid A sparked our interest in investigating the immunostimulatory activity of its LPS. Activation of TLR4, the main receptor able to recognize lipid A, triggers the Nuclear Factor kappa-lightchain- enhancer of activated B cells (NF-kB) pathway which in turn is responsible for regulating the expression of various pro-inflammatory genes and therefore it represents a key mediator of the inflammatory response [159]. As such, we used human embryonic kidney-blue (HEK-Blue) tohoku hospital

pediatrics-1 (THP-1) cells stably transfected with human TLR4 and MD-2/ CD14 featuring an NF-κB/AP-1-inducible secreted embryonic alkaline phosphatase (SEAP) reporter gene to evaluate the TLR4- dependent NF-κB response upon stimulation with LPS. In these experiments, EPS, which underwent additional steps of purification to remove traces of bacterial cells, was also tested and its activity compared to that of the LPS. We stimulated HEK-Blue hTLR4 cells with various concentrations (1–10–100 ng mL1) of both *Polaribacter* sp. SM1127 LPS and EPS. HEK-Blue hTLR4 cells stimulated with Escherichia coli LPS (1–10–100 ng mL1) were used as a positive control, while unstimulated cells were used as a negative control. Both *Polaribacter* sp. SM1127 LPS and EPS treatment resulted in a significantly lower TLR4 activation than E. coli LPS at all tested concentrations (*Polaribacter* LPS vs *E. coli* LPS $p < 0.01$ at 1 and 10 ng mL1, $p < 0.001$ at 100 ng mL1; *Polaribacter* EPS vs E. coli LPS $p < 0.001$ at all concentrations, *Figure 10.7 A*). Interestingly, treatments with 1 and 10 ng mL1 of EPS were associated with an even weaker activation of TLR4 compared to *Polaribacter* LPS used at the same concentrations (*Polaribacter* EPS vs *Polaribacter* LPS $p < 0.01$ at 1 and 10 ng mL1, *Figure 10.7a*). No significant differences were detected between *Polaribacter* sp. SM1127 LPS and its EPS at 100 ng mL1. Although we cannot fully exclude the presence of trace amounts of bacterial debris in the EPS preparations, which may contribute to the observed TLR4-mediated signaling at 100 ng mL1, this finding is in line with other studies reporting that certain polysaccharides can activate TLR4 even at concentrations lower than those typically required for such molecules (i.e., 1–500 μgmL1) [93], [160]. To further investigate the immunological properties of LPS and EPS in real immune cells, we evaluated their effect on Tohoku Hospital Pediatrics-1 (THP1)-Blue NF-κB cells. Once differentiated into macrophages, Quanti blue assay was conducted upon stimulation of cells with LPS or EPS from *Polaribacter* at 10 and 100 ng mL1, as well as with E. coli LPS used again as positive control. THP1 cells stimulated with *Polaribacter* LPS (10 and 100 ng

mL1) showed reduced NF-kB activation compared to that observed for the same concentrations of E. coli LPS (*Polaribacter* LPS vs *E. coli* PS $p < 0.05$ at both concentrations, *Figure 10.7b*). Likewise, EPS behaved as an even weaker activator compared to E. coli LPS (*Polaribacter* LPS vs EPS $p < 0.01$ at 10 ng mL1 and $p < 0.0001$ at 100 ng mL1, *Figure 10.7b*). Finally, *Polaribacter* sp. SM1127 LPS and EPS exhibited different immunostimulatory capacity also in THP-1 as NF-kb activation was significantly lower in THP1 cells treated with EPS compared to those stimulated with LPS at both concentrations used (*Polaribacter* EPS vs *Polaribacter* LPS $p < 0.01$ at 10 ng mL1, $p < 0.001$ at 100 ng mL1, *Figure 10.7b*).

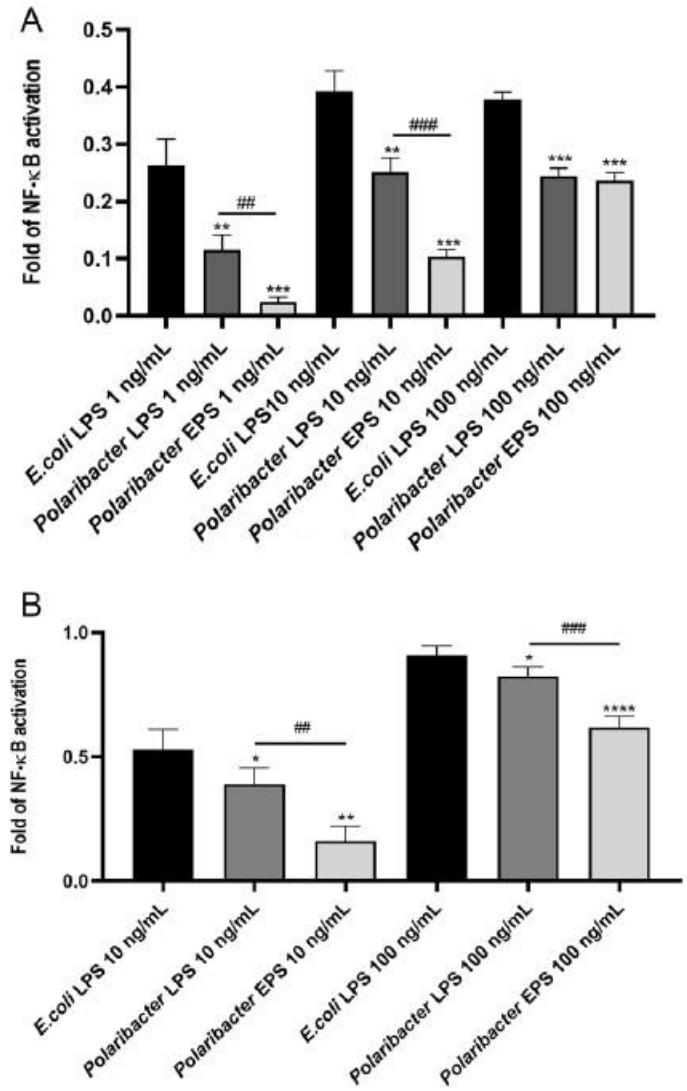

Figure 10.7*:* (A) HEK-Blue hTLR4 cells were stimulated with increasing concentrations (1, 10, 100 ng/mL) of *E. coli* LPS, *Polaribacter* LPS, or EPS. SEAP levels (OD 620 nm) were measured using the Quanti-Blue assay (B) PMA-differentiated THP1-Blue NF-κB cells were stimulated with 10 or 100 ng/mL of the same compounds, and SEAP levels were similarly assessed. Data are normalized to unstimulated controls and presented as mean ± SD. Statistical significance was tested via unpaired t-test, comparing *Polaribacter* LPS or EPS to E. coli LPS (*$p < 0.05$, **$p < 0.01$, ****$p < 0.0001$) and *Polaribacter* LPS vs EPS (##$p < 0.01$, ###$p < 0.001$).

10.5 Conclusion

Marine bacteria have long been recognized for their biotechnological potential in food, cosmetics, and pharmaceuticals [141]. In this study, we analyzed for the first time the LPS, EPS, and Lipid A components of *Polaribacter* sp. SM1127. Lipid A was extracted using two distinct protocols, i.e. cold ethanol precipitation followed by acidic hydrolysis ($LipA_{abh}$), and ultracentrifugation with small-scale extraction ($LipA_{sse}$), both yielding identical mass spectra, confirming the reliability of the methods. MALDI-TOF MS and MS/MS in negative mode revealed extensive structural variability in Lipid A, consistent with the bacterium adaptation to Arctic conditions. The presence of tetra- and penta-acylated Lipid A species with diverse acyl chain lengths and hydroxylation levels suggests a finely tuned biosynthetic mechanism for maintaining membrane fluidity under extreme cold. Similar adaptations are observed in other psychrophilic species, such as *Pseudoalteromonas tetraodonis*, *Psychromonas arctica*, and *Psychrobacter cryohalolentis*, which utilize unsaturated and branched acyl chains to enhance membrane flexibility [159]. Notably, the unsaturated chains in *Polaribacter* sp. SM1127 appear to be primary rather than secondary, indicating a unique strategy for cold adaptation and nutrient uptake.

Moreover, we evaluated the immunostimulatory activity of *Polaribacter* sp. SM1127 LPS. Compared to *E. coli* LPS, *Polaribacter* sp. SM1127 LPS induced significantly lower TLR4 activation, likely due to its hypoacylated structure and single phosphate group, features associated with reduced inflammatory potential [159]. THP-1 cell assays confirmed attenuated NF-κB pathway activation, highlighting the immunomodulatory potential of this Arctic-derived LPS for applications such as vaccine adjuvants and immunotherapeutics [161]. Additionally, we analyzed the bacterium EPS, known for its wound-healing and cryoprotective properties. EPS exhibited even weaker NF-κB activation than its LPS and *E. coli* LPS, reinforcing its suitability for pharmaceutical use due to its low immunogenicity and tissue-repair capabilities [158]. In summary, the structural and functional features of *Polaribacter*

sp. SM1127 Lipid A and EPS underscore their promise as novel biomolecules for immunomodulatory and tissue-protective applications.

References

[155] P. G. Williams, "Panning for chemical gold: marine bacteria as a source of new therapeutics," *Trends Biotechnol*, vol. 27, no. 1, pp. 45–52, Jan. 2009, doi: 10.1016/j.tibtech.2008.10.005.

[156] S. Dong *et al.*, "Cultivable Alginate Lyase-Excreting Bacteria Associated with the Arctic Brown Alga Laminaria," *Mar Drugs*, vol. 10, no. 11, pp. 2481–2491, Nov. 2012, doi: 10.3390/md10112481.

[157] B. Avcı, K. Krüger, B. M. Fuchs, H. Teeling, and R. I. Amann, "Polysaccharide niche partitioning of distinct Polaribacter clades during North Sea spring algal blooms.," *ISME J*, vol. 14, no. 6, pp. 1369–1383, Jun. 2020, doi: 10.1038/s41396-020-0601-y.

[158] N. Hassan *et al.*, "Temperature Driven Membrane Lipid Adaptation in Glacial Psychrophilic Bacteria," *Front Microbiol*, vol. 11, May 2020, doi: 10.3389/fmicb.2020.00824.

[159] Q. Guo *et al.*, "NF-κB in biology and targeted therapy: new insights and translational implications," *Signal Transduct Target Ther*, vol. 9, no. 1, p. 53, Mar. 2024, doi: 10.1038/s41392-024-01757-9.

[160] X. Wang, C. Zhang, F. Shi, and X. Hu, "Purification and Characterization of Lipopolysaccharides," 2010, pp. 27–51. doi: 10.1007/978-90-481-9078-2_2.

[161] F. Zhou *et al.*, "Polysaccharide Isolated From Tetrastigma hemsleyanum Activates TLR4 in Macrophage Cell Lines and Enhances Immune Responses in OVA-

Immunized and LLC-Bearing Mouse Models," *Front Pharmacol*, vol. 12, Mar. 2021, doi: 10.3389/fphar.2021.609059.

Chapter XI

Materials and Methods

All bacteria analyzed in this thesis were kindly provided by collaborators: *Phocaeicola vulgatus PVCL10T00C06, ΔM0N98_0427, ΔM0N98_0428-29, PVCL09T03C04, and ΔAntisigma* (Chapter VI) was provided by Professor Laurie Comstock from The University of Chicago, Department of Microbiology. Segatella copri (Chapter V) was provided by ……..

Bacteroides xylanisolvens (Chapter VIII) was provided by ……

Cellulophaga baltica NNO 15840^T, *tyrosinoxydans* EM41^T, and *algicola* ACAM 630^T (Chapter IX) was provided by ……
*Polaribacter sp. SM1127 (Chapter X) was provided by**……***

11.1 Preliminary Washes

Before initiating any LPS extraction protocol, preliminary manipulations of the lyophilized bacterial cells can be performed. These include either washing the bacterial cells or subjecting them to ultracentrifugation. The washing steps may begin with distilled H_2O, followed by centrifugation (10,000 × g, 10 °C, 20 minutes). Ethanol can then be used in subsequent washes. The material obtained is analyzed by means of ^1H NMR spectroscopy to monitor the extraction efficiency. Ultracentrifugation involves resuspending the bacterial cells and evenly distributing them into ultracentrifuge tubes. Samples are then centrifuged using a Beckman

Coulter ultracentrifuge (Brea, CA, USA) at forces ranging from 100,000 to 500,000 × g at 4 °C for 6 hours.

11.2 Extraction of R-LPS and S-LPS

While this PhD project, two main methods were employed for the extraction of LPS. The first is the PCP extraction method, which involves the use of a solvent mixture of phenol, chloroform, and light petroleum in a 2:5:8 volume ratio. The bacterial cells are suspended in this mixture at room temperature and stirred for 90 minutes. After this incubation, the sample is centrifuged at 8,000 × g for 30 minutes. The supernatant is collected in a round-bottom flask and the entire extraction procedure is repeated two additional times. The combined extract is concentrated by vacuum evaporation to remove chloroform and light petroleum, leaving phenol as the only remaining solvent. This phenolic phase is transferred to a Falcon tube, to which a few drops of cold water are added. A final centrifugation step (8,000 × g, 1 hour, room temperature) allows for the recovery of any precipitated material containing the LPS fraction. The resulting pellet is then rehydrated and lyophilized [162]. The second extraction strategy employed is the hot phenol/water method. In this protocol, pre-warmed water is added to the bacterial cells—either after the PCP extraction or directly to the freeze-dried pellet—followed by the addition of an equal volume of hot phenol. The suspension is stirred for 2 hours at 70 °C, then centrifuged at 8,000 × g for 30 minutes at 4 °C. The aqueous phase (supernatant) is collected, and the extraction is repeated twice more. Both the aqueous and phenolic phases are then dialyzed against distilled water using dialysis membranes with a molecular weight cut-off ranging between 8 and 14 kDa. After completion of the dialysis, the fractions are recovered and lyophilized. [162]

11.3 Enzymatic Hydrolysis and Extract Validation

To eliminate residual cellular contaminants, especially relevant for samples obtained using the hot phenol/water extraction method, enzymatic digestion is performed. This includes treatment with RNase (Roth), DNase (Roth), and Proteinase K (Roth) at 37 °C and 56 °C respectively. This step is followed by an additional dialysis step to ensure purity. Upon completion, the final product is recovered in distilled water and subsequently lyophilized [116]. The last step involves verification of the LPS extract using SDS-PAGE electrophoresis on a 12.5% acrylamide gel, followed by various staining methods. These include Alcian Blue staining [163], silver nitrate staining [116], [164], or PAS staining. If protein contamination is suspected, detection is carried out using Coomassie Blue staining solution (0.5% w/v Coomassie Brilliant Blue G-250 in 40% methanol, 5% acetic acid) [165]

11.4 Acetylated O-methyl glycosides (AMG)

For the analysis of monosaccharide composition in the sample (purified LPS, core oligosaccharide, or O-antigen), an aliquot of approximately 0.5 mg was subjected to acidic methanolysis by treatment with 300 µL of 1.25 M HCl/CH_3OH. The reaction was carried out at 80 °C for 16 hours. Upon completion, the mixture was neutralized through repeated methanol washes. Acetylation of hydroxyl groups was then performed by adding acetic anhydride (25 µL) and pyridine (25 µL), with the reaction maintained at 80 °C for 30 minutes. The resulting acetylated glycosides were extracted using chloroform and water washes. The organic phase was subsequently dried under airflow, and the residue was dissolved in 100 µL of acetone for analysis by gas chromatography–mass spectrometry (GC-MS) [166], [167]

11.5 Acetylated Alditols (AA)

To analyse the monosaccharide composition, approximately 0.5 mg of the freeze-dried sample was subjected to hydrolysis using 2 M trifluoroacetic acid (TFA) at 120 °C for 2 hours. Following hydrolysis, the sample was dried under a gentle stream of air. The resulting free monosaccharides were subsequently reduced to alditols by treatment with sodium borohydride ($NaBH_4$) in ethanol. The reduction products were then acetylated using 25 µL of acetic anhydride and 25 µL of pyridine at 80 °C for 30 minutes. After acetylation, the sample was evaporated under airflow, reconstituted in 100 µL of acetone, and analyzed by gas chromatography-mass spectrometry (GC-MS) [166], [167]

11.6 Partially Methylated Alditol Acetates (PMAA)

For linkage analysis, approximately 1 mg of freeze-dried sample was first dissolved in dimethyl sulfoxide (DMSO), followed by the addition of powdered sodium hydroxide. The suspension was stirred at room temperature, allowing complete dissolution and activation of hydroxyl groups. Subsequently, methylation was initiated by the addition of 300 µL of methyl iodide (CH_3I), and the reaction was allowed to proceed under continuous stirring for 16 hours at room temperature. After completion, the sample was exposed to a stream of air for one hour to evaporate any residual reagents. The methylated material was extracted with sequential washes of chloroform and water; the organic phase was then isolated and evaporated. The dry product underwent acid hydrolysis using 4 M trifluoroacetic acid (TFA) at 100 °C for 4 hours and was again dried and neutralised with repeated methanol washes. The resulting monosaccharides were subjected to carbonyl group reduction by treatment with sodium borodeuteride ($NaBD_4$) in ethanol under stirring for 16 hours at room temperature. The reaction was quenched by the addition of 2 M hydrochloric acid and neutralised once more with methanol. Finally, free hydroxyl

groups were acetylated with a mixture of acetic anhydride and pyridine at 80 °C for 30 minutes. The resulting partially methylated alditol acetates were then analyzed by GC-MS. [166], [167]

11.7 Octyl-glycosides

For the stereochemical analysis of monosaccharides, approximately 1 mg of the freeze-dried sample was taken and divided into two separate aliquots. To the first, 100 µL of enantiomerically pure 2-(+ or −)-octanol was added, while the second aliquot was treated with 100 µL of racemic 2-(±)-octanol in a separate vessel. In both preparations, 15 µL of acetyl chloride were introduced to initiate glycosylation, and the mixtures were incubated at 60 °C overnight to ensure complete reaction. Following the reaction, the samples were dried under a stream of air to remove any residual solvents and reagents. Subsequently, each sample was acetylated using a standard mixture of acetic anhydride and pyridine (80 °C, 30 minutes). The final derivatised octyl glycosides were then subjected to GC-MS analysis and compared with known standards for configurational assignment.[166], [168]

11.8 Gas Chromatography Mass Spectrometry

GC-MS analyses were carried out using an Agilent Technologies 7820A gas chromatograph system, coupled with a mass selective detector model 5977B. Chromatographic separation was achieved using an HP-5 capillary column (30 m × 0.25 mm, Agilent, Milan, Italy), with helium as the carrier gas at a constant flow rate of 1 mL/min. Specific temperature programs were employed based on the nature of the analytes. For the identification of acetylated O-methyl glycosides (AMG) and

octyl glycosides (OGA), the oven was initially held at 140 °C for 3 minutes, followed by a ramp to 240 °C at a rate of 3 °C/min. For partially methylated alditol acetates (PMAA), the temperature program was as follows: 90 °C for 1 minute, then raised to 140 °C at 25 °C/min, followed by an increase to 200 °C at 5 °C/min, then to 280 °C at 10 °C/min, and held at 280 °C for 10 minutes. In the case of fatty acid analysis, the oven was initially set at 150 °C for 5 minutes, then increased to 280 °C at 3 °C/min and maintained at that temperature for an additional 5 minutes [166], [168]

11.9 isolation on Lipid A

To isolate the lipid A moiety, an aliquot of the purified LPS was suspended in 1% acetic acid and subjected to mild acid hydrolysis at 100 °C for 4 hours. Following incubation, the mixture was centrifuged at 8,800 × g for 60 minutes at 4 °C, allowing phase separation: the insoluble pellet, enriched in lipid A, was collected, while the supernatant contained the oligo-/polysaccharidic components.

The lipid A-containing pellet was then subjected to sequential washes using a freshly prepared Bligh and Dyer solvent system composed of chloroform, methanol, and water in a 2:2:1.8 (v/v/v) ratio. The mixture was vortexed thoroughly and centrifuged again at 8,800 × g for 20 minutes at 4 °C. The organic (chloroform) layer, containing the lipid A, was carefully recovered, dried under vacuum, and subsequently analyzed by MALDI-TOF MS and tandem MS^2 (MS/MS) to elucidate its structural features. [169], [170]

11.10 Nuclear Magnetic Resonance (NMR)

All structural assignments of the core OS and the O-antigen from *Phocaeicola vulgatus PVCL10T00C06*, *ΔM0N98_0427*, *ΔM0N98_0428-29*, *PVCL09T03C04*, and *ΔAntisigma* (Chapter V), *Segatella copri* (Chapter VI) *and Bacteroides xylanisolvens* (Chapter VIII) were carried out as followed.

Nuclear Magnetic Resonance (NMR) spectra, including both one-dimensional (1D) and two-dimensional (2D) experiments, were acquired in D2O at 298 K, maintaining a pD of 7, using a Bruker 600 DRX spectrometer equipped with a cryogenic probe. Chemical shifts were referenced internally to acetone (δ_H = 2.225 ppm, δ_C = 31.45 ppm). Phosphorus-31 (^31P) NMR spectra were recorded on a Bruker DRX-400 spectrometer, using aqueous 85% phosphoric acid as an external standard (δ = 0.00 ppm). For homonuclear correlation experiments, total correlation spectroscopy (TOCSY) was performed with a spinlock duration of 100 ms, utilizing data matrices of 4096 × 256 points. Rotating-frame Overhauser enhancement spectroscopy (ROESY) and nuclear Overhauser enhancement spectroscopy (NOESY) were conducted with 4096 × 256 data points, mixing times between 100 and 300 ms, and 16 scans per experiment. Double-quantum-filtered phase-sensitive correlation spectroscopy (DQF-COSY) experiments used data matrices of 4096 × 512 points. In all homonuclear experiments, zero-filling was applied in both dimensions to achieve 4K × 2K data points, followed by resolution enhancement with a cosine-bell window function prior to S5 Fourier transformation. Coupling constants were extracted from the 2D phase-sensitive DQF-COSY spectra [149]. Heteronuclear experiments included ^1H,^13C heteronuclear single quantum coherence (HSQC) and heteronuclear multiple bond correlation (HMBC) performed in ^1H-detection mode, using single-quantum coherence with proton decoupling in the ^13C channel. Data matrices of 2048 × 256 points were employed. The HSQC spectra were acquired with sensitivity enhancement and phase-sensitive mode, incorporating echo/antiecho gradient selection and multiplicity editing. HMBC

experiments were optimized for long-range couplings (~6 Hz) with a low-pass J-filter to suppress one-bond correlations, and gradient pulses were applied for selection. A 60 ms delay was used for evolution of long-range correlations. Additionally, ^1H,^31P HSQC experiments were conducted optimized for an 8 Hz coupling constant. The heteronuclear data matrices were extended to 2048 × 1024 points using forward linear prediction extrapolation to improve resolution.

11.11 MALDI-TOF Mass Spectrometry and MS2

Mass spectrometry (MS) analyses were carried out using an AB SCIEX TOF/TOF™ 5800 mass spectrometer (Applied Biosystems) equipped with a neodymium-doped yttrium aluminum garnet (Nd:YAG) laser operating at 349 nm, with a 3 ns pulse width and a maximum repetition rate of 1000 Hz. All spectra were acquired in both positive and negative ion modes under reflectron conditions. For MS acquisition, each spectrum was generated by averaging approximately 2000 laser shots, while tandem MS (MS/MS) spectra were obtained by accumulating between 5000 and 7000 shots. All experiments were performed in replicate to ensure reproducibility [149]. Lipid A samples, extracted and purified as described, were dissolved in a chloroform/methanol mixture (1:1, v/v) prior to analysis. The matrix solution used for MALDI-TOF was 2,4,6-trihydroxyacetophenone (THAP), prepared at a concentration of 75 mg/mL in a mixture of methanol, 0.1% trifluoroacetic acid (TFA), and acetonitrile in a 7:2:1 volumetric ratio. Equal volumes (1:1, v/v) of the sample and matrix solution—less than 1 µL in total—were co-spotted onto a stainless-steel MALDI target plate and air-dried at room temperature. The resulting spectra were used to determine the structural features of lipid A by both MS and MS/MS analysis [149]

11.12 Preparation of fecal supernatant

To analyses LPS and Lipid A from healthy and food-allergic subjects, faces from healthy (CT) and food-allergic (FA) subjects randomly selected from the MATFA study population database were sampled. For all samples, the characteristics of the gut microbiota were analyzed using shotgun methodology [105] fecal supernatants were prepared by the addition of a quantity of phosphatase-buffered saline (PBS) in a ratio of 1:1 to weight in grams. The resulting mixture was subjected to serial centrifugation until a homogenous suspension was obtained. The supernatants obtained were then filtered and subsequently stored at -80°C. The samples were then subjected to cycles of lyophilization and resuspension in H2O for cell culture (ThermoFisher Scientific).

11.13 Extraction and purification of fecal LPS

For the isolation and characterization of LPS from the faces of CT and FA subjects, the supernatants were subjected to enzymatic digestion with DNase, RNase and Protease prior to the actual extraction step. Following enzymatic digestion, the samples undergo dialysis to remove contaminants. The deionized samples are then lyophilized and subjected to a hot H2O/phenol extraction protocol. Extracts from both the phenol and aqueous phases are analyzed via SDS-PAGE with silver staining to verify the nature of the extraction and the degree of purity of the extract. This process was useful to verify that only the aqueous fraction is the sample, so the aqueous fractions of all samples were subjected to ultracentrifugation. The ultracentrifugation precipitates are then further purified by gel filtration chromatography on a Sephacryl column. Following column purification, each sample was washed with CHCl3/CH3OH and CHCl3/CH3OH/H2O mixtures to remove any contaminating phospholipids. To purify the sample from the presence of any lipoproteins/lipopeptides, a clean-up described by Hirschfeld et al. (2000) was

performed [108]. Following these procedures, a further check was carried out via SDS-PAGE with silver staining and Coomassie's Blue to validate the degree of purification of the samples. LPS from *E. coli* was used as a positive control.

11.14 Compositional analyses of fecal LPS

Through the derivatization of acetylated O-methyl glycosides (AMG), it was possible to determine the content of monosaccharides in LPS extracted from fecal samples. The absolute configuration of the sugars present in the samples was obtained by O-octyl glycoside (OGA) derivatization [74]. All analyses performed in this way were validated by comparing the samples to specially prepared standards. About the fatty acid content, this was determined using a protocol involving 4M HCl followed by treatment with NaOH. The protocol then proceeds to adjust the pH until a slight acidity is reached. After this, the sample is then treated in CHCl3, methylated and finally analyzed via GC-MS. The extraction products were also subjected to other protocols, such as the one using HCl/CH3OH and subsequent extraction with hexane. Hexane in this case represents the solvent that retains the fatty acids in the form of methyl ester derivatives and was therefore analyzed to study their lipid composition.

11.15 MALDI-TOF analysis of fecal Lipide A

To prepare the sample for analysis via MALDI-TOF, freeze-dried samples of fecal material were taken and treated with mixtures of CHCl3/CH3OH and with CHCl3/CH3OH/H2O for washing and then subjected to centrifugation steps. The material was then lyophilized and prepared for analysis via MALDI-TOF. The supernatants of the samples were treated with a protocol already found in the literature

[115], which uses an isobutyric acid/ammonium hydroxide solution followed by repeated cycles of vertexing and sonication. Following this procedure, the samples are centrifuged, and their supernatant collected and subjected to repeated passages of lyophilization and washing with MeOH. They too were then lyophilized and analyzed via MALDI-TOF. For the best resolution of the spectra, and to obtain an optimal signal-to-noise ratio, different ratios of sample to MALDI matrix were tested, with the conclusion that the best ratio was 1:1. Samples spotted on the MALDI matrix were allowed to dry at room temperature before being analyzed. LPS from *E. coli* obtained by acid hydrolysis in the laboratory was used as the standard for each experiment. All experiments were recorded in technical triplicate.

11.16 Blood sampling and isolation of peripheral blood mononuclear cells

To procure mononuclear cells, peripheral blood samples were taken from three healthy children (Caucasian males with a negative history of allergic conditions and not at risk of atopic disorders). Mononuclear cells were isolated by centrifugation on a density gradient at room temperature. After centrifugation, an opaque interface representing the mononuclear cells was observed. The latter was aspirated using Pasteur, and the cells thus extracted were subjected to repeated washing with PBS and subsequent centrifugation. The supernatant was then removed, and the pellet, representing the cells, was collected.

11.17 PBMCs stimulation for cytokines and monocytes and statistical analysis

Cells extracted from peripheral blood as described in the previous sections were stimulated by Lipid A and LPS extracted from fecal samples. The experiments were performed at varying times and doses, using cells without stimulation as a negative control. Following the incubation period with the materials extracted from the fecal samples, the cells were harvested for analysis by flow cytometry, and the supernatants

collected to assess their production of cytokines such as IL-4, IL-13, IL-10 and IL-12. The evaluation of cytokine expression in the samples was possible by using the ELISA technique. The analysis of the T-reg and monocyte populations was done by classifying the T-reg as CD4+/CD25+/FoxP3+ positive cells, and the monocytes as CD14+/CD16++ positive cells by flow cytometry analysis. For the statistical analysis, the Kolmogorov-Smirnov test was used for the analysis of variables, the differences between the three groups were calculated by means of the ANOVA one way test, followed by the Tukey post-hoc test. Pearson's correlation coefficient "r" was used for the evaluation and correlation between the continuous variables. Differences that are considered significant are those for a p-value < 0.05. The database used for the analysis is GraphPad Prism 7.

11.18 Cell Culture

HEK-Blue™ hTLR4, HEK-Blue™ hTLR2, HEK-Blue™ TLR2/1, HEK-Blue™ TLR2/6 and THP1-Blue™ NF-κB reporter cell lines (InvivoGen, Toulouse, France) were used for the cell-based assays. HEK-Blue™ hTLR4, HEK-Blue™ hTLR2, HEK-Blue™ TLR2/1 and HEK-Blue™ TLR2/6 cells were maintained in Dulbecco's Modified Eagle's Medium (DMEM, 4 g/L glucose) supplemented with 10% heat-inactivated fetal bovine serum (FBS), 1% penicillin/streptomycin (Pen/Strep), 2 mM L-glutamine, and 100 µg/mL Normocin. To ensure plasmid maintenance and selective pressure, HEK-Blue™ Selection reagent was added to the culture medium following the manufacturer's recommendations. THP1-Blue™ NF-κB cells were cultured in RPMI 1640 medium supplemented with 10% heat-inactivated FBS, 1% Pen/Strep, 2 mM L-glutamine, 25 mM HEPES, 100 µg/mL Normocin, and 10 µg/mL Blasticidin.All cell lines were incubated at 37 °C in a humidified atmosphere containing 5% CO_2. Cell culture reagents, including FBS, Pen/Strep, DMEM, RPMI 1640, L-glutamine, and HEPES, were obtained from Thermo Fisher Scientific (Gibco

brand), while Normocin, Blasticidin, and HEK-Blue™ Selection were supplied by InvivoGen (Toulouse, France).

11.19 LPS Stimulation of HEK and THP-1 Cells

HEK-Blue™ hTLR4, HEK-Blue™ hTLR2, HEK-Blue™ TLR2/1 and HEK-Blue™ TLR2/6 cells were seeded in 96-well plates at a density of 3×10^4 cells/well. After overnight attachment, cells were stimulated for 18 h with lipopolysaccharide (LPS) from *Escherichia coli* O111:B4 (InvivoGen, Toulouse, France) at various concentrations (1, 10, and 100 ng/mL for HEK-Blue™ hTLR4 and HEK-Blue™ hTLR2 cells; 100 ng/mL for HEK-Blue™ TLR2/1 and HEK-Blue™ TLR2/6 cells). NF-κB activation was quantified using the Quanti-Blue™ assay (InvivoGen, Toulouse, France), which measures secreted embryonic alkaline phosphatase (SEAP) activity. As positive controls for receptor activation, HEK-Blue™ hTLR2 and HEK-Blue™ TLR2/1 cells were treated with 500 ng/mL Pam_3CSK_4 (InvivoGen), a synthetic triacylated lipopeptide known to activate TLR2/TLR1 heterodimers. Likewise, HEK-Blue™ TLR2/6 cells were stimulated with 100 ng/mL FSL-1 (InvivoGen), a diacylated lipopeptide specific for TLR2/TLR6 heterodimer activation. THP1-Blue™ NF-κB cells were seeded in 96-well plates at a density of 6×10^4 cells/well and differentiated through a 24 h exposure to 5 ng/mL phorbol 12-myristate 13-acetate (PMA; Thermo Fisher Scientific, Kandel, Germany), followed by a 72 h resting period in PMA-free medium. Differentiated cells were then stimulated for 24 h with increasing concentrations of *E. coli* LPS (0.1, 1, 10, 100, and 1000 ng/mL). SEAP levels released in the supernatants of HEK-Blue™ and THP1-Blue™ NF-κB cells were quantified to assess NF-κB activation upon LPS stimulation using the Quanti-Blue™ assay. Absorbance was measured at 620 nm using a TECAN Infinite® M Plex spectrophotometer (Tecan, Grödig, Austria). For competition assays, HEK-Blue™ hTLR4 cells were pre-treated for 4 h with LPS derived from *Rhodobacter sphaeroides* (RS-LPS; #tlrl-prslps, InvivoGen, Toulouse, France) at

concentrations of 1, 10, and 100 ng/mL, and subsequently stimulated with 10 ng/mL *E. coli* LPS for 16 h. Results from Quanti-Blue™ assays were expressed as percentages relative to the response induced by 10 ng/mL *E. coli* LPS, which was set as 100%.

11.20 3-(4,5-Dimethylthiazol-2-yl)-2,5-diphenyltetrazolium bromide (MTT) Assay

Cell viability was evaluated by means of the MTT assay in PMA-differentiated THP1 cells. MTT reagent (#BID2165, Apollo Scientific) was prepared as a 5 mg/mL stock solution in phosphate-buffered saline (PBS) and filtered through 0.22 µm pore-size membranes. After 24 h of stimulation with *Escherichia coli* LPS, culture supernatants were carefully removed, and cells were incubated with medium containing 0.5 mg/mL MTT for 3 h at 37 °C. Subsequently, the medium was discarded, and the resulting formazan crystals were solubilized in dimethyl sulfoxide (DMSO). Absorbance was measured at 570 nm with background subtraction at 630 nm using a TECAN Infinite® M Plex spectrophotometer (Tecan, Grödig, Austria). Cell viability values were normalized to those of unstimulated control cells.

11.21 Enzyme-Linked Immunosorbent Assay (ELISA)

Tumor necrosis factor-α (TNF-α) concentrations in the supernatants of PMA-differentiated THP1 cells stimulated for 24 h with *Escherichia coli* LPS were quantified using DuoSet® ELISA kits (R&D Systems, Bio-Techne, Minneapolis, USA), according to the manufacturer's instructions. Optical density was measured at 450 nm with background subtraction at 570 nm using a TECAN Infinite® M Plex spectrophotometer (Tecan, Grödig, Austria).

11.22 Peripheral Blood Mononuclear Cell (PBMC) Isolation

Peripheral blood mononuclear cells (PBMCs) were isolated from peripheral blood samples collected from healthy adult donors using density gradient centrifugation with Ficoll-Paque™ PLUS (GE Healthcare, Chicago, IL, USA). No identifying donor information was recorded. All procedures were conducted in accordance with institutional ethical guidelines and the principles outlined in the Declaration of Helsinki.PBMCs were seeded at a density of 2×10^6 cells per well in 6-well plates, using 2 mL of RPMI 1640 medium supplemented with 10% fetal bovine serum (FBS) and 1% penicillin-streptomycin (Thermo Fisher Scientific, Waltham, MA, USA).

11.23 Cytokine Production in PBMCs upon LPS Stimulation

PBMCs were stimulated for 24 h with lipopolysaccharide (LPS) from *Escherichia coli* at concentrations of 1 ng/mL and 10 ng/mL. Following stimulation, the production of key cytokines—interleukin-10 (IL-10), interleukin-6 (IL-6), and tumor necrosis factor-α (TNF-α)—was quantified using the ultrasensitive ELLA-Simple Plex® system (ProteinSimple, Bio-Techne, San José, CA, USA) with a customized microfluidic cartridge.

11.24 Statistical Analysis

All data are presented as mean ± standard deviation (SD), unless otherwise specified. For ELLA assays, cytokine levels are expressed as mean ± standard error of the mean (SEM). Statistical differences were analyzed by ordinary one-way ANOVA for experiments conducted on HEK cells and for MTT assays on THP1 cells. NF-κB activation and TNF-α release in THP1 cells, as well as cytokine production in PBMCs, were evaluated using unpaired *t*-tests.

For all statistical analyses, a p-value < 0.05 was considered statistically significant. Analyses were performed using GraphPad Prism software (version 9.1.2; GraphPad

Software, CA, USA). Immune cell population frequencies obtained by CyTOF were expressed as percentages (%), and non-parametric one-way ANOVA followed by Tukey's post hoc multiple comparison test was applied. Significance was set at $p < 0.05$ for all comparisons.

References

[162] C. Galanos, O. Lüderitz, and O. Westphal, "A New Method for the Extraction of R Lipopolysaccharides," *Eur J Biochem*, vol. 9, no. 2, pp. 245–249, Jun. 1969, doi: 10.1111/j.1432-1033.1969.tb00601.x.

[163] J. Corzo, R. Pérez-Galdona, M. León-Barrios, and A. M. Gutiérrez-Navarro, "Alcian blue fixation allows silver staining of the isolated polysaccharide component of bacterial lipopolysaccharides in polyacrylamide gels," *Electrophoresis*, vol. 12, no. 6, pp. 439–441, Jan. 1991, doi: 10.1002/elps.1150120611.

[164] C.-M. Tsai and C. E. Frasch, "A sensitive silver stain for detecting lipopolysaccharides in polyacrylamide gels," *Anal Biochem*, vol. 119, no. 1, pp. 115–119, Jan. 1982, doi: 10.1016/0003-2697(82)90673-X.

[165] W.-H. Dong, T.-Y. Wang, F. Wang, and J.-H. Zhang, "Simple, Time-Saving Dye Staining of Proteins for Sodium Dodecyl Sulfate–Polyacrylamide Gel Electrophoresis Using Coomassie Blue," *PLoS One*, vol. 6, no. 8, p. e22394, Aug. 2011, doi: 10.1371/journal.pone.0022394.

[166] P. Garcia-Vello, I. Speciale, F. Di Lorenzo, A. Molinaro, and C. De Castro, "Dissecting Lipopolysaccharide Composition and Structure by GC-MS and MALDI Spectrometry," 2022, pp. 181–209. doi: 10.1007/978-1-0716-2581-.

[167] C. De Castro, M. Parrilli, O. Holst, and A. Molinaro, “Microbe-Associated Molecular Patterns in Innate Immunity,” 2010, pp. 89–115. doi: 10.1016/S0076-6879(10)80005-9.

[168] M. D. Pither *et al.*, “Bacteroides thetaiotaomicron rough-type lipopolysaccharide: The chemical structure and the immunological activity,” *Carbohydr Polym*, vol. 297, p. 120040, Dec. 2022, doi: 10.1016/j.carbpol.2022.120040.

[169] U. Piantini, O. W. Sorensen, and R. R. Ernst, “Multiple quantum filters for elucidating NMR coupling networks,” *J Am Chem Soc*, vol. 104, no. 24, pp. 6800–6801, Dec. 1982, doi: 10.1021/ja00388a062.

[170] M. Rance, O. W. Sørensen, G. Bodenhausen, G. Wagner, R. R. Ernst, and K. Wüthrich, “Improved spectral resolution in COSY 1H NMR spectra of proteins via double quantum filtering,” *Biochem Biophys Res Commun*, vol. 117, no. 2, pp. 479–485, Dec. 1983, doi: 10.1016/0006-291X(83)91225-1.

Conclusions

During my PhD studies, I had the opportunity to explore one of the most fascinating and complex aspects of human biology: the way in which the gut microbiota communicates with and modulates the immune system through an extremely precise molecular language. Lipopolysaccharides have traditionally been regarded as endotoxins, inherently linked to inflammatory responses and to the pathogenic potential of Gram-negative bacteria. However, the findings presented in this work reveal a far more nuanced and unexpected reality. **Behind the term "LPS" lies an enormous diversity of chemical structures**, many of which appear to have co-evolved with the host—not only avoiding chronic inflammation but even contributing to the proper development of immune homeostasis at the organismal level.

Over these years, I have learned how even minimal structural variations—such as a single phosphorylation, a different acylation pattern, or the addition of one sugar residue—can profoundly alter the immunological fate of a molecule. What may seem like a minor structural detail often proves crucial for its recognition by immune receptors. This concept, which forms the basis of my thesis, represents one of the most intriguing and least understood aspects of the human microbiota and its dense network of signals governing host homeostasis.

Recognizing that **not all LPS molecules trigger an alarm response, and that some are instead capable of regulating, attenuating, or even educating the immune system**, opens new conceptual and translational perspectives. The differences observed between the LPS profiles of healthy children and those with food allergies suggest that this early molecular dialogue may steer immune development toward physiological or pathological trajectories, highlighting the evolutionary role of the microbiota in shaping immunity. The characterization of commensal Gram-negative bacteria presented in this thesis provides a concrete insight into the structural complexity of LPS and into the diverse ways they can either activate or suppress immune responses. Even the studies conducted on extremophilic bacteria—although peripheral to the central focus of this work—have further broadened this perspective:

in extreme environments, where survival requires unconventional biochemical strategies, LPS adopt even more elaborate configurations, sometimes displaying unexpectedly anti-inflammatory properties that may hold biomedical potential.

In conclusion, this doctoral journey has allowed me to reinterpret **LPS not simply as "inducers of inflammation," but as subtle mediators of the symbiotic dialogue between the gut microbiota and its host**. I conclude this work with the awareness that much remains to be discovered, but also with the strong conviction that the host–microbiota dialogue represents one of the most extraordinary biological stories of our time, and that deciphering its molecular language may pave the way for new perspectives in human health.